ABSTRACT

Title of Document: SYSTEMATIC INVESTIGATION OF QUORUM SENSING IN *Escherichia coli*

JUN LI, Doctor of Philosophy, 2007

Directed By: Professor, William E Bentley, Chemical and Biomolecular Engineering

High throughput techniques and advanced mathematical tools have enabled systematic investigations of biological systems with unparalleled precision. Not only molecular interactions between components but mechanisms and the dynamic behaviors associated with these systems are revealed, suggesting that comprehensive systems biology can be realized in the near future. Quorum sensing, especially the auto-inducer2 (AI-2) system, has been extensively studied due to its commonality among bacteria and connections to pathogenic phenotypes.

In this study, the *E. coli* quorum sensing AI-2 system was studied combing system-based mathematical modeling and high throughput genomic profiling. First, a Stochastic Petri Network (SPN) model was constructed based on available regulatory information. Simulations together with experimental data demonstrated that the apparent stimulation of AI-2 in the presence of glucose is not from the increased transcriptional or translational expression of AI-2 synthases *luxS* and *pfs*, nor from the increased metabolic flux associated with LuxS-related pathways but from an

alternative AI-2 synthesis pathway. The conversion of adenosine with cellular extracts from both *luxS* and *pfs* mutants validated our prediction about the existence of an alternative non-LuxS related AI-2 synthesis pathway. Second, AI-2 uptake regulatory network was investigated in detail: *lsrR*-lacZ, *lsrK*-lacZ fusion reporters were constructed and the analysis found that *lsrR* is subject to its own repression and is induced by both *lsrK* and *luxS*. Further transcriptome analysis demonstrated that *lsrR* and *lsrK*, together with quorum signal AI-2, coregulate *lsrRK* regulon, which influences phenotypes (biofilm, small RNAs). Importantly, this regulation is in a distinctly different manner than that mediating the *lsr* operon. We hypothesize that *lsrR* acts together with AI-2 to mediate cellular processes and that the phosphorylation of AI-2 molecule through *lsrK* triggers different response pathways. These investigations demonstrated that *lsrR*, *lsrK* are indispensable for AI-2 uptake. These newly elucidated regulatory mechanisms and associations undoubtedly broaden the scope of the AI-2 quorum sensing system, and provide a solid foundation for further mathematical modeling of the dynamics and system behaviors in *E. coli*. Finally, a tight coupling of experimental manipulation with mathematical analysis, as demonstrated in this study, provides a good example for systematically investigating biological systems.

SYSTEMATIC INVESTIGATION OF QUORUM SENSING IN *Escherichia coli*

By

Jun Li

Dissertation submitted to the Faculty of the Graduate School of the
University of Maryland, College Park, in partial fulfillment
of the requirements for the degree of
Doctor of Philosophy
2007

Advisory Committee:
Professor William E Bentley, Chair
Associate Professor, Cheng Lee, Dean's representative
Associate Professor, Nam S Wang
Associate Professor, Evanghelos Zafiriou
Assistant Professor, John P Fisher

Dedication

I would like to dedicate this work to my beloved mother, Wangping Hu, to whom I am always indebted.

Acknowledgements

I would like to take this opportunity to appreciatively acknowledge my advisor, Dr William E. Bentley, for his invaluable time, guidance, support, advice and encouragement during all these years of my studies. I would also like to thank all my committee members, Dr Cheng Lee, Dr Nam S. Wang, Dr Evanghelos Zafiriou and Dr John P. Fisher for their wonderful suggestions and help.

I really appreciate all the love and support from my beloved husband and partner, Daniel E. Mitchell. I am truly blessed with the birth of my son and daughter, Danny and Pearl, during my Ph.D studies.

I would also like to extend my sincere thankfulness to all the Bentley lab members, for all their wonderful discussions and great friendship. I would like to acknowledge B. L. Bassler, H. Aiba, R. Kolter, A. Hochschild, L. I. Rothfield, and M. Berlyn for generously providing strains and plasmids used in this study. I would like to thank Mr. Alvaro Godínez for assistance in the DNA microarray experiments, Tim Maugel for scanning electron microscopy (SEM) experiments. This work was supported by the National Science Foundation and the Center for Biosystems Research, UMBI.

Table of Contents

Dedication ii
Acknowledgements iii
Table of Contents iv
List of Tables vi
List of Figures vii
Chapter 1: Introduction 1
Life beyond the Central Dogma 1
Genetic Regulatory Network (GRN) 6
Systems Biology 10
Quorum Sensing Systems 16
Gram-negative LuxI/LuxR system 17
Small Peptide Mediated Quorum Sensing 21
The LuxS/AI-2 system 23
Multi-Channel Quorum sensing systems 27
Stochastic Petri Network Simulations 30
Research Motivation 36
Chapter 2: A Stochastic Model of *E. coli* AI-2 Quorum Signal Circuit Reveals Alternative Synthesis Pathways 39
Abstract 39
Introduction 40
Materials and Methods 43
Plasmid, bacterial strains, and culture conditions. 43
AI-2 Activity Assay. 43
RNA preparation and Northern blot analysis 44
Real-Time RT-PCR. 45
SDS-PAGE analysis 46
Results 47
Model construction 47
AI-2 production in LB medium is partially influenced by Pfs & LuxS 54
Glucose provides enhanced flux through the LuxS synthesis pathway 60
Is Conversion of 4,5-dihydroxy-2, 3-pentanedione a High-flux Reaction? 66
Experiments demonstrating existence of alternative AI-2 synthesis pathways 70
Discussions 74
Acknowledgements 78
Chapter 3: Transcriptional Analysis of *lsrR* and *lsrK* 80
Abstract 80
Introduction 81
Materials and Methods 82
Bacterial strains and growth conditions. 82
Plasmid construction. 83
RT-PCR 84
β-galactosidase assays 85
Expression and purification of the LsrR repressor protein. 86

Gel motility shift assay. 86
Result 87
Transcriptional regulation of *lsrR* by LsrR and CRP 87
lsrK and *lsrR* belong to the same operon 90
Overexpression of *lsrR* represses in vivo *lsr* transcription 93
Discussions 97
Chapter 4: Quorum Signal AI-2 Uptake Regulators in *Escherichia coli* Affects Biofilm Architecture and sRNA Regulations 98
Abstract 98
Introduction 99
Materials and Methods 103
Bacterial strains and growth conditions 103
RNA isolation 103
cDNA synthesis and labeling 103
Microarray hybridization, washing and scanning 104
Data analysis 104
Motility assays 105
Biofilm and time course assays 105
SEM (Scanning Electron Microscopy) 106
Real-Time RT-PCR 106
Autoaggregation assay 107
Flow cell biofilm experiments and image analysis. 107
Results 109
Deletion of the E. coli W3110 *lsrR*, *lsrK* gene does not affect growth or motility but biofilm architecture. 109
Genomic transcriptional analyses of the *lsrR*, *lsrK* mutations 111
l*srR* and *lsrK* regulate biofilm architecture and formation through the colanic acid synthesis gene, *wza*, and the autotransporter gene, *flu* 124
Small RNAs (sRNAs) are mediated by *lsrR* and *lsrK* 129
Discussion 132
Acknowledgements 139
Chapter 5: Conclusions and Future Directions 140
Bibliography 146

List of Tables

Table 2-1 Baterial strains and plasmids used in this study 44
Table 2-2 Primers used in real-time PCR 46
Table 2-3 Initial markings used in AI-2 circuit 51
Table 2-4 Rate constants in AI-2 synthesis and uptake circuit 52
Table 2-5 AI-2 synthesis and uptake rate constants in simulations 56
Table 2-6 *LuxS*, *pfs* mRNA level from real-time PCR and comparison to quantified Northern blot data 56
Table 2-7 AI-2 synthesis rate constant comparison under simulations with different DPD levels 69
Table 3-1 Bacterial strains and plasmids used in this study 83
Table 3-2 Primers used in this study 85
Table 4-1 Genes co-regulated by *lsrR*, *lsrK* 113
Table 4-2 Genes regulated by *lsrR* only 119
Table 4-3 Genes regulated by *lsrK* only 122
Table 4-4 Biofilm related gene mediated by *lsrR*, *lsrK* 125
Table 4-5 Confocal analysis results of biofilm flow cell assay 127
Table 4-6 Small RNAs affected by *lsrR*, *lsrK* 131

List of Figures

Figure 1-1 The Central dogma of molecular biology 2
Figure 1-2 The genetic flow of molecular biology 5
Figure 1-3 Genetic regulatory network as a cellular input-output device 7
Figure 1-4 Approaches utilized by System Biology 12
Figure 1-5 LuxR-type quorum sensing in Gram-negative bacteria 22
Figure 1-6 Quorum sensing in Gram-positive bacteria..... 22
Figure 1-7 LuxS catalyzed AI-2 biosynthesis pathway and related equilirium of different AI-2 molecules 25
Figure 1-8 Three parallel quorum sensing systems in *V. harveyi* 29
Figure 1-9 An example of SPN..... 33
Figure 2-1 AI-2 synthesis and uptake pathways in *E. coli* 47
Figure 2-2 Schematic of SPN for AI-2 synthesis and uptake circuit 49
Figure 2-3 Transcription rate for AI-2 synthase LuxS, Pfs 53
Figure 2-4 *LuxS*, *pfs* mRNA decay rate 54
Figure 2-5 Effects of glucose on AI-2 production and *luxS*, *pfs*, *speD* mRNA levels 55
Figure 2-6 *LuxS, pfs* overexpression partially influences AI-2 formation in LB medium 59
Figure 2-7 *LuxS, pfs* overexpression affects AI-2 formation in the presence of glucose 61
Figure 2-8 Glucose affect AI-2 formation by increasing fluxes through AI-2 pathway modulating AI-2 synthesis rate 64
Figure 2-9 Modulating flux from DPD to AI-2 significantly affects AI-2 formation 68
Figure 2-10 AI-2 produced from reactions with substrate adenosine and SAH 71
Figure 3-1 Transcriptional regulation of *lsrR* expression 89
Figure 3-2 Deletion of *rpoS* increase *lsrR* expression 90
Figure 3-3 Transcriptional regulation of *lsrK* expression..... 91
Figure 3-4 Transcriptional analysis for *lsrRK* operon 92
Figure 3-5 LsrR overexpression represses *lsr* transcription 94
Figure 3-6 LsrR purification and detection by Comassie stain and Western blot 94
Figure 3-7 Determination of LsrR binding site on *lsr*, *lsrR* promoter 95
Figure 4-1 Regulation of AI-2 uptake network..... 101
Figure 4-2 Genomic deletion of lsrR, lsrK does not affect growth, motility..... 110
Figure 4-3 Crystal violet estimation of biofilm formation..... 110
Figure 4-4 Biofilm structure from Scanning Electron Microscope 111
Figure 4-5 Correlation of microarray and Real Time PCR..... 112
Figure 4-6 Three different groups gene regulated by *lsrR* and *lsrK* 112
Figure4-7 Autoaggregation assay of W3110, and *lsrR*, *lsrK* mutants 117

Chapter 1: Introduction

Life beyond the Central Dogma

The central dogma forms the backbone of traditional molecular biology and is represented by four major stages: (1) Replication- a double stranded nucleic acid is duplicated to give identical copies for perpetuating the genetic information; (2) Transcription- a DNA is read and transcribed into messenger RNA (mRNA); (3) Splicing- pre-mRNA are generally processed where introns are cut off and mRNA migrates from the nucleus to the cytoplasm (this step is necessary for eukaryotic cells because the genetic material in the nucleus is physically separated from the site of protein synthesis in the cytoplasm in the cell); (4) Translation-ribosomes read the information coded by mRNA (three codons every time) and translate them into amino acid for protein formation. The central dogma, first elucidated by Francis Crick, deals with the detailed residue-by-residue transfer of sequential information and states that such information can only linearly flows from DNA to RNA to protein (48) (Fig 1-1, adapted from http://users.ugent.be/~avierstr /principles/centraldogma.html).

Since 1970, there is immense amount of evidence contradictory to the central dogma: (1) flow from RNA to DNA does occur, retroviruses in viruses and retrotransposons in higher animals including humans are good examples. These retroviruses have the enzymatic ability to reverse the flow of information from RNA back to DNA using a special enzyme called reverse transcriptase. This phenomenon was first discovered by Howard M. Temin and David Baltimore independently (11, 266), which upset the widely held belief

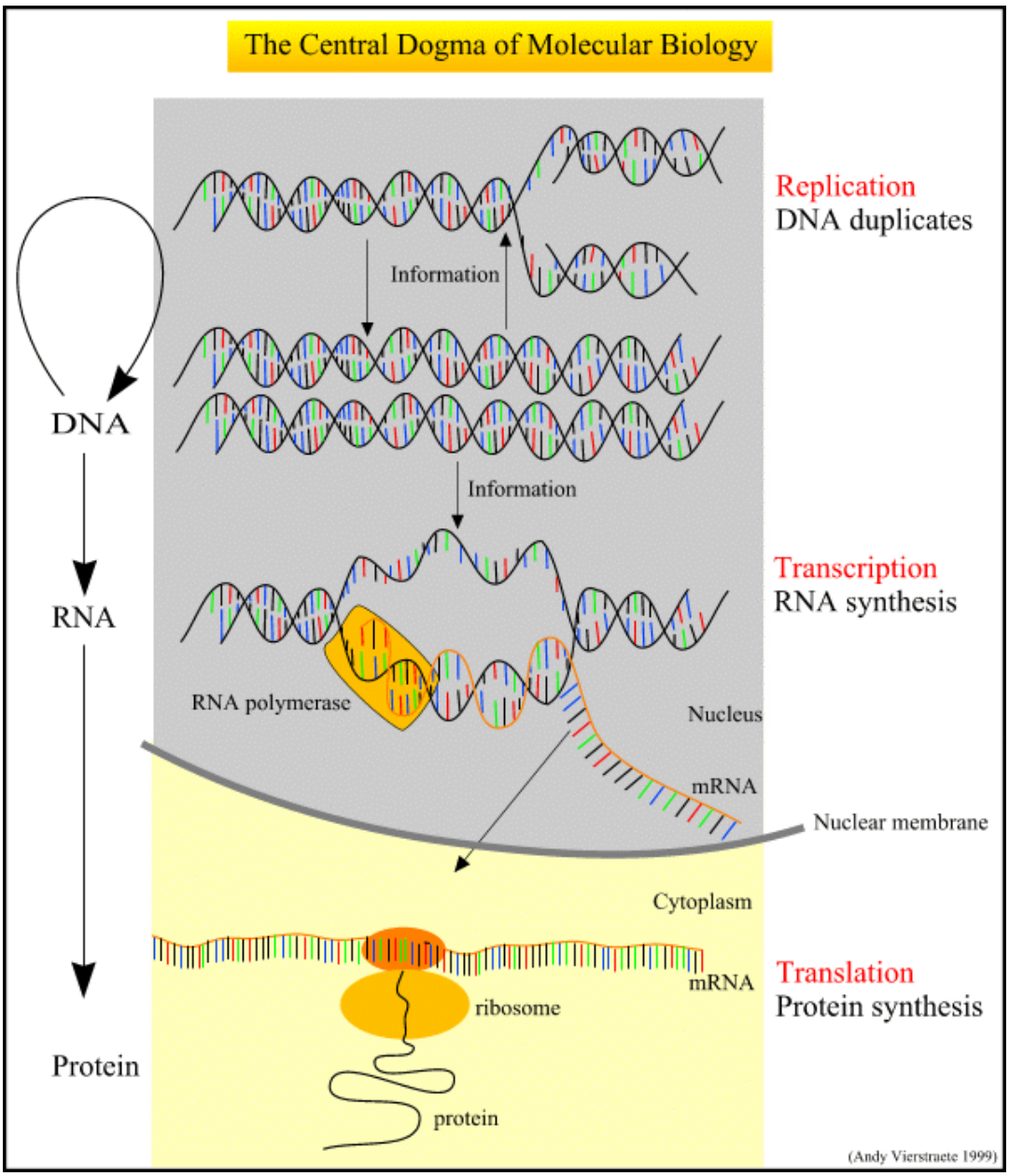

Figure 1-1 The Central dogma of molecular biology

(Adapted from http://users.ugent.be/~avierstr /principles/centraldogma.html)

about genetic information exclusively flowing from DNA to RNA at that time. (2) flow from RNA to protein where genomic information was stored in RNA instead of DNA. RNA viruses are good examples of this type of genetic information flow, such as Hepatitis C virus (42, 152). (3) Flow from RNA to RNA. RNA molecule's true power was long upstaged by its siblings DNA and protein until some double stranded RNA was found to quash gene expression in biological systems (81, 106). After 1990s, lots of RNA molecules, including small interfering RNA (siRNA), micro RNA (miRNA), small non-coding RNAs (sRNA), have been demonstrated as cellular regulators instead of just being drones. Generally, these RNA trigger gene silencing at the post-transcriptional level by virtue of their sequence complementary to their target mRNAs (106, 107). Biologist now believe that this RNA interference silencing is a genome immune system in host defense pathways against harmful foreign DNA or viruses (80). Recently small RNA molecules were demonstrated to be associated with epigenetic alterations of the genome, such as histone conformational modifications and DNA methylation (229, 262). (4) flow from protein to protein, prions are good examples: they propagate themselves by making conformational changes in other molecules of the same type of protein. This change affects the behavior of the biological organisms (4). In some organism, as fungi, this change can be passed from one generation to the next (282).

After the discovery of reverse transcriptase, Francis Crick modified his ideas about the central dogma (47) and accept the exceptions of genetic flow from RNA to DNA, from DNA directly to protein (the latter one has no examples yet). He also postulates that the information flow from protein to DNA,

RNA, or protein will never occur. Unfortunately, the discovery of prion demonstrated that the genetic flow from protein to protein does exist. Therefore, it is possible that other predicted impossible genetic flow by the central dogma may actually exist too. With all these exceptions to the central dogma, now the genetic information flow can be summarized as in Fig 1-2.

These exceptions to the central dogma demonstrated that there is no simple one to one interaction during the genetic flow in organisms. The linear information flow from DNA to RNA, and RNA to protein is proven to be an over-simplification. Other formalism of genetic flow, other than those associated with the Central Dogma, resulted in a more complex and various genetic regulations in biological systems. Therefore, it is easy to understand why organisms are functionalized through complicated crosstalk between pathways and environments instead of just simply hardwired in their genetic makeup. It is also no wonder why genetic mechanisms and regulations are tanglesome and intricate.

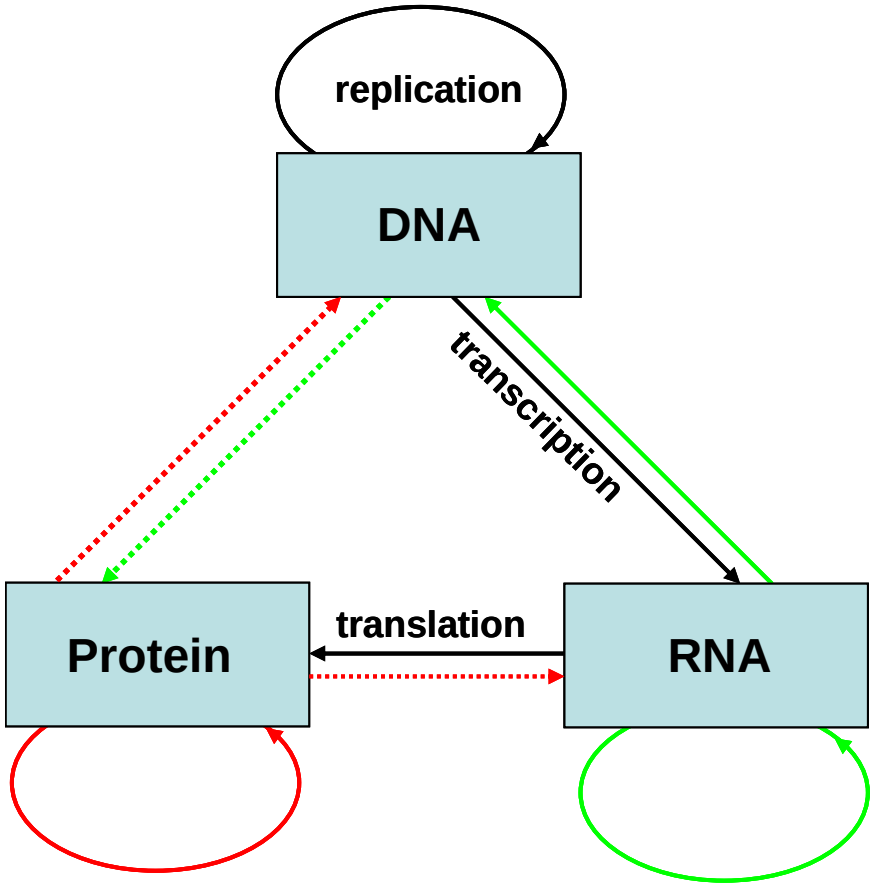

Figure 1-2 The genetic flow of molecular biology

The solid line represents validated genetic flow existing in life circuitry, while dashed line represents possible genetic flow. Black line represents existing genetic flow predicted by the Central Dogma, Green line represents possible existing genetic flow predicted by the Central Dogma, and Red line represents impossible existing genetic flow predicted by the Central Dogma

Genetic Regulatory Network (GRN)

As stated above, gene regulation in the life sciences is not a simple linear process but a complex nonlinear phenomenon. Usually the regulation of gene expression is achieved through various interactions between environmental stimuli and different types of genetic flow which form genetic regulatory systems or "circuits". For example, bacterial cell-to-cell communication involves extracellular events, such as the diffusion of a signaling molecule, which subsequently triggers intracellular events (signal transduction), such as the regulation of gene expression (transcription), which ultimately produces a communication system for the cell to act as a three-way coincidence detector in the regulation of a variety of genes, including those responsible for bioluminescence, type III secretion, and metalloprotease production (118). The Mitogen-activated Protein Kinase (MAPK) signaling cascades represent another example of natural genetic network: the transmission of extracellular stress, including growth factor signals (hormone, cytokines), into their final intracellular targets is mediated by a network of interacting proteins. This transmission will results in cell proliferation, differentiation, development, stress response, and apoptosis etc (231). Genetic regulatory network also controls functioning and development of organisms, for example, the *endo16* gene controls endomesoderm specification in the sea urchin embryo (51). In all these systems, the interactions between signal molecules and the target gene responses formed a cellular input-output device. The signaling molecule and its synthesis gene can be viewed as input while the trigged gene expression can be viewed as a primary output which in

turn, results in an ultimate output including cellular phenotype and function changes (Fig 1-3).

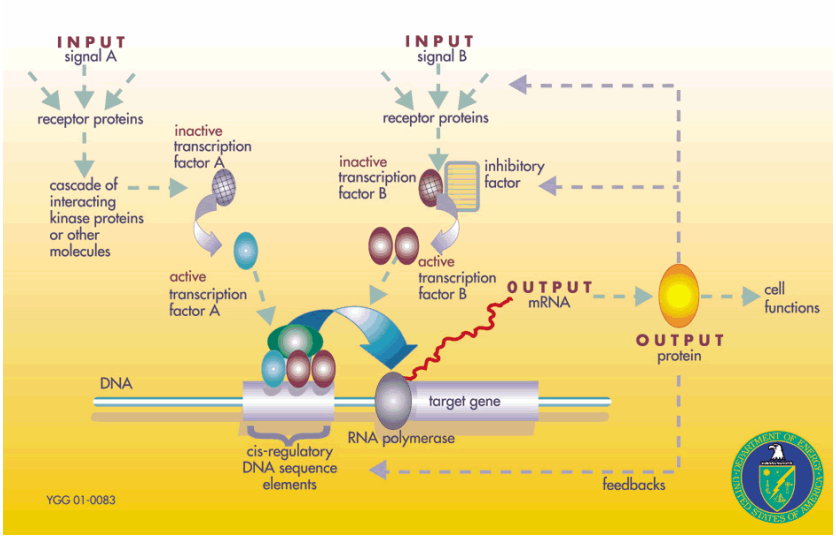

Figure 1-3 Genetic regulatory network as a cellular input-output device

(Adapted from U.S. Department of Energy Genomics:GTL Program, http://genomicsgtl.energy.gov)

A single organism generally includes an array of remarkably various interacting genetic regulatory networks that monitor environmental and intracellular parameters and affect cellular response to changes in these parameters. Therefore, organisms can be viewed like biochemical reaction systems constructed by different interacting components. Nevertheless, these biochemical systems are originated from interactions between molecular components such as genes, transcriptional factor, protein etc, where feedback is a ubiquitous control mechanism that probably help for

the genetic maintenance or adaptation to the environmental evolutions. For example, sequential feedback inhibition and activation in MAPK cascade resulted in an ultrasensitive response for mediating cellular processes such as mitogenesis, cell fate induction and oocyte maturation (125). In the case of *E. coli lac* operon, the mutual activation of inducer allolactose and its permease LacY led to discontinuous, multistable responses (156). Interlocked positive and negative feedbacks entail the bistability and switching dynamics in lysis/lysogeny genetic regulatory network of λ phage (269). Self-regulated negative feedback loop speeds up the response time of transcription networks (218). Recently, positive and negative feedback were demonstrated to affect the intrinsic and external noise at transcriptional and translational level (263). These feedback regulations and mediations generally lead to nonlinear dynamics and results in hierarchical interactions between GRNs. Therefore, life systems are highly complex in their organization and sometimes can exhibit a number of emergent properties including bistability and ultrasensitivity (8, 21).

Towards this end, these examples illustrate the interconnectivity that exists both within and across genetic circuits and how the synchronous organization of multiple genetic events consummates as a living physiochemical process. Gene expression in a cell is also stochastic in nature and can consist of various trajectories including oscillations. Even more challenging, it has been demonstrated that there is rarely a one-to-one relationship between individual gene and overall function (254). Instead, concomitant expression of multiple genes is likely responsible for altering phenotype. Therefore the majority of cellular functions stem from the coordinated activity of the products of multiple genes. This necessitates our focus shifting from

single parameter markers to multiple measurement patterns as descriptors of cellular behavior. A detailed understanding of the interconnectivity between genetic sequence and associated nonlinear cellular responses is necessary to effectively engineer phenotypes and pathways for improved performance.

Mathematical models of GRNs thus have been developed to study the nonlinear interactions and stochastic processes, to predict the dynamic profile, and eventually to modify the cellular behaviors. Various modeling techniques have been used, including "logical" ("binary approach"), "chemical kinetics" ("rate-equation") approach and "stochastic kinetics" approach. In logical approach, all elements are treated with either ON or OFF two discrete states, and describe how groups of interacted elements act to change other's states. Stuart Kauffman was among the first to utilizes this type of formalism to modeling GRN (97, 137). This abstract ON/OFF state makes it unbearable for including details of GRN. In rate equation approach, a set of ordinary differential equations (ODE) generally used to describe accumulation rate of products and consumption rate of reactants. This type of formalism can model nonlinear dynamics in GRN, which makes it a promising avenue for analyzing biological systems. However, ODE does not consider random noises or components associated with GRN, which makes it invalid for the nonlinear systems near chemical instable state, and impossible to capture the bifurcation sometimes (8). Stochastic kinetics modeling consider possible noise and fluctuations associated with GRN, therefore provide the most detailed description of the biochemical reaction system and can correctly differentiated distinct developmental pathways due to small fluctuations (8). However, this achievement is fulfilled at the expense of high

computational cost and lost in immediate analytical treatment (168). Generally, the models are validated by comparing the predicted qualitative behaviors with experimentally-measured profiles.

With these promising mathematical tools to analyze the mechanisms and dynamic profiles associated with GRN, the synthetic biology is now immerging as a promising platform to engineering desired genetic circuits and pathways. Lots of researchers already successfully redesigned the genetic pathways or reconstructed recombinant metabolic pathways for redirecting the genetic flow into needed directions (112, 298). With the beginning understanding of the genetic regulatory networks, the biology area shifts from traditional molecular-based reductionism approach, attempting to deduce the functions for each gene, to system biology, assisting to uncover the holistic picture of the biological systems. The system biology utilizes the combinatorial efforts of the mathematical modeling together with the high through output experiments.

Systems Biology

As stated above life circuitry not only contains the theory of Central Dogma but also involves hierarchy and complexity from entangled metabolic pathways and genetic modules which possess interconnected interactions between DNA, RNA, proteins and small molecules (200). New technologies, such as cDNA microarrays, and other "-omics" techniques, have inundated researchers with a deluge of data and information on genes, proteins, metabolites and stress responses to environmental stimuli. In order to provide useful information for genetic regulations and

mechanisms, these data need to be interpreted and structured to understand comprehensively about the architectures of genetic regulation. Furthermore, the holistic picture of how these biological networks interacting with each other and then ticking the whole organism still lacks. To accomplish these formidable tasks will, by necessity, incorporate mathematical modeling and automated strategies of all processes. In responses to the evolution of alterations of the central dogma and the advances of modern technologies, system biology now pushes to the forefront.

Systems biology, although no precise definition yet, most would agree it aims to understand the dynamics of the system theoretically, computationally, and experimentally in a concerted way through cooperation of math, computation and molecular biology (143)(Fig 1-4). That is, system biology is the combination of advanced mathematical simulations (either differential equation modeling of GRN or statistical analysis of high throughput data) together with the experimental manipulation, including high through output measurements such as cDNA microarray, proteomics etc as well as traditional molecular biology approach. Both components and the interactions between all components are essential for understanding behaviors at system level.

Therefore, we can overall understand where prediction, control, and design the biologic system is feasible. Systems biology has experimental aspects (such as the empirical side protemomics, metaboliomics, as "-omics") as well as modeling aspects, while theory connects these two parts. Within this context, (1) understanding of system structure, such as gene regulatory and biochemical networks, as well as physical structures, (2) understanding of dynamics of the system, both quantitative

and qualitative analysis as well as construction of theory/model with powerful prediction capability, (3) understanding of control methods of the system, and (4) understanding of design methods of the system, are key milestones for understanding the systems.

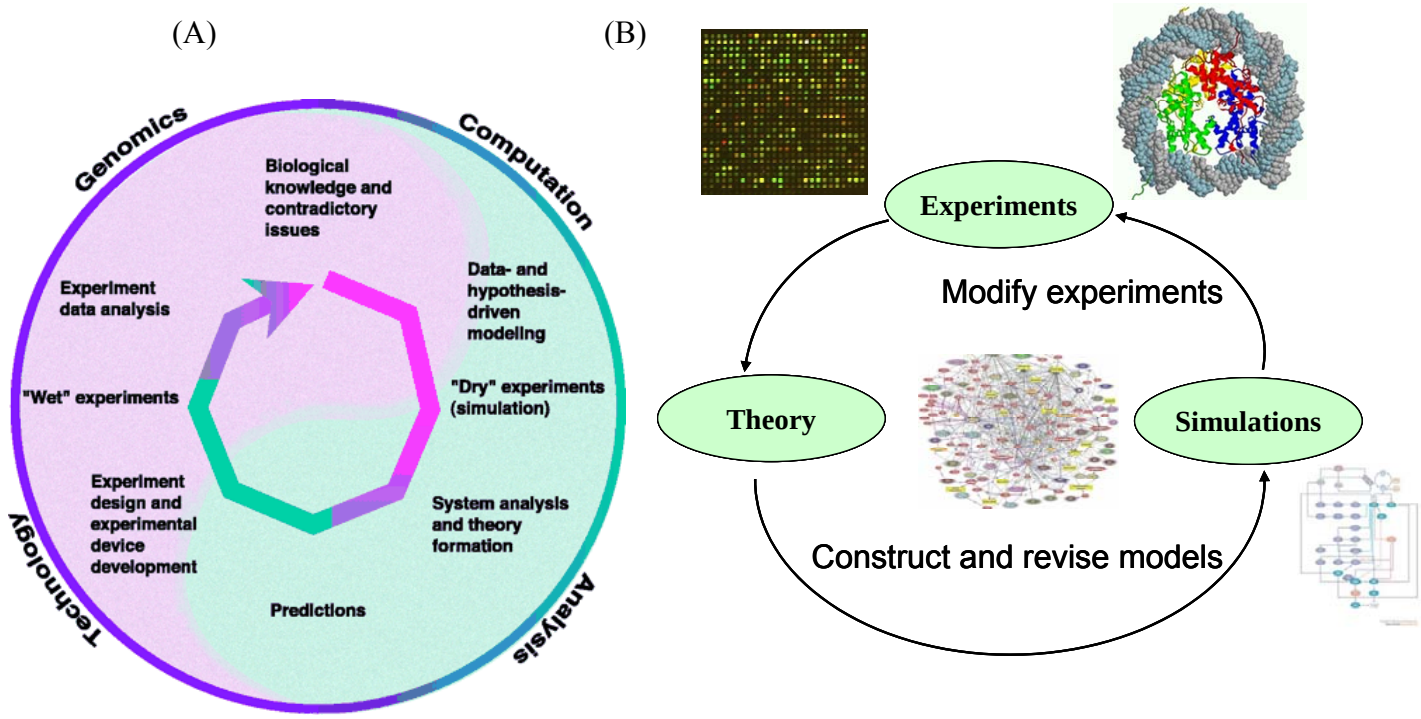

Figure 1-4 Approaches utilized by System Biology

((A) Adapted from Kianto, System Biology: a Brief review. *Science* (295):1662 – 1664, 2002, (B) The combining approach of Systems Biology)

There are two major areas in Systems biology: qualitative and quantitative Systems biology. Qualitative Systems biology includes the major following technology platform: (1) DNA microarrays, Serial Analysis of Gene Expression (SAGE) and Single Nucleotide Polymorphism (SNP) of single nucleotide variation (2) two dimensional gel electrophoresis and mass spectrometry for protein, (3) metabolomics for intracellular metabolite in different organisms. Systems biology modeling includes mathematical simulation of biological system based on available knowledge of GRN, and statistical analysis and map of multi-dimensional data from high throughput approaches. Generally, the experiments provides measurement and manipulation of the system while the modeling side is mining data and reverse engineering pathways from the experimental data (163, 172). It's the tight coupling between experimental biology and very sophisticated computational modeling methodologies that ultimately drives Systems biology.

Many researches have successfully utilized Systems biology approach and yield promising results. For examples, Hwang *et al* demonstrated two types of cardiomypathies existed between two distinct pathways by differential gene expression profiling (241). Dubba-Subramanva *et al*. found a novel pathway involving the expression of synthetase genes from DNA microarray analysisof alpocia areata patients (69). Li *et al*. reconstructed the triglyceride and urea synthesis pathways in a heptatocullar system by genetic algorithm and partial least square analysis (163). Another striking result originated from Systems biology approach is the emergence of synthetic biology, which integrate the cellular systems and reconstruct desired recombinant systems based on the system level understanding of

dynamics and the associated mechanisms (13). This propels advancement of functional biological circuits.

Systems biology has the potential to impact biological areas. For example, the Department of Energy just launched a Systems biology project called Genome to life for focusing on environmental cleanup and new energy sources.The impacts of Systems biology on the health care have also been proposed since diseases such as caner, diabetes, and HIV are found to be related to system behaviors associated with GRN and environmental stimuli. Cancer research has been focused for a long time on the molecular difference between normal cell and tumor cells. However, the picture is totally different because the tumor developmental processes associated with various interactions between numerous macromolecules and environmental cues which formed hierarchical GRN (123). For type 2 diabetes, the systematic, multi-factorial character makes its treatment very difficult even though intense researches have been conducted (84, 134). Therefore, pharmaceutical companies are now shifting from "one gene-one enzyme-one drug" approach to "systematic network based rational drug" design, to derive more effective and safer drugs for the right patient groups. The introduction of personalized drugs and the development of novel therapeutics are conjectured and may become reality as a small number of biotechnology companies have started using this systems biology driven approach. For example, last year Roche and the Competence Center for Systems Physiology and Metabolic Diseases (CC-SPMD) of SystemsX (in Sweden) started a joint research project to identify novel pathways for drug development in diabetes as well as new biomarkers of beta cell failure for diagnostics through system biology approaches

(http://www.innovations-report.de/html/berichte/biowissenschaften_chemie/bericht-52932.html). However, the correct predictions rely upon our ability to understand and quantify the roles that specific genes possess in the context of human and pathogen physiologies. Undoubtedly, the power of mathematical modeling and prediction with the combining effect of experimental techniques will help researchers to ultimately find the prerequisite knowledge and amazing tools. Mathematical models have also been started to integrate heterogeneous pre-clinical and clinical data to reveal new information about known molecular pathways, to discover new pathways and to predict clinical performance of compounds with a high degree of accuracy, which in turn will increase the clinical trial success rates and advancing overall R&D productivity of efficient drug design. Millions of these "in silico" experiments are run on computers in a fraction of time and expense it would take to test similar predictions in a wet lab. Gene Network Science Inc is one of good example for running the modeling system biology approach (http://www.genenetworksciences.com/). Then based on these initial predictions, probable candidates will go through further experimental tests and screening. All in all, the combining mathematical simulations and carefully designed approach will lead to experiments more effective drugs and more rational health treatment in our daily life.

Even though Systems biology is in its infancy, there are numbers of exciting and profound issues that are actively investigated in systems biology, such as robustness of biological systems, network structures and dynamics, and applications to drug discovery. With the development of accumulation in-depth knowledge of

molecular nature of biological systems, we believe systems biology going to be the main stream in biological sciences in this century.

Quorum Sensing Systems

Quorum sensing is the ability of bacteria to communicate and coordinate behaviors via signaling molecules. Specifically, bacteria produce and release some small chemical molecules into the environment as the cell population-density increases. When a threshold stimulatory level of signals (also called autoinducers) is achieved, it can be detected and a signal transduction cascade is initiated that ultimately results in a change in the social behavior of the bacteria. This process is accomplished via cooperative function of the colony through self-organization of hierarchical spatial-temporal patterning. The communications and coordination between bacteria provide the degree of plasticity and flexibility required for better colonial adaptability and endurability in a dynamic environment, where they can modify the environment and obtain environmental information for further self-improvement.

The first organisms in which quorum sensing was observed were Myxobacteria and Streptomyces species. However, the most popular example is *Vibrio fischeri* (http://en.wikipedia.org/wiki/Quorum_sensing). Most of the bacteria thus far identified that utilize cell-to-cell communication (i.e. quorum-sensing systems) are associated in some way with plant or animal hosts. The nature of these relationships can be amicable, as characterized by symbiotic bacteria, or adversarial, as seen with pathogenic bacteria (196, 219, 247). A most popular example of the

symbiotic relationship is the regulation of light production in *V. fischeri*, a marine luminous bacterium that lives as a symbiont in the light organ of *Euprymna scolopes* (a Hawaiian bobtail squid) (219). When *V. fischeri* cells are free-living, the autoinducer is at low concentration and thus cells do not emit bioluminescence. When they are in the light organ of the squid, they are highly concentrated (about 10^{11} cells/ml) and the transcription of luciferase is induced, leading to bioluminescence emission. An adversarial example is that Enterohemorrhagic *Escherichia coli* (EHEC) uses a hormone epinephrine signal (AI-3) to "sense" that it is within the intestine and activate expression of its virulence genes essential for intestinal colonization (247). Another adversarial example is a highly virulent *Enterococcus faecalis* strain which secret cytolysin to sense and lysis target cells: *E. faecalis* actively secretes two components of cytolysin (a virulence factor), an autoinducer and an anti-autoinducer. The anti-autoinducer is a toxin component and effectively tags the target for destruction. In the absence of target cells, these two interact and prevent the autoinducer from inducing high-level expression of the cytolysin. In the presence of the target cell, however, the anti-autoinducer binds to the target cell and allows the autoinducer to accumulate to a threshold level required for quorum induction of the cytolysin operon (43).

Gram-negative LuxI/LuxR system

There are several types quorum-sensing regulated systems elucidated since 1970s. The most widely studies quorum sensing system is the *V. fischeri* LuxI /LuxR system, which existed in more than 70 species of Gram-negative bacteria. In general, a freely diffusible Acyl-homoserine lactone (AHL) is used as quorum sensing signal.

These molecules share a common homoserine lactone moiety with difference in the length and oxidation state of the acyl side-chain (176). In this type of quorum sensing, bacteria utilize LuxI-type protein to synthesize AHL molecule and use LuxR-type protein as receptor to bind autoinducer for triggering target gene expression (89). For example, in *Vibrio fischeri*, at low cell density, the concentration of AHL is low, *luxICDABEG* is transcribed at a basal level, and therefore only a low level of light is emitted. As population of the bacterium increases, autoinducer AHL accumulates in the growth medium and inside the cells. When it reaches a threshold concentration, this molecule interacts with receptor protein LuxR to form a positive transcriptional complex, which then significantly stimulates transcription of the *luxICDABEG* operon (Fig 1-5). This results in the emission of bioluminescence and in the positive autoregulation of *luxI*. The transcriptional complex of the LuxR-AHL also negatively regulates the expression of *luxR* itself, which reduces transcription of the *luxICDABEG* operon in a feedback loop.

LuxR is a 250-amino acid polypeptide (135) that requires the presence of the GroESL molecular chaperones to enable folding into an active form (2, 3). Indeed, the instability of LuxR resulted from the absence of these chaperones may render its activity (3). LuxR does not contain a membrane-spanning domain but it localizes to the cytoplasmic face of the inner membrane, which does not subject to the influence of autoinducer (146).

Genetic analysis of LuxR suggests that it is composed of two functional domains: an amino-terminal domain with an AHL binding region and a carboxy-terminal transcription regulation domain, which includes a helix-turn-helix DNA

binding motif (240). The DNA-binding domains share sequence similarity with a LuxR or FixJ superfamily (133). Amino-terminal deletion of LuxR polypeptides shows an AHL-independent activation of *lux* genes, which suggest that the amino-terminal of LuxR protein blocks the function of the DNA-binding domain in the absence of AHL. The interaction with the AHL molecules abolishes this inhibition and allows transcriptional activation of target gene (41). The carboxy-terminal are important in multimerization of LuxR that plays a role in transcriptional activation (251-253). In the autoinduction of the *lux* operon, LuxR is considered to bind a 20 base pair inverted repeat, known as the *lux* box (63). Similar binding sequences as *lux* box are found upstream of some LuxR-type proteins regulated promoters in other bacteria (88, 220).

The LuxR-type proteins contain relatively conserved sequence in their DNA binding domains, probably due to the specificity in gene regulation associated with the unique structures of the AHL signals. Amino acid sequence alignments of LuxR with its homologues reveal them to be surprisingly disparate in terms of sequence identity (18–25%). Only five residues are completely conserved in all of the LuxR homologues for which sequence data are currently available (89). In addition to the role in activating gene expression, there are studies suggesting that some LuxR homologues such as EsaR, YenR, and ExpR, appear to act as repressors, and binding by the autoinducers inhibits their functions (89, 179).

In 1996, two separate groups demonstrated that LuxI type protein can synthesize homoserine lactone from probable substrate (182, 226). The eventual elucidation of AHL molecules revealed that S-adenosylmethionine (SAM) provides

the main amino acid substrate during AHL synthesis while the acyl carrier protein (ACP) are the most likely donors for the fatty acid side chain of AHL (73, 280). Based on these, a model of how LuxI type protein sequentially acts on SAM and acylated ACP to produce AHL molecules were proposed: SAM binds to the active site of LuxI type enzyme and the appropriate acyl group is transferred to this complex from a charged ACP. Then the acyl group forms an amide bond with the amino group of SAM. Subsequent lactonisation results in the synthesis of the acyl HSL and the by-product, 5′-methylthioadenosine (MTA) (198, 226).

Some synthase/receptor system other than LuxI/LuxR family existed. LuxM in *Vibrio harveyi* and Ains in *Vibrio fischeri*, are a second family of AHL synthases (15, 108). Due to the diversity of the AHL molecules, the LuxR-type proteins contain relatively conserved sequence in their DNA binding domains, only about 18-25% identity between LuxR homologues (89). Therefore, sequence analysis of the LuxR homologues does not offer any clues as to which acyl HSL is preferentially bound by each protein(74). Unfortunately, one cannot predict which acyl HSL(s) will be synthesised by different LuxI homologues through comparative sequence analysis either. The type of acyl HSL produced by a particular species can be strain-dependent. This may reflect the differing habitats in which individual strains reside and probably explains the diverse activities controlled by this type of quorum sensing. For example, AHLs have been shown to play an important role in the establishment and course of bacterial infections (56, 138).

Small Peptide Mediated Quorum Sensing

In contrast to *V. fisheri* system, Gram-positive bacteria generally use a secreted autoinducing peptide (AIP) for controlling quorum sensing behaviors. This system was first described in *Lactococcus lactis* and *Streptococcus pneumonia* (114, 151). Subsequently, this AIP mediated quorum sensing behavior was found in many species, including *Bacillus subtilis*, *Staphylococcus aureus Enterococcus faecalis* (153, 183, 270). AIP are ribosomally synthesized as precursor peptides and exported by a dedicated ATP-binding cassette (ABC) transporter. The AIPs are sensed by the transmembrane receptor component of a two-component signal transduction module (TCS), consisting of a membrane-located receptor protein histidine protein kinase and an intracellular response regulator (100, 145, 194). This two-component system relay sensory information by phosphorylation/dephosphorylation cascades, where a membrane-bound sensor kinase protein initiates information transfer by autophosphorylation, and a response regulator protein typically controls transcription of downstream target genes (145, 176). A general scheme for Gram-positive quorum sensing is shown in Fig. 1-6.

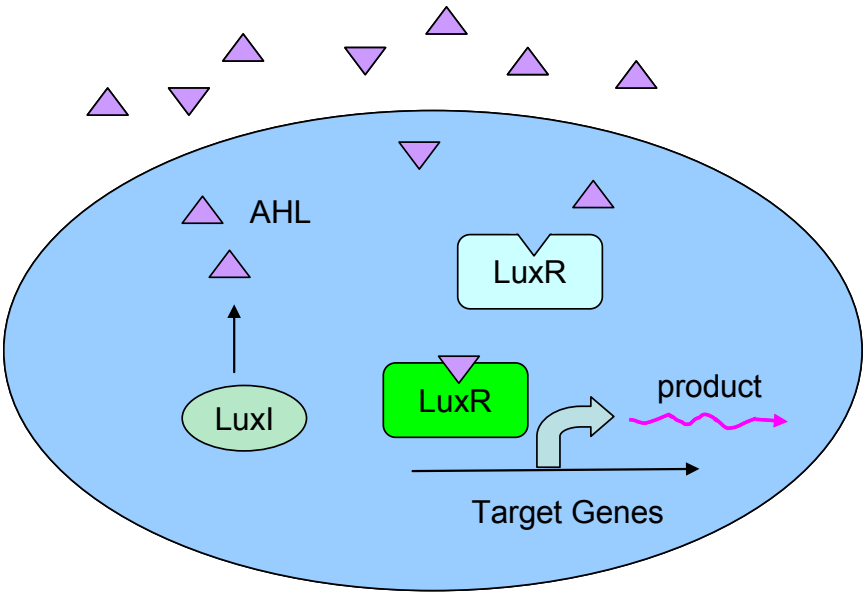

Figure 1-5 LuxR-type quorum sensing in Gram-negative bacteria

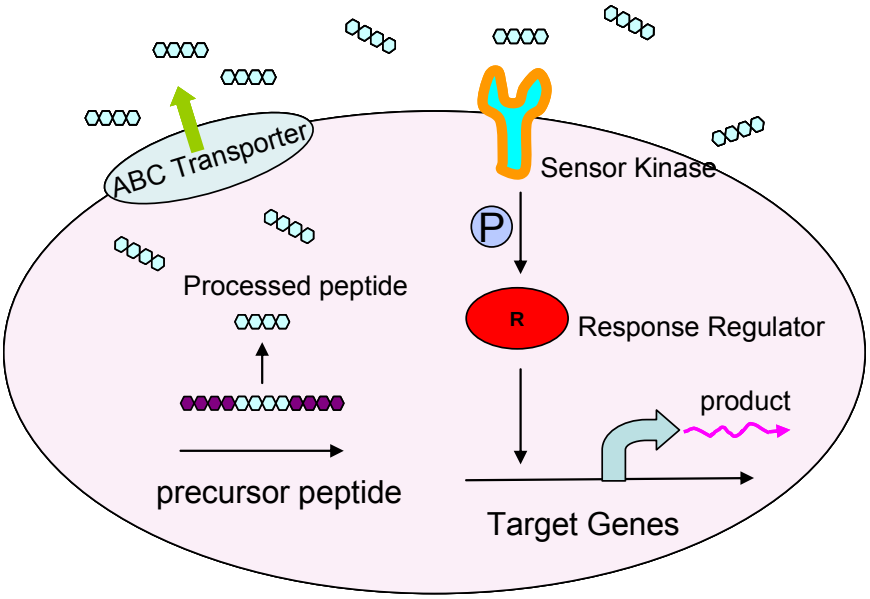

Figure 1-6 Quorum sensing in Gram-positive bacteria

The AIPs show a variety of structures but share a small size, are ribosomally synthesized, and are some cases subject to posttranslational modifications that add to their functionality and stability. The regulatory genes involved in these AIP mediated quorum sensing show high genetic polymorphism among species and strains. The highest sequence diversity is in the N-terminal and linker part of the receptor histidine kinase, and in the autoinducing peptide and peptide-processing genes. Diversity and specificity has been well studied for the *agr*-system in *S. aureus* (71, 129), and the competent system in *B. subtilis* (270) and *Streptococcus spp* (115). For these systems, the induction activity of each AIP appeared to be specific toward its cognate receptor, indicating the existence of distinct phenotypes.

The LuxS/AI-2 system

The only quorum-sensing system shared by both Gram-positive and Gram-negative bacteria involves the biosynthesis of autoinducer-2 (AI-2) catalyzed by LuxS. Indeed, database searches revealed the presence of a *luxS* homolog in many Gram-negative and Gram-positive bacterial species (259, 292). LuxS is conserved among ~50% of the sequenced bacteria (256, 285, 287). Therefore, AI-2 is suggested as a language for interspecies communication (292). This quorum sensing system has been intensively studied in the past decade, mostly in relation to the AI-2 molecule and the downstream effects of *luxS* knockouts. Phenotypes associated with LuxS/AI-2, such as bioluminescence, regulation of virulence factors and biofilm formation, have been described (197, 272, 292).

Although LuxS was identified in 1999 (259), in fact it had already been described in the 1960s as the S-ribosylhomocysteine (SRH) cleavage enzyme (160,

174). AI-2 is produced from S-adenosylmethionine (SAM), a methyl donor for cellular processes, in at least three enzymatic steps (227). Consumption of SAM produces S-adenosylhomocysteine (SAH), which is subsequently detoxified by the nucleosidase Pfs to yield adenine and S-ribosylhomocysteine (SRH). SRH is converted to 4,5-dihydroxy-2,3-pentanedione (DPD) and homocysteine. This reaction is catalyzed by LuxS (160). DPD spontaneously rearranges into AI-2 (227). LuxS plays an important function in the activated methyl cycle of the cell because it is necessary for recycling of the toxic intermediate (285). Except for some symbionts and parasites, all organisms have a pathway to recycle SAH, either using a two-step enzymatic conversion by the Pfs and LuxS enzymes to produce adenine, homocysteine and DPD, or a one-step conversion using SAH hydrolase (SahH) (287). No AI-2 is produced through the SAH-hydrolase pathway (256, 287).

More than 55 bacterial species have a *luxS* homolog, but only two AI-2 structures have been elucidated: a furanosyl borate diester (3A-methyl-5,6-dihydro-furo(2,3-D) (1,3,2)dioxaborole-2,2,6,6A-tetraol; S-THMF-borate) in *V. harveyi* and (2R,4S)-2-methyl-2,3,3,4-tetrahydroxy-tetrahydrofuran (R-THMF), which lacks boron, in *Salmonella. typhimurium* (39, 178). The

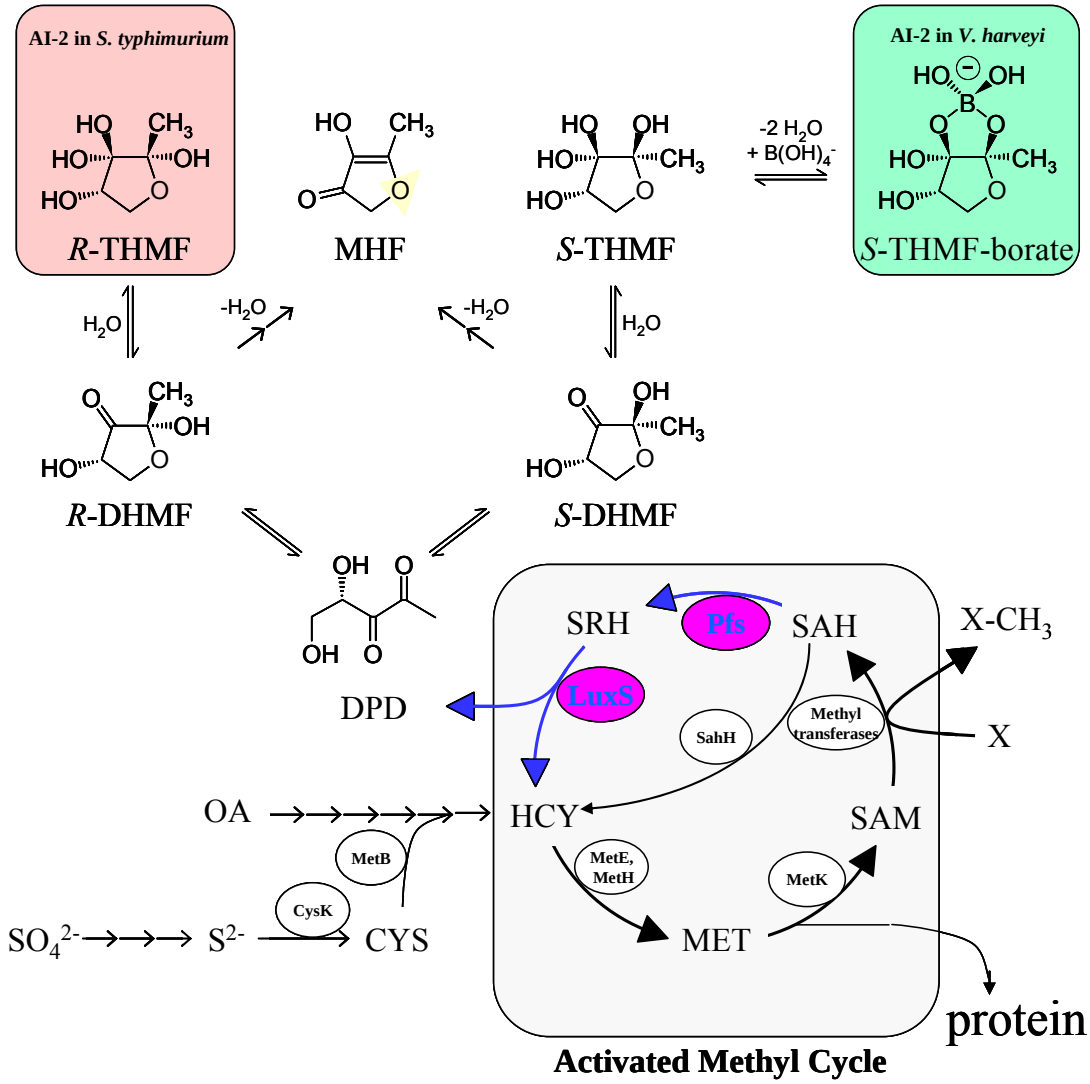

Figure 1-7 LuxS catalyzed AI-2 biosynthesis pathway and related equilirium of different AI-2 molecules

molecules DPD, R-THMF and S-THMF-borate are in equilibrium with one another (Fig 1-7). However, "pure" DPD has never reported as existing other than mixture or equilibrium with its anomers (55, 171). Niether pure AI-2 structure has been elucidated without its cognate receptor (39, 178) 'AI-2', therefore, is actually a collective term for DPD-derived and interconvertible molecules that can promote cross-communication (291). Other un-identified AI-2 molecules existed in other bacteria has been assumed as R-THMF or S-THMF-borate, or similar molecules derived from DPD. Furthermore, only a few cases with direct cell–cell signaling processes related to LuxS have actually been demonstrated (for recent review, see (272)), for example, in *Vibrio* species (177). Further work still need to determine if LuxS does actually influence intercellular signaling. More knowledge about the structures of different members in the AI-2 molecule family will help us gain the specific role of the molecule.

Until now, among most of the studies associated with LuxS/AI-2 system, few have focused on the *luxS* gene and protein activity itself. However, LuxS is also an integral component of the activated methyl cycle in bacteria. Ongoing attempts to dissect the metabolic and signaling roles of LuxS leave little doubt that unraveling the regulation of *luxS* expression and cellular LuxS activity is the key to understanding LuxS-based quorum sensing (54).

LuxS is a small metalloenzyme (±170 amino acids) with two identical active sites that are formed at the dimer interface by residues from both subunits (120, 160, 210). Sequence alignment reveals an invariant His-Xaa-Xaa-Glu-His motif, which is important in the catalytic activity of LuxS (302). However, only a few regulatory

elements of *luxS* have been described across all of the species examined and no direct binding of regulatory proteins to the promoter region of *luxS* has been shown. For example, in *E. coli* AI-2 synthesis is subject to catabolite repression through the cAMP–CRP complexs' indirect repression on *luxS* transcription, where the cAMP–CRP complex does not bind to the *luxS* promoter (276). The effect of glucose on *luxS* transcription is reflected in the LuxS protein level (109). In *S. typhimurium*, transcription and translation of *luxS* is reported to be constant through all phases of growth and AI-2 production is tightly correlated to *pfs* transcription (18).These results suggest that AI-2 production is regulated at the level of LuxS substrate (SRH) availability, and that AI-2-dependent signaling in *S. typhimurium* is a reflection of the metabolic state of the cell and not of cell density (18). We have also shown that AI-2 communicates with the metabolic state of cells when cells are transformed with expression vectors for the synthesis of recombinant proteins (Insert DeLisa Paper). Also, in *Streptococcus bovis*, *luxS* transcription is not directly related to AI-2 production. However, in contrast to the *S. typhimurium luxS*, *S. bovis luxS* expression is not constitutive but is linked to the availability of glucose in the medium and the growth rate of the cells (9).

Multi-Channel Quorum sensing systems

It was not new that several quorum sensing signal systems coexisted in one bacterium. For example, *V. harveyi* possesses three parallel quorum sensing systems to control gene expressions (118) (Fig 1-8):an AI-1 system, where a AI-1 synthase LuxML produces a 4-hydroxyl C4 homoserince lactone molecular and that is detected via its cognate sensor LuxN (15, 35); an AI-2 system, where a 3A-methyl-5,6-

dihydro-furo(2,3-D)(1,3,2)dioxaborole-2,2,6,6A-tetraol synthesized by *luxS* gene and perceived by LuxPQ complex sensor, a CAI-1 system, where a CAI molecule is produced by CsqA and recognized by CsqS. Among these communications system, AI-1 system is an intra-species communications system, AI-2 is a highly conserved inter species communication system, and CAI-1 system is also an inter species communication system but not widely spread out like AI-2 system (14, 118, 259). All three systems work in tandem to regulate a variety of genes including bioluminescence, type III virulence factor and metalloprotease (VhpA) production. Simultaneous presence or absence of three signals imposes maximal effect on gene expression and each signal needs a different critical concentration to trigger gene expression. For example, when cells grow on agar surface, the buildup of the critical concentrations of the autoinducers required to switch their cognate sensors from kinase mode to phosphatase mode occurs in the following order: CAI-1, then HAI-1, then AI-2 (118).

Similarly, there are three different quorum-sensing systems exist in *V. cholerae*: the CAI-1-CqsS system and the AI-2-LuxPQ system, and an unidentified third circuit (System 3) that acts through LuxO. The mechanistic model of *V. cholerae* mirrors that of *V. harveyi*, and orthologs of quorum sensing AI-2 system with receptor LuxPQ and downstream cascade LuxO, LuxU, small RNAs repressor and LuxR (HapR in *V. cholerae*) (177, 178, 303). The CAI-1 mediated quorum sensing system in *V. cholerae* similar to that one in *V. harveyi* but *V. cholerae* does not have a similar AI-1 sensing system like *V. harveyi* (118). The putative system 3

acts in tandem with LuxO and HapR to control virulence gene but signal probably is not an extracellular one (177).

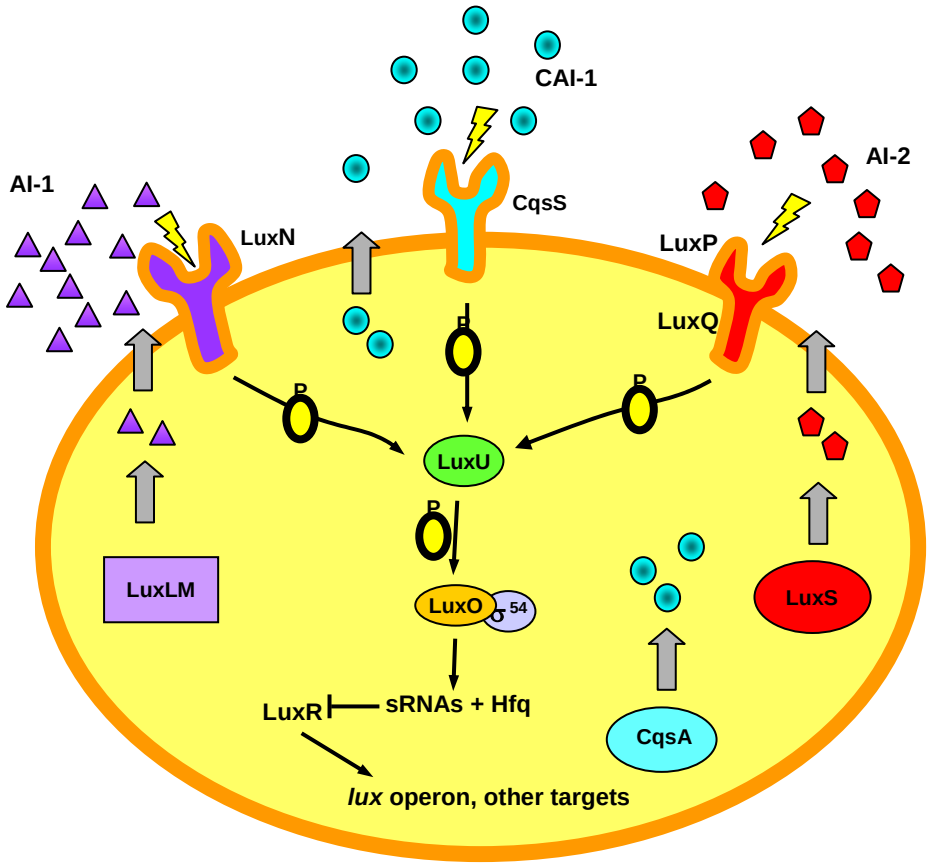

Figure 1-8 Three parallel quorum sensing systems in *V. harveyi*
(Adapted from Liang Wang' Dissertation, 2004, UMCP)

Several multi-channeled hybrid quorum sensing systems, including a hybrid two-component-type sensors that respond to two types of signals, 3-hydroxy-C4-homoserine lactone and AI-2, exist in all different types of *Vibrio* organisms, such as *V. cholerae, V. vulnificus, V. parahaemolyticus, V. anguillarum* and *V. fischeri*. LuxO homologues from *V. harveyi*, *V. cholerae* and *V. fischeri* have been shown to negatively regulate the expression of their respective transcriptional activators *luxR*, *hapR* and *litR* (180, 303). LuxO homologues are demonstrated to work via activation of small RNAs together with Hfq protein (159). This mechanism is suggested to be a general regulatory mechanism in *Vibrios* (180, 211).

Stochastic Petri Network Simulations

Modeling can sharpen our understanding of fundamental processes, provide a guide for training exercise and scenario development, guide risk assessment, aid forensic analysis, predict future trends. When experimentation or field trials are often prohibitively expensive or unethical or impossible, or no real data is available, mathematical model becomes an important experimental and analytical tool for summarizing data, exploring hidden mechanisms, and providing reasonable predictions. Components of biochemical network systems are sufficiently numerous and their interactions are complicated and that intuition alone is insufficient to fully understand the dynamics of such systems (53, 57).

Due to the complexities of living systems, many attempts have been made to simulate important cellular processes, genetic interactions and phenotypic variation in bacterial and viral systems (8, 23, 168, 190, 250, 289). Mathematical modeling and simulation of signal transduction mechanisms (150, 223), genetic regulatory

mechanisms and carbohydrate uptake in certain metabolic pathways (22, 149) have also been active area of research. These modeling use formal methods to describe the regulatory system unambiguously and predict behaviors in a systematic way. The resulted elucidation of the hidden mechanisms and interactions about the biochemical networks lead to the emergence of engineering of synthetic genetic circuits, including genetic toggle switch, intracellular oscillators, autogenous and nonautogenous response genetic network (17, 33, 91, 290).

Different types of formalisms have been used in modeling biological systems (53, 228). Petri nets, originated from a mature theoretical background, are a graphical-oriented modeling formalism, analyzing and simulating discrete events with inherent concurrency (165, 201). Its first application in biochemical pathways was carried out by Reddy *et al.*, in 1993, wherein Petri nets were used to qualitatively simulate biochemical pathways (213). In recent years there are numerous examples for analysis both quantitatively and qualitatively by Petri Nets in molecular biological system (a detailed review see (110)).

The importance of stochastic simulations of gene expression systems was stressed by Berg and Gillespie (20, 95) and more recently by others (46, 75, 141, 236). When reactions take place far from equilibrium (102, 131), their reactions rates generally depend on metabolite concentrations and sometimes involve very small molecule numbers (101). Such features motivate mesoscopic approaches where intracellular stochastic characteristics and fluctuation are considered (72).

The stochastic approach for a reaction system generally employs a single differential-difference equation (the “master equation”) to describe the time evolution

of the system as a random-walk process (170). This equation generally intractable to solve, therefore Gillespie proposed a systematic computational method to solve this master equation and validated its capability in different types of chemical reaction systems, which is now called as Gillespie algorithm. Specifically, a rigorously derived Monte Carlo technique called "inversion method" was employed to generate random numbers for describing the inherent fluctuations of the chemical reaction system. Therefore, the probability of what reaction will occur at what time is determined through the reaction probability density function thus the random walk process that the master equation describes analytically is efficiently simulated (95, 96).

Stochastic Petri Nets (SPN), a mathematical formalism developed in computer science, derived from the combination of stochastic simulation and Petri net theory, and has been a popular simulation tool (8, 99, 249, 250). A stochastic Petri net consists of places, tokens, transitions, input gates and output gates, connected by arcs. Fig 1-9 gives an example of the graphical representation of Petri nets. Places (species) are denoted by circles, tokens (markings) are denoted by dots, transitions (activities) are denoted by thin bars or rectangles, input gates denoted by triangles with their points connected to the transitions they control, output gates denoted by triangles with their base connected to a transition and arcs denoted by arrows.

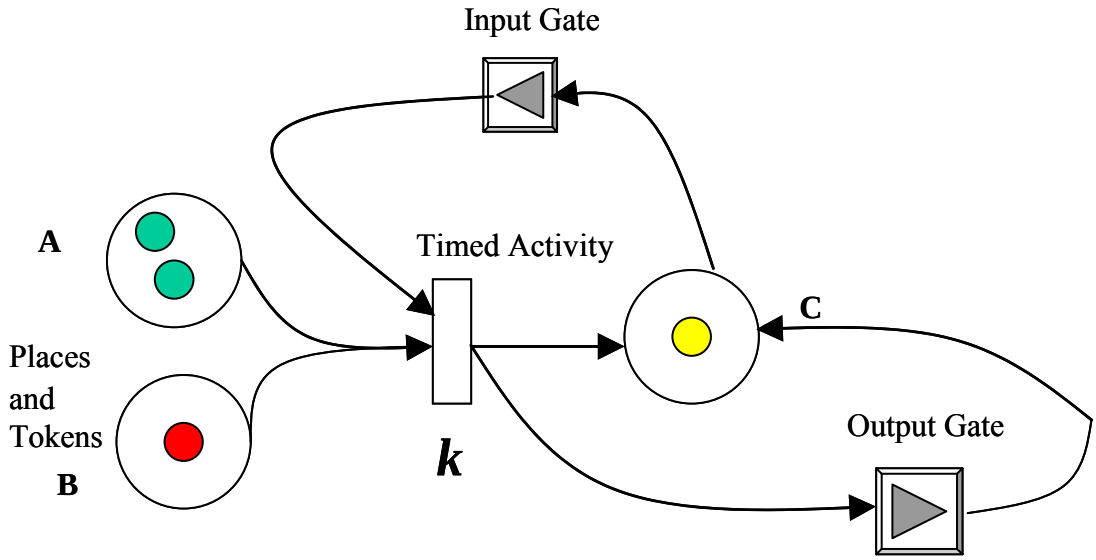

Figure 1-9 An example of SPN

The tokens represent the chemical species; the transitions represent chemical reactions. The transitions can be divided into instantaneous transitions and timed transitions. The former one fires immediately, the later one fires with a certain delay. A transition is said to be enabled when the required minimum token (one if the reaction is first order) is present in the input place connect to them. When an enabled

transition fires (executes), reactant molecules are consumed, that is, tokens removed from the input place, product molecules formed, that is, tokens added to output place. The rate of a reaction is represented by a weight function associated with the transition. Input gates control the enabling of the activities and define marking changes when activities are completed. Output gates define marking changes that will occur when activities complete.

The Gillespie algorithm is applied in SPN simulations. Specifically, in SPN, the occurrence of any reaction is determined by a weighted negative exponentially distribution function, with the weighting of the function is determined by rate constant and the number of tokens. If the system has $X_1, \cdots X_N$ molecules and there are $1, \cdots, M$ reactions, the function is illustrated in equation 1-1 (95):

$$P(\tau, \mu) = a_\mu \exp(-a_0 \tau) \text{ (if } 0 \le \tau < \infty \text{ and } \mu = 1, \cdots, M \text{)} \quad (1\text{-}1)$$

Where $a_\mu = \beta_\mu \times h_\mu$ and $a_0 = \sum_{v=1}^{M} a_v$, β_μ is the stochastic rate constant, h_μ is the number of molecular reactant combinations in reaction μ. If more than one potential reaction can occur, the time when each reaction will occur is determined randomly from this probability density function. The simulation is terminated when a predetermined criterion is met.

If there is only a first order reaction in the system, say $A \xrightarrow{\beta} B$, number of A molecules is X_A, the probability density function can be simplified as equation 1-2:

$$f(t) = X_A \beta \exp(-X_A \beta \times t) \quad (1\text{-}2)$$

From equation 1-2, we can know that the mean delay of a first order reaction is $1/X_A\beta$, which means in the presence of more molecules and larger rate constants, the resultant mean delay is shorter.

The stochastic rate constant is related to the deterministic rate constant (76): as the number of molecules tends to infinity, the stochastic rate of a reaction is equal to the deterministic kinetic rate (154). For monomolecular reaction (first order reaction) of the form

$$A \xrightarrow{k} B \tag{1-3}$$

Where k is the deterministic rate constant, the stochastic rate constants β are equal to deterministic rate constants k. When the order of the reaction is larger than one, the relationship of the stochastic rate constant to the deterministic rate constant is determined by the volume of the reaction system and the numbers of each reactant required for the reaction (76, 154). For example, for a second order reaction like

$$A + B \xrightarrow{k} C \tag{1-4}$$

The stochastic rate constant is:

$$\beta = \frac{k}{VN_A} \tag{1-5}$$

Where k is the deterministic rate constant, V is the cell volume, N_A is Avogadro's number (96, 99).

There are quite a few biochemical systems are modeled successfully by SPN. For example, the σ^{32} stress-circuit regulatory network was successfully modeled (249). The model transiently analyzed ethanol shock and compared this with experimental data, predicting σ^{32} distribution in the regulatory pathway and how it responded to the overexpression of recombinant proteins. The simulation results were validated against experimental results.

Research Motivation

The study of quorum sensing has attracted lots of intentions for quorum-quenching bacterial infection (64, 65), quorum sensing drive recombinant protein production (185) and programmed cell death (298). As stated above, the LuxS/AI-2 mediated quorum sensing system is widely spread and involved in lots of important activities such as virulence factor expression (178, 192), antibiotics synthesis (62), biofilm formation (207) and recombinant protein production (60).

First, we were fascinated by the dramatic increase of AI-2 signal activity when cells grow in the presence of glucose. Even though it was attributed to the repression of AI-2 uptake transporter (277, 293), but there is no direct validation yet. It is also interesting that cells utilize a delicate feedback transport system to import AI-2 signal back inside the cell via the regulation of AI-2 uptake repressor LsrR and its cognate kinase LsrK. This system is like the MAPK transduction cascade in eukaryotic system, where extracellular signals including hormones or cytokines transmitted intracellular through continuous processing and eventually results in the cell proliferation and differentiation etc. Therefore, lots of questions arise: what genotype and phenotype are controlled by this delicate uptake regulatory system and

its regulators? What other genetic regulatory network are interacting with this uptake systems? Or what other regulators are mediating this auto-inducible uptake processes? Is this network just one phosphorylation process imbedded among lots of sequential phosphorylation signal transduction network? Answering these questions undoubtedly will help us understanding this auto-inducible system and help improve the performance of its utilization. The elucidation of the mechanisms will also provide valuable information about quorum sensing for other similar organism such as *S. typhimurim*.

In the first part of this study, we constructed a stochastic model based on partially elucidated AI-2 synthesis and uptake pathways to simulate the apparently increased AI-2 level with the presence of glucose in culture medium. In the second part of this study, we constructed lacZ transcriptional reporters to investigate the transcriptional regulations associated with quorum sensing repressor LsrR, kinase LsrK. We also utilized the genomic DNA microarray to investigate the genes regulated by the quorum sensing regulators. The stochastic simulations discovered the existence of a glucose related alternative AI-2 synthesis pathway. Further transcriptional analysis revealed that quorum sensing repressor *lsrR* cooperates with AI-2 molecule to fulfill its signaling function, and that uptake kinase LsrK deactivate AI-2 signal's function through phosphorylaton of signaling molecule. These regulations entangle with each other thus form a complex regulation circuit for AI-2 uptake. The transcriptional analysis also revealed that quorum sensing regulators *lsrR*, *lsrK* interacts with the small RNA regulators, and demonstrated that biofilm architecture formation was subject to the regulation of AI-2 uptake regulators'

coordinated mediations on different genes. The elucidated regulatory mechanism and associated hierarchy once again pushed the mathematical simulations to the front. Hopefully, the combination of mathematical simulations and experimental manipulation will lead us to a more clear understand for this quorum sensing AI-2 system since the combined approach already unmasked a hidden glucose-associated AI-2 synthesis pathway . Hopefully, further mathematical analysis based on current knowledge of AI-2 uptake from this study will lead to new insight about the mechanisms and interactions in AI-2 uptake process, point new directions for future research for this complex biological system.

Chapter 2: A Stochastic Model of *E. coli* AI-2 Quorum Signal Circuit Reveals Alternative Synthesis Pathways

Abstract

Quorum sensing (QS) is an important determinant of bacterial phenotype. Many cell functions are regulated by intricate and multimodal QS signal transduction processes. The LuxS/AI-2 QS system is highly conserved among Eubacteria and AI-2 is reported as a "universal" signal molecule. To understand the hierarchical organization of AI-2 circuitry, a comprehensive approach incorporating stochastic simulations was developed. We investigated the synthesis, uptake, and regulation of AI-2, developed testable hypotheses, and made several discoveries: (1) the mRNA transcript and protein levels of AI-2 synthases, Pfs and LuxS, do not contribute to the dramatically increased level of AI-2 found when cells are grown in the presence of glucose; (2) a concomitant increase in metabolic flux through this synthesis pathway in the presence of glucose only partially accounts for this difference. We predict that "high-flux" alternative pathways or additional biological steps are involved in AI-2 synthesis; and (3) experimental results validate this hypothesis. This work demonstrates the utility of linking cell physiology with systems-based stochastic models that can be assembled *de novo* with partial knowledge of biochemical pathways.

Introduction

Bacteria utilize an intricate communication system for the sensing and interpretation of environmental cues that has recently been shown to mediate coordinated population-based behavior. This process, termed "quorum sensing", involves the production, the release and detection of small chemical signal molecules, called autoinducers. Conceptually, a threshold stimulatory concentration of autoinducer is achieved, then a signal transduction cascade is initiated that ultimately results in a change of the "collective" behavior of the organism (86, 176, 184). Quorum sensing (QS) has been found a regulator of cellular processes such as bioluminescence production (16, 176), virulence gene expression (303), biofilm formation (10, 297), cell division, motility, metabolism, and recombinant protein production (58, 59, 248). Indeed, quorum sensing is an integral component of global gene regulatory networks (288), and has been suggested to be "a language for bacteria", mediating social engagements between prokaryotes and eukaryotes (247, 272, 284).

There are several types of quorum sensing systems including: (1) an acylated homoserine lactone (AI-1) system utilized by a variety of Gram-negative bacteria (87); (2) a post-translationally modified peptide signaling system of Gram-positive species (255); and (3) a system mediated by a highly conserved autoinducer synthase, LuxS, which appears among a variety of Gram-negative and Gram-positive bacterial species (78, 247, 259, 292). Because of its cross-species and even pro-eukaryotic connectivity, the *luxS*-mediated system has been the topic of the intense research. The

most well studied *luxS*-derived autoinducer, AI-2, is a product of the activated intracellular methyl cycle, and the flux of metabolites through this cycle affects the rate of its formation (203, 287). Indeed, the production rate of AI-2 has been shown linearly proportional to cell growth rate (58). Alternatively, its level in batch cultures in the extracellular medium appears modulated by a sophisticated autoregulated energy-dependent mechanism, suggesting an important cellular function (293). Understanding the intricacies of AI-2 mediated regulation and the mechanisms by which AI-2 influences transcription and/or cellular phenotype will naturally play a role in deciphering the behaviors of these *luxS*-containing bacteria in various environments.

Large scale system biology platforms for transcriptomics, proteomics and metabolomics enable transient experimental mapping of biological systems, however, the conceptual framework of these genetic systems cannot be fully developed without computational or simulation approaches. That is, the mathematical models serve to integrate experimental data as well as facilitate hypotheses that can be tested, and serve to provide valuable insights into the general principles of biological system organization (279).

In this work, a stochastic model based on the algorithms of Gillespie (95) was used to simulate the AI-2 circuit of *E. coli* K12. Specifically, a Stochastic Petri Net (SPN) model, a mathematical approach succinctly reviewed by Goss and Peccoud (99) and successfully used for modeling several biological systems (8, 166, 249), was developed for the appearance and disappearance of AI-2 in extracellular fluids of laboratory batch cultures of *E. coli*. This stochastic approach can accommodate large

and discrete transitions in its reacting species (94, 169); and favorably contrasts the deterministic approach which assumes that the time evolution of a chemically reacting system is continuous. That is, for biological systems, such as genetic regulatory networks with species at very low concentrations (or number) and slow reaction rates, random fluctuations can exist due to inherent stochastic events. These, in turn, can yield significant variability in system behavior particularly when modeled stochastically (93, 167, 173, 242).

Our particular interest was the apparent stimulation of AI-2 due to the presence of glucose, as its presence appears to interfere with QS signaling in *E. coli*. Based on initial simulation and experimental results in LB medium, we investigated several experimental and computational hypotheses related to redistribution of metabolic flux within the AI-2 biosynthesis pathway. Results suggest the existence of an alternative glucose-regulated pathway for autoinducer AI-2 synthesis. We subsequently discovered the conversion of nucleic acid precursor, adenosine, to AI-2 via a pathway other than the well known Pfs-LuxS pathway. That is, upon interrogating our model simulations and the enzymatic synthesis of AI-2 *in vitro* (178, 227), we discovered the existence of an alternative pathway for its synthesis, which is shown here. Other attributes of this SPN approach to investigate bacterial quorum sensing are revealed: 1. the stochastic approach formally enables estimation of variance for the simulated concentrations which can be compared to experimental data, 2. the simulated genetic circuit can be assembled from "subcircuits" as the complexity and interconnectivity with the rest of metabolism is established, 3. inferences from the literature concerning metabolic flux and other events such as

transcription, translation, and biomolecular assembly formation can be tested, and perhaps most importantly, 4. this approach enables a computational framework that allows one to postulate mechanisms and concepts that can ultimately be tested using bacterial genetics.

Materials and Methods

Plasmid, bacterial strains, and culture conditions. pTrcHisC (Invitrogen) was used for construction of pTrcHis-pfs and pTrcHis-luxS. Detailed methods for plasmid construction are outlined elsewhere (Hashimoto et al., in preparation). These plasmids were subsequently transformed into strains DH5α and NC13: DH5α carrying pTrcHis-pfs, and NC13 carrying pTrcHis-luxS, for overexpressing Pfs and LuxS, respectively. Glucose, biotin (30) and IPTG, when present, were added at 0.8%, 10 ng/ml and 1 mM, respectively. Bacterial strains and plasmids used in this paper are summarized in Table 2-1.

AI-2 Activity Assay. *E. coli* cell-free culture supernatants were tested for the presence of AI-2 using the *Vibrio harveyi* reporter strain BB170 (258). Briefly, 20 µl of AI-2 cell-free supernatant was mixed with 180 µl of BB170 suspension, which was prepared by 5000-fold dilution of a 16-hour overnight culture in AB medium. 20 µl growth medium (AB and LB medium) was added to 180 µl BB170 suspension as negative controls. All cultures were grown at 30°C, 225 rpm (New Brunswick Scientific); bioluminescence was measured hourly. Fold activation was calculated by the bioluminescence from experimental samples divided by that of the negative controls, and then normalized by cell optical density.

Table 2-1 Baterial strains and plasmids used in this study

Strain/plasmid	Relevant genotype and property	Source or reference
Strains		
E. coli W3110	Wild type	Laboratory stock
E. coli LW3	ZK126 Δ*luxS*::Kan^r	Laboratory stock
E. coli MDAI2	W3110 Δ*luxS*::Tc^r	Laboratory stock
E. coli NC13	RK4353 *Δpfs (8-226)*::Kan^r	(30)
E. coli DH5α	*recA1 supE44 endA1 hsdR17 gyrA96 relA1 thiΔ (lac-proAB)* F' [*traD36 proAB+ lacI^q lacZΔM15*]	Invitrogen
E. coli LW2	ZK126 Δ*crp*::Kan	(276)
V. harveyi BB152	BB120 *luxL::*Tn5 (AI-1$^-$, AI-2$^+$)	(258)
V. harveyi BB170	BB120 *luxN*::Tn5 (sensor 1$^-$,sensor 2$^+$)	(15)
Plasmids		
pFZY1	*galk'-lacZYA* transcriptional fusion vector, Ap^r	(147)
pLW10	pFZY1 derivative, containing *luxS* promoter, Ap^r	(276)
pYH10	pFZY1 derivative, containing *pfs* promoter, Ap^r	(276)
pHA7E	pBR322 derivative, *crp*$^+$ Ap^r	(132)
pIT302	pACYC184 derivative, *cya*$^+$ Cm^r	(142)
pTrcHis C	Cloning vector, Ap^r	Invitrogen
pTrcHis-luxS	pTrcHis C derivative, *luxS*$^+$ Ap^r	Hashimoto *et al.* ,in preparation
pTrcHis-pfs	pTrcHis C derivative, *pfs*$^+$ Ap^r	Hashimoto *et al.*, in preparation

RNA preparation and Northern blot analysis. Overnight cultures grown in LB were diluted 100-fold into fresh LB and grown to mid-exponential phase, then diluted again into LB or LB with glucose at OD_{600} near 0.03. Cultures were then incubated at 30°C with shaking at 250 rpm. Total RNA was isolated and diluted on an OD equivalent basis from culture volumes equivalent to 1 mL at an OD_{600} of 1.0 using a Qiagen RNeasy mini kit (Qiagen, Valencia, CA). Same amount of RNA was loaded on a 1% formaldehyde agarose gel and then transferred to a positively charged nylon

membrane. A digoxygenin (DIG) DNA labeling and detection kit (Boehringer Mannheim) was used for labeling DNA probes and detection according to the manufacture's instructions. For probe construction, the following olignucleotides were used: *luxS1* 5'-CTAGATGTGCAGTTCCTGCAA-3' and *luxS2* 5'-ATGCCGTTAGATAGCTTC-3' for a *luxS*-specific probe; *pfs1* 5'-AATCGGGCTTATCGCGAGTAAA-3' and *pfs2* 5'-GCAAGTTTCTGCACCAGTGACTC-3' for a *pfs*-specific probe; *speD1* 5'-GCGCGACGGTTATATTATATC-3' and *speD2* 5'-CGCTAATCAATGGTTACGATATCGGA-3' for a *speD*-specific probe. Northern results were repeated in triplicate and quantified using NIH ImageJ software.

Real-Time RT-PCR. cDNA was synthesized from total RNA with random hexamers using the SuperScript™ III First-Strand Synthesis System for RT-PCR (Invitrogen) according to the manufacturer's instructions. Primers were designed and purchased from Integrated DNA Technologies (Coralville, IA). Regular PCR was used to check the uniqueness of the primers before using the cDNA for quantification PCR. Real-time RT-PCR was performed in 50 μl of reaction mixture containing the Platinum SYBR Green qPCR Supermix UDG (Invitrogen), 0.2 μM of primers, and cDNA (50°C, 2 min; 95°C, 2 min; 95°C, 15 s, 40 cycles; 60°C, 1 min). The reaction and detection of dye-labeled PCR products were performed with an Applied Biosystems 7300 Real-Time PCR System (Appled Biosystems). *16S rRNA* was used as the endogenous control and primers were listed in Table 2-2. Samples obtained from the 3 hr time points of the LB with 0.8% glucose cultures were used to normalize data.

Table 2-2 Primers used in real-time PCR

Gene	Direction	Primer Sequence
16S rRNA	Upstream	5'-CAGCCACACTGGAACTGAGA-3'
	Downstream	5'-GTTAGCCGGTGCTTCTTCTG-3'
luxS	Upstream	5'-CATACCCTGGAGCACCTGTT-3'
	Downstream	5'-TGATCCTGCACTTTCAGCAC-3'
pfs	Upstream	5'-GAGGTTGCGCTTCTGAAATC-3'
	Downstream	5'-GACAACGATATCGCCCACTT-3'

SDS-PAGE analysis. Culture volumes equivalent to 2 ml at an OD_{600} of 1.0 were withdrawn at the growth of 6 h time point and spun down at 12,000 rpm for 5 min in a microcentrifuge. The cell pellets were resuspended and lysed in 300 μl BugBuster protein extraction reagent (Novagen) under room temperature for 30 minutes, and then spun down at 12,000 rpm for 10 min. The soluble cell extract was 1:1 (v/v) mixed with SDS sampling buffer (12.5% 0.5 M Tris-HCl (pH 6.8), 10% glycerol, 2% sodium dodecyl sulfate (SDS), 5% β-mercaptoethanol, 0.0025% bromophenol blue), heated at 100^{o}C for 5 min, and vortexed. Samples were loaded onto a 15% SDS polyacrylamide gel for electrophoresis. Proteins were visualized by staining with Coomassie blue and quantified after developing linearized standard curves with purified proteins.

Results

Model construction

AI-2 biosynthesis and uptake pathways in *E. coli* (Fig.2-1) have been partially elucidated (227, 293): AI-2 is derived from S-adenosylmethionine (SAM), a major methyl donor in metabolic processes. SAM transfers a methyl group to methyl acceptors by methyltransferases, such as CheR (296),

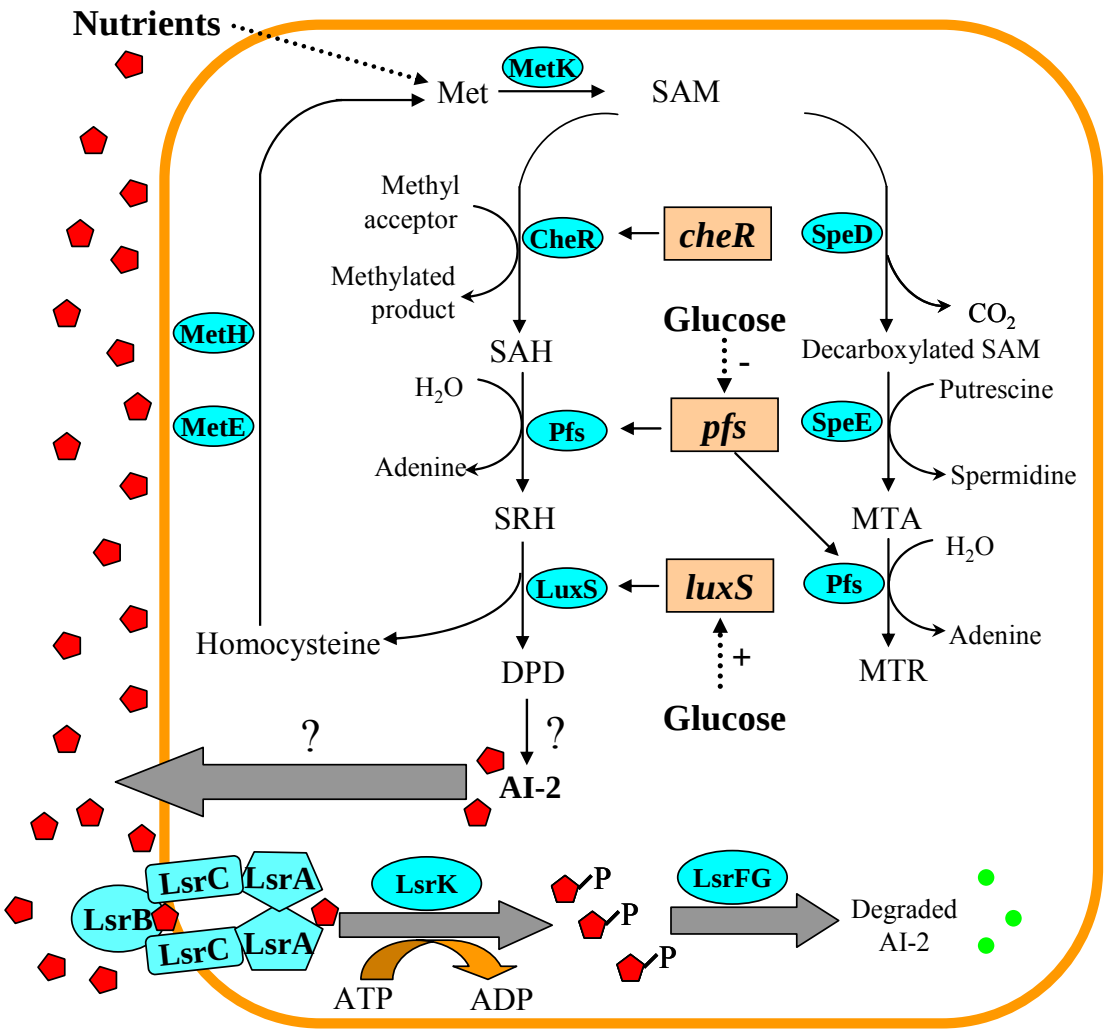

Figure 2-1 AI-2 synthesis and uptake pathways in *E. coli*
(Adapted Wang *et al.*, J Bacteriol (187): 2066-2076)

yielding *S*-adenosylhomocysteine (SAH). SAH is hydrolyzed to S-ribosylhomocysteine (SRH) by a nucleosidase, Pfs, with a concomitant release of adenine. LuxS cleaves the thioether linkage of SRH and yields homocysteine and 4,5-dihydroxy-2, 3-pentanedione (DPD). It has been reported that AI-2 results from the autocyclization of DPD in at least two additional reactions (39, 178, 232). SAM, together with diamine and putrecine, is also decarboxylated to form a major triamine, spermidine. This triamine plays an important role in proliferation and differentiation of *E. coli* (44). This reaction also releases a toxic by-product 5'-thiomethyladenosine (MTA), which is then acted upon by Pfs, yielding adenine and 5'-thiomethylribose (MTR). MTR is reportedly excreted to the medium in *E. coli* (230). The export mechanisms of AI-2 are unknown. Extracellular AI-2 is transported into the cell by an ABC transporter, Lsr (260, 276). Its uptake was recently shown to be glucose dependent (276). The role of AI-2 beyond regulating its uptake remains unresolved in *E. coli* K12, although many targets have been proposed (58, 59).

A Stochastic Petri Net (SPN) model (Fig. 2-2), was constructed for the AI-2 biosynthesis and uptake pathways (Fig. 2-1). The SPN circuit includes both SAM utilization branches, because Pfs acts on both SAH and MTA, which may enable pathway competition.

Experiments with wild type *E. coli* have demonstrated that extracellular AI-2 accumulates in the exponential phase and then is rapidly depleted at the onset of the stationary phase (258). Extracellular AI-2 level is presumed to be a function of synthesis and uptake (260, 276, 287). Our observations, which are consistent with these hypotheses, are that

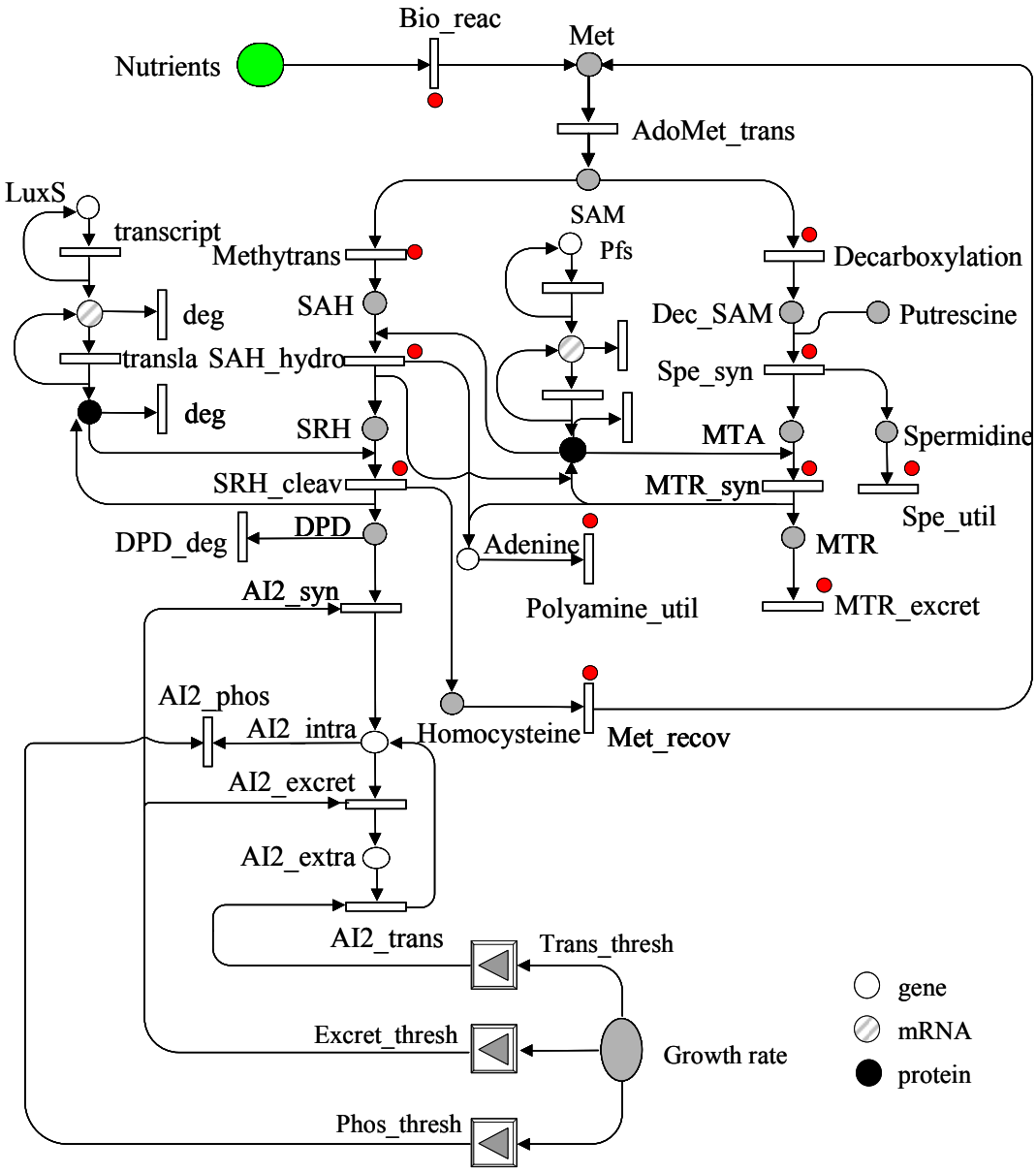

Figure 2-2 Schematic of SPN for AI-2 synthesis and uptake circuit

Circles represent places (hollow, genes; dotted, mRNA; solid dark, proteins; grey, other components). Rectangles represent transitions either transcription, translation, or flux-associated reactions (e.g., enzyme-mediated). The reactions indicated by red circles are altered by the presence of glucose.

AI-2 is stable in spent culture media devoid of cells (data not shown here), so that intrinsic instability of AI-2 is negligible. Thus, for simplicity, we partitioned our SPN so that AI-2 accumulation and uptake are two independent processes. Hence, a quorum signal "switch" was included to control the AI-2 synthesis and uptake transition. Three input gates (Trans_thresh, Excret_thresh, Phos_thresh) together with a growth rate indicator were used to control the switching process (Fig. 2-2). The instantaneous specific growth rate, which was calculated from experimental data, was used to determine the stage of cell growth and to 'open' specific input gates.

All initial markings and their appropriate references are listed in Table 2-3. For all species, one token represents a single molecule and this was taken as 1 n*M* concentration (8). Similarly, all rate constants and their original sources are listed in Table 2-4. Most of these rate constants were collected from literature data of earlier studies (66, 155, 212), such as rates of transcription, translation, and metabolic enzyme activity. *LuxS* and *pfs* transcription rates were derived from a typical transcription rate (212) modified by our transcriptional promoter probe data (Fig. 2-3), while their mRNA degradation rates were determined from previous reports (155) together with our NIH-image quantified Northern blotting data (Fig 2-4). These deterministic rate constants were transformed into stochastic constants based on the relationship between mRNA synthesis, degradation, and the cell volume.

A base model was constructed for growth in LB medium wherein an AI-2 synthesis rate was found to match our AI-2 data. To be specific, a piece-wise constant optimization routine was carried out using an identically constructed ODE model

Table 2-3 Initial markings used in AI-2 circuit

Name	Token Number	References
Nutrients	28350	(199)
Methionine	2248	(127)
SAM	10000	(203)
SAH	320	Hashimoto *et al*., in preparation
SRH	300	Hashimoto *et al*., in preparation
DPD	300	Hashimoto *et al*., in preparation
AI-2	60	Hashimoto *et al*., in preparation
LuxS mRNA	16	(127)
LuxS protein	400	(186)
Pfs mRNA	32	(276)
Pfs protein	800	(186)
Adenine	596	(70)
Homocysteine	300	(217)
Intracellular AI-2	60	Hashimoto *et al*., in preparation
Extracellular AI-2	60	Hashimoto *et al*., in preparation
Decarboxylated SAM	220	(26)
Putrescine	4400	(44)
MTA	296	(70)
MTR	180	(230)
Spermidine	940	(44)

with median output quantities for state variables. The AI-2 uptake rate was based on AI-2 uptake experiments in *luxS* mutant strains MDAI2 and LW3 (162), together with *lsr* transcription rate results (276). AI-2 excretion and AI-2 phosphorylation rates were based on intracellular AI-2 experiments indicating that intracellular AI-2 was insignificant as compared to extracellular levels (data not shown here).

ODE parameter optimization was executed using a Matlab® optimization toolbox (http://www.mathworks.com/access/helpdesk/help/toolbox/optim/optim.shtml). AI-2 circuit simulations were run using Mobius on a laptop PC, kindly provided by Dr. William Sanders (Center for Reliable and High Performance Computing at the University of Illinois at Urbana-Champaign: http://www.mobius.uiuc.edu/).

Table 2-4 Rate constants in AI-2 synthesis and uptake circuit

Reactions	Reaction symbol	Deterministic rate constants	Reference
Bio-reaction[3]	Bio_reac	0.01 min^{-1}	Derived from Delisa, 2001
Methionine Adenosyl transfer[3]	AdoMet_trans	0.962 min^{-1}	(265) (189)
Methyl transfer[3]	Methytrans	0.015 min^{-1}	(235)
SAH Hydrolysis[3]	SAH_hydro	$1.32x10^{5}$ $M^{-1}\cdot min^{-1}$	(70) (61)
SRH Cleavage[3]	SRH_cleav	$4.86x10^{5}$ $M^{-1}\cdot min^{-1}$	(301)
AI-2 Synthesis[a2]	AI2_syn	$6.7x10^{-4}$~0.1 min^{-1}	(202) (128) This study, fitted to data
AI-2 excretion[a2]	AI2_excret	0.25 min^{-1}	This study, fitted to AI-2 data
AI-2 transport[1]	AI2_trans	0.006~0.03 min^{-1}	(162)
AI-2 phosphorylation[a2]	AI2_phos	0.5 min^{-1}	This study, fitted to data
SAM Decarboxylation[3]	Decarboxylation	0.055 min^{-1}	(283) (294)
Spermidine Synthesis[3]	Spe_syn	$8.73x10^{2}$ $M^{-1}\cdot min^{-1}$	(294) (26)
MTR Synthesis[3]	MTR_syn	$4.81x10^{3}$ $M^{-1}\cdot min^{-1}$	(70)
Spermidine Utilization[3]	Spe_util	$2.11x10^{-2}$ min^{-1}	(136)
LuxS transcription [b1]	tanscript	1.25min^{-1}	(212) (276)
LuxS translation[2]	transla	0.74 min^{-1}	(27)
Pfs transcription [b1]	Not denoted	2.1 min^{-1}	(212) (276)
Pfs translation[2]	Not denoted	0.54 min^{-1}	(27)
LuxS mRNA degradation[c1]	deg	0.03 min^{-1}	(155) Fitted to data
Pfs mRNA degradation[c1]	Not denoted	0.022 min^{-1}	(155) Fitted to data
LuxS protein degradation[2]	deg	0.012 min^{-1}	Assumed
Pfs protein degradation[2]	Not denoted	0.003 min^{-1}	Assumed

Derived deterministic rate constants were transformed into stochastic rate constant through equation 1-5, cell volume is 4.0e-16 Liter.
a : Fitted to experimental data in this study, stated in text
b: *luxS*, *pfs* transcription rate fitted to β-galatosidase data in Wang *et al*., 2005, see supplemental figure 1
c: See supplemental figure 2
1: adjusted according to experimental data in presence of glucose
2: retained as constant irrespective of glucose
3: increased 50% due to presence of glucose

As our simulations monitor constituents in a single cell, each simulation was terminated at a cell's doubling. For example, during the exponential phase, doubling time was 35 minutes, the simulation was terminated at 35 min and constituents' levels were divided by two and set as initial markers for the subsequent run.

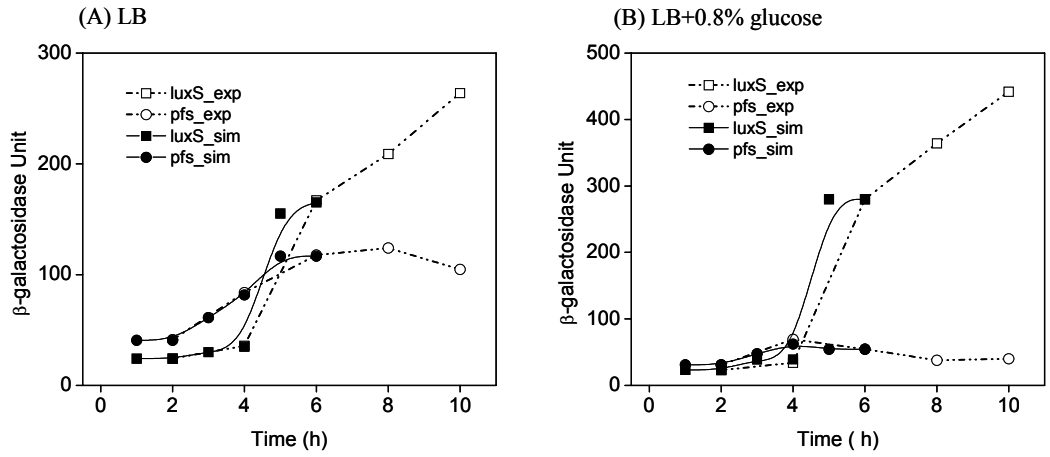

Figure 2-3 Transcription rate for AI-2 synthase LuxS, Pfs

luxS, *pfs* transcription rate determined from their β-galactosidase data, respectively. The dotted line represents experimental data, while the solid line shows resultant calculated transcription rate. A constant was used for the transformation of β -galactosidase units into transcription rate.

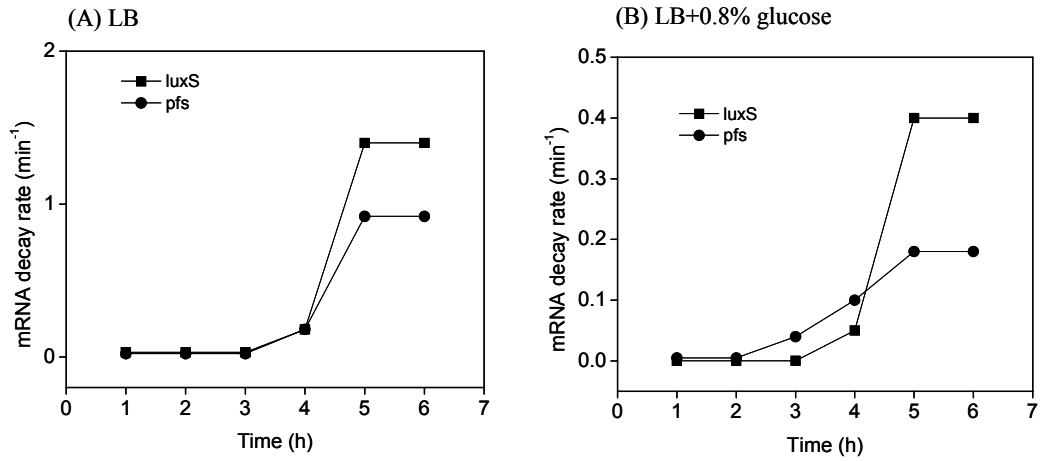

Figure 2-4 *LuxS, pfs* mRNA decay rate
luxS, *pfs* mRNA decay rates were determined from their quantified northern blotting data and previously determined transcription rates, respectively. A constant was used for the transformation of quantified northern blotting data to mRNA level for calculating each corresponding mRNA decay rate.

AI-2 production in LB medium is partially influenced by Pfs & LuxS

AI-2 activity exists in LB medium of cells grown without glucose, although at a much lower level than with glucose (276). Simulations were performed on the AI-2 circuit for cells cultured in LB medium without glucose. During these simulations and because there exists solid literature data on most remaining constants, the AI-2 synthesis rate (k_{syn}) was optimized by minimizing the variance between the simulated results and corresponding experimental data. Hence, the optimized synthesis rate, which enables good agreement with experimental data, is a piecewise constant that increases with time ("LB_sim"in Fig. 2-5 A and Table 2-5). That the reaction rate increased with time is an interesting result that will be

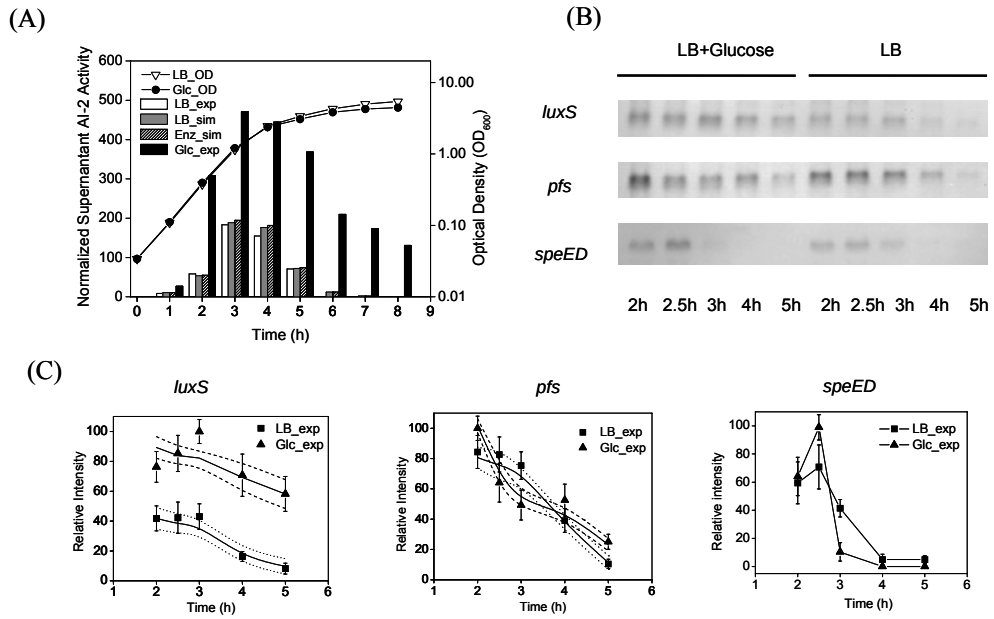

Figure 2-5 Effects of glucose on AI-2 production and *luxS, pfs, speD* mRNA levels

(A) Overnight cultures of W3110 were diluted 1:100 in LB and grown to mid-exponential phase, then diluted again into different mediums at OD_{600} of 0.03. At different time points, aliquots were collected for measurement of OD_{600} and AI-2 activity. Data shown are representative of three independent experiments. Replicate assays agreed to within 10%. (B) Northern blot analyses of *luxS*, *pfs*, and *speED* mRNA levels. (C) Densitometric analyses of the Northern blot data shown in (B) and the simulated results of *luxS*, *pfs* mRNA. Amount of transcript was represented as normalized by the peak levels. Simulated results of absolute mRNA numbers are transformed into relative level by a constant. Experimental points with error bars from densitometric analyzed data of Northern blots, solid lines represents simulated results, dotted or dashed lines represent simulation results +/- standard deviation.. "sim" represents simulation data while "exp" respresent experimental data.

Table 2-5 AI-2 synthesis and uptake rate constants in simulations

Growth phase		Synthesis rate in exponential phase (min^{-1}) (k_{syn}, k_{synGlc})						Uptake rate in Stationary phase (min^{-1})		
Time/min		35	35	35	35	35	35	70	140	140
Run #		1	2	3	4	5	6	7	8	9
LB_sim	k_{syn}	6.7e-04	6.7e-04	0.0045	0.0045	0.1	0.1	0.01	0.03	-
Enz_sim	k_{syn}	6.7e-04	6.7e-04	0.0045	0.0045	0.1	0.1	0.006	0.006	0.006
LBOver_sim	k_{syn}	6.7e-04	6.7e-04	0.0045	0.0045	0.1	0.1	0.01	0.03	-
GlcOver_sim	k_{syn}	6.7e-04	6.7e-04	0.0045	0.0045	0.1	0.1	0.006	0.006	0.006
GlcFlx_sim	k_{syn}	6.7e-04	6.7e-04	0.0045	0.0045	0.1	0.1	0.006	0.006	0.006
Glc_sim1	k_{synGlc}	0.0012	0.0012	0.05	0.05	0.05	0.05	0.006	0.006	0.006
Glc_sim2	k_{synGlc}	0.0012	0.0012	0.05	0.05	0.05	0.05	0.006	0.006	0.006

Note: LB_sim represents simulations in LB, Enz_sim represents simulations when *luxS* and *pfs* transcripts change due to the presence of glucose, LBOver_sim and GlcOver_sim represents simulations of LuxS and Pfs overexpression in LB without and with glucose respectively (denoted LuxS_sim or Pfs_sim in Figures 2-6 & 2-7, respectively). GlcFlx_sim, Glc_sim1, Glc_sim2 represent three different simulations in the presence of glucose (Fig.2-8).

Table 2-6 *LuxS*, *pfs* mRNA level from real-time PCR and comparison to quantified Northern blot data

Gene	Time (hour)	Real-time PCR Fold Change		Relative mRNA level (mRNA in Glc divided by mRNA in LB)			
				Real time PCR		Quantified Northern blot	
		LB	Glc	Exp	Sim	Exp	Sim
luxS	2	0.47±0.12	0.75±0.20	1.60	1.21	1.82	1.93
	2.5	0.62±0.10	0.906±0.13	1.44	1.76	2.02	2.20
	3	1.38±0.29	<u>1.00±0.11</u>	0.72	1.45	2.32	2.22
	4	1.11±0.03	1.97±0.19	1.79	1.68	4.34	4.30
	5	0.84±0.14	1.87±0.20	2.23	2.48	7.10	5.98
pfs	2	0.65±0.10	0.72±0.04	1.10	1.00	1.18	1.26
	2.5	0.75±0.02	0.86±0.11	1.14	1.23	0.77	0.92
	3	0.99±0.19	<u>1.00±0.12</u>	1.01	1.42	0.65	0.78
	4	0.90±0.13	1.27±0.16	1.41	1.39	1.34	1.22
	5	0.52±0.08	0.95±0.15	1.84	1.68	2.39	2.04

"Glc" represents LB with 0.8% glucose. "Exp" represents experimental data, "Sim" represents simulation data. RT-PCR results are normalized to 3 hr time point (underlined).

discussed later. Our decision to optimize the AI-2 synthesis rate as opposed to uptake rate was based on our experimental observations that *luxS* and *pfs* transcript levels are high during exponential growth and that *lsr* transcription is not initiated until late exponential phase (276, 277). Hence, synthesis is regulated first followed by uptake.

It has also been reported that glucose can stimulate AI-2 synthesis. In Wang *et al*. (276), we demonstrated that the rates of *luxS* transcription were increased due to the presence of glucose and this increase was mediated by the cAMP-CRP complex. In Fig. 2-5 and Table 2-6, we show the *luxS*, *pfs*, and *speED* mRNA levels, detected by both Northern blot and qRT-PCR, in cells grown with and without glucose. Interestingly, the Northern data suggest a 2 to 7-fold increase in *luxS* mRNA in glucose-grown cells, while the qRT-PCR data track the transcription rate data obtained previously (~ 1.5 to 2-fold increase, Wang et al; 2005a). Because of the apparent variability in mRNA data based on the two measurement techniques, the rates of *luxS* and *pfs* transcription were calculated twice, corresponding to both data sets (Table 2-6) and both sets of simulation results indicated only a 10% increase in calculated AI-2 (Fig. 2-5A, only "Enz_sim" shown here for the Northern data). Importantly, irrespective of the mRNA quantities, the experimentally observed AI-2 levels were 3-fold higher than predicted by SPN. Not seen in these simulations are the estimated variances calculated by the stochastic model. In particular, the AI-2 variance was less than 5% of the mean throughout the simulation period. The most widely varied constituents were indeed the levels of *luxS* and *pfs* mRNA (~16%) as indicated in Fig. 2-5C, which roughly correspond to the standard errors associated with the Northern blot measurements.

These results suggest that changes in the levels of these key enzymes do lead to the stimulation of AI-2 production, but at levels much less than needed to rectify simulation with experimental results from cultures containing glucose.

In order to test this enzyme dependence further, the AI-2 circuit was experimentally perturbed by *luxS* and *pfs* overexpression. IPTG inducible expression vectors for the production of LuxS and Pfs were introduced into W3110 cells, which, in turn, were grown in the presence and absence of glucose. First, in the absence of glucose and consistent with Fig. 2-5, *luxS* overexpression resulted in only a small AI-2 increase (about 16%) relative to the control (plasmid without *luxS* insertion) (Fig. 2-6A). Interestingly, *pfs* overexpression resulted in no clear trend and no appreciable difference relative to the control (plasmid without *pfs* insertion) (Fig. 2-6A). In order to mimic the effects of *luxS* and *pfs* overexpression on the AI-2 SPN, their transcription rates were increased 200-fold, respectively. This is a much more severe test of the reaction network's dependency on LuxS and Pfs expression than the simulations above (Fig. 2-5). The resultant LuxS and Pfs protein levels were calculated to be around 200 to 300-fold higher than wild type cells in the mid-exponential phase (Fig. 2-6D). While not shown, the levels of these enzymes in the wild-type cells does not change significantly with time (i.e., they roughly correspond to transcript levels in Fig 2-5C). The corresponding calculated AI-2 levels were raised by less than 10% (Fig. 2-6C). These simulation results corroborate the experimental

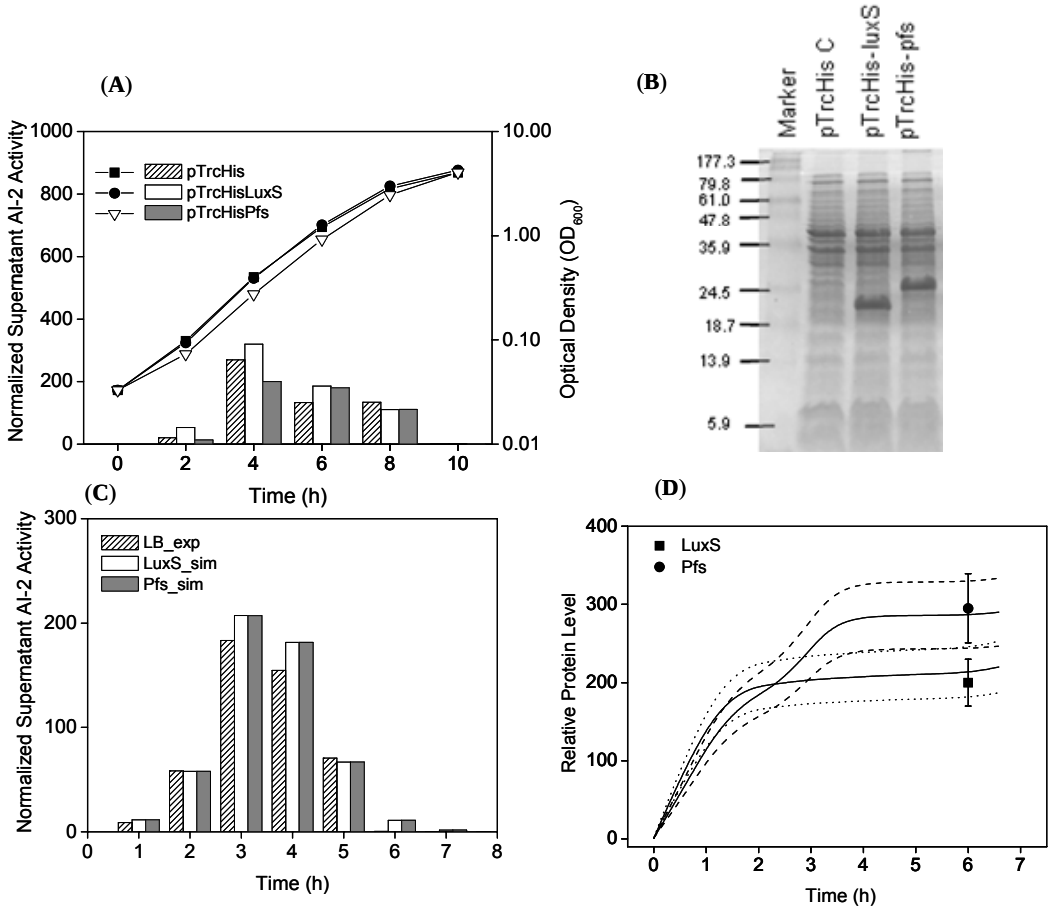

Figure 2-6 *LuxS, pfs* overexpression partially influences AI-2 formation in LB

(A). Overnight cultures were diluted 1:100 in LB medium; IPTG was added to cultures at 1 mM (*trc* promoter) at time zero. Aliquots were collected for measurement of OD_{600} and AI–2 activity. Replicate assays agreed to within 10%. **(B)**. Overexpression of LuxS and Pfs was confirmed by SDS-PAGE using samples taken at 6 hr. **(C).** Simulation results of *luxS* and *pfs* overexpression are compared to experimental data from LB cultures; corresponding protein levels are indicated in (**D**). Relative protein level was obtained from the simulated protein molecule at time t divided by the initial protein molecule at initial time t_0. The relative experimental data was obtained from the image quantified protein molecule divided by the same initial protein molecule as in simulations. Solid lines represent simulated LuxS and Pfs levels, broken lines represent mean values plus/minus variance (LuxS, dotted; Pfs, dashed)

findings that *luxS* and *pfs* overexpression only minimally influences AI-2 production in LB medium without glucose.

In Fig. 2-7A, cells overproducing each of the synthases in the presence of glucose exhibited significantly higher levels of AI-2. In the case of LuxS, the increase was more immediate than with Pfs. The levels of LuxS and Pfs in these overproducing cells were estimated to be 200-fold greater than the uninduced controls (quantified results in Fig.2-7D). By increasing *luxS* mRNA (due to the presence of glucose) in the network, and performing the similar *luxS* or *pfs* overexpression simulations as stated in LB medium, we saw only similarly increased AI-2 levels (less than 10%, data not shown here).

Taken together, these simulations have demonstrated that the expression level of LuxS and Pfs enzymes can not notably enhance AI-2 production. However, experiments have clearly demonstrated that overexpression of LuxS and Pfs can effectively increase AI-2 production when glucose is present. This discrepancy suggests that the increase in AI-2 production due to the presence of glucose may result from factors other than LuxS and Pfs, in ways that have yet to be revealed. This is partially explored by examining carbon flux through the biosynthesis pathways.

Glucose provides enhanced flux through the LuxS synthesis pathway

Based on Holms' flux analysis of *E. coli* grown with different carbon sources (122) and the work of Liao and co-workers (191), the presence of glucose and varied carbon sources can significantly enhance the flux through central metabolic pathways (CMPs). According to their data, a 50% increase in the flux of material through the AI-2 circuit due to the presence of glucose is

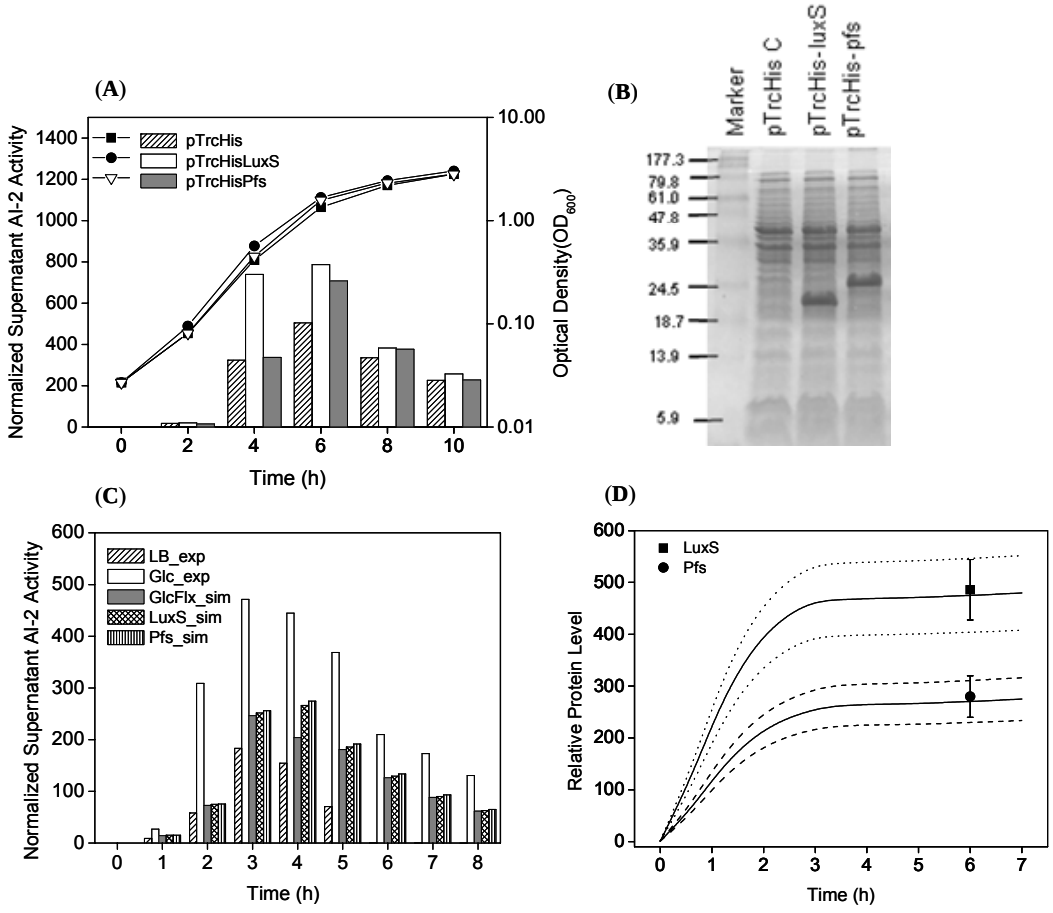

Figure 2-7 *LuxS, pfs* overexpression affects AI-2 formation in the presence of glucose

Overnight cultures were diluted 1:100 in LB + 0.8% glucose medium, IPTG was added to cultures at 1 mM (*trc* promoter) at time zero. **(A)**. Aliquots were collected for OD_{600} and AI–2 activity measurement. Replicate assays agreed to within 10%. **(B).** Overproduction of LuxS and Pfs was confirmed by SDS-PAGE using samples taken at 6 hr. **(C).** Simulation results of *luxS*, *pfs* overexpression on AI-2 production in presence of glucose. **(D).** Corresponding protein levels are indicated (fold-increase relative to control). Relative protein level was obtained same as described in Fig. 2-6. Solid lines represent simulated LuxS and Pfs levels, broken lines represent mean values plus/minus variance (LuxS, dotted; Pfs, dashed). Points are NIH-image quantified results based on standard curve.

reasonable. Hence, we carried out several "what if" simulations whereby metabolic fluxes other than the AI-2 synthesis rate from DPD and its uptake were up-regulated 50% as compared to without glucose. In the first set of simulations (GlcFlx_sim, Fig. 2-7C), the 2-fold increase of *luxS* mRNA due to glucose was included, but without overexpression of *luxS* and *pfs*. The calculated AI-2 increased 35% over that without glucose. The addition of *luxS* and *pfs* overexpression to the case of increased metabolic flux only marginally increased AI-2 levels (LuxS_sim, Pfs_sim in Fig. 2-7C).

In Fig. 2-7A, cells overproducing each of the synthases in the presence of glucose exhibited significantly higher levels of AI-2. In the case of LuxS, the ~2-fold increase was more immediate than with Pfs. In Fig. 2-7B, the levels of LuxS and Pfs in these overproducing cells was estimated to be 200-fold greater than the uninduced controls (quantified results are depicted in Fig. 2-7D). Simulations with glucose present (ie., higher initial *luxS* mRNA), predict that both *luxS* and *pfs* overexpression enhance AI-2 production over the LB SPN calculations but by less than or near 2-fold (Fig. 2-7C, Fig. 2-6C). Interestingly, the simulated levels of LuxS and Pfs were higher than those without glucose (Fig. 2-7D, Fig. 2-7D). It is again noteworthy that the LuxS and Pfs protein levels were within the variances calculated by the SPN. Also, experimental observations indicated a more immediate response in the case of LuxS overexpression, yet there was no distinct difference in calculated AI-2 even though the calculated LuxS level appeared to increase more quickly than Pfs. We note that in experiments, the peak AI-2 levels were similar in both overexpression cases (~800 normalized activity units, Fig. 2-7A), and roughly 1.5-fold higher than the +glucose

case without enzyme overexpression (Fig. 2-7A). That the SPN captured the relative increase in AI-2 (~1.5 – 2 fold) due to the enzyme overexpression in the presence of glucose was both interesting and noteworthy, but our simulations still missed the overall enhancement resulting from glucose itself. Most importantly, an approximately 250 to 500-fold increase in each enzyme resulted in only a maximum 2-fold increase in AI-2.

Trends in all of the above simulations are consistent with our experimental results and a previous report that flux increases do stimulate AI-2 production (203). Because the simulated AI-2 remained much lower than the experimental data, we hypothesized that the rate of AI-2 synthesis from DPD was itself a function of glucose, with an as yet to be determined functional form. This has varied ramifications as will be discussed.

In order to set up further simulation experiments, we performed a piecewise linear optimization analysis to "find" the AI-2 synthesis rate constant (k_{synGlc}) that best matched the experimental data with glucose present. Since our simulation rate constants are most grounded in events associated with transcription, translation and flux in the enzyme-mediated reactions, we optimized the AI-2 synthesis rate under the condition of 50% increased metabolic flux. In Fig. 2-8, the corresponding best fit simulation results for the glucose case are, as expected, in close agreement with the data (Fig. 2-8, Glc_sim1). The experimental results and the previous GlcFlx_sim from Fig. 2-7C are also included. In Table 2-5, the corresponding synthesis rates for the conversion of DPD to AI-2 increased ~10-fold over the previous case during the

period of maximum AI-2 increase (2-3 hrs). The maximum difference between calculated results and measurements was less than 15%.

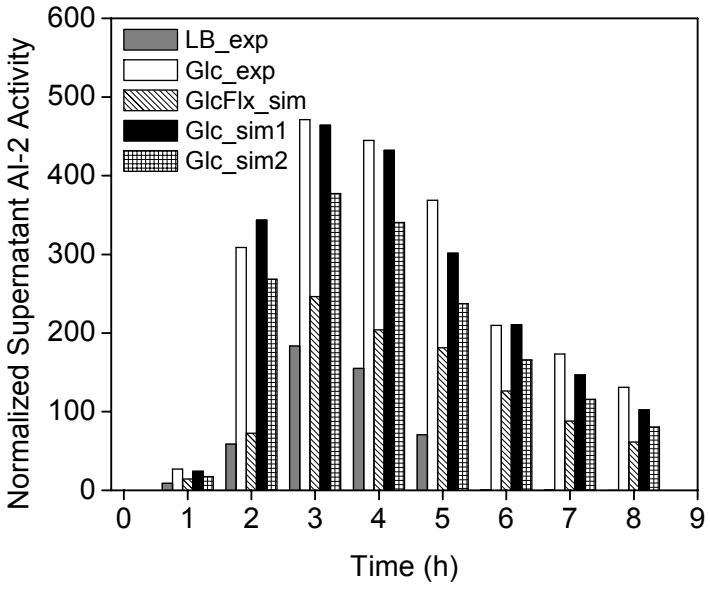

Figure 2-8 Glucose affect AI-2 formation by increasing fluxes through AI-2 pathway modulating AI-2 synthesis rate

AI-2 experimental data in LB, grey bar; AI-2 experimental data in LB+0.8% glucose, white bar; "GlcFlx_sim" (striped bar) denotes results for 50% increase in flux of reactions noted by red circles in Fig. 2-2.; "Glc_sim1" (black bar) denotes results of optimized AI-2 synthesis rate together with a 50% increase in flux of reactions denoted by red circles in Fig. 2-2; "Glc_sim2" (rectangular bar) denotes results of optimized AI-2 synthesis rate only.

A second simulation was run in which the "optimized" AI-2 synthesis rate was run without enhanced metabolic flux (Fig. 2-8, Glc_sim2). This tests whether the influence of glucose on the well-studied synthesis pathway is the potential problem in our SPN circuit. The results are again significantly different from the experiments, reinforcing the suspicion that our model construction from DPD to AI-2 is flawed. That is, the net result of these simulations demonstrated that increases in "upstream" metabolic flux do stimulate AI-2 production, but that the apparent non-enzymatic conversion of DPD to AI-2 may be the basis for discrepancy. One explanation is that there are alternative pathways other than those well-documented (as shown in Fig.2-1) for AI-2 synthesis. These may be induced and/or undergo dramatic flux increase due to the presence of glucose.

Alternatively, when cells enter stationary phase, AI-2 uptake takes place. As stated above, the AI-2 uptake rate was determined in the initial model based on LB medium (162). However, in the presence of glucose (0.8% glucose in LB), AI-2 uptake was observed to be slower as compared to without glucose, due to the CRP mediated repression of glucose on AI-2 uptake (260, 276). A reduced uptake rate would increase the extracellular AI-2 level. While not noted earlier, a revised AI-2 uptake rate (reduced by more than 40%) was used in the above simulations representing glucose addition (Table 2-5). However, when the AI-2 uptake rate constant was lowered 10-fold to reflect nearly complete repression of uptake, there was no depletion of AI-2 level in supernatant (not shown here). This is inconsistent with the experimental results which clearly demonstrated AI-2 uptake, even in cells devoid of the active *lsr* uptake transporter (276). A further modification is envisioned

wherein uptake and synthesis are coordinated so that cessation of synthesis ends after AI-2 uptake begins. Our experimental evidence with *lsrK* knockouts however, demonstrates that AI-2 synthesis indeed ends at switch times or conditions as indicated, and AI-2 levels remain the same during the stationary phase (276). If there were still AI-2 synthesis under the condition without any uptake, we would see a continually increased AI-2 activity.

Is Conversion of 4,5-dihydroxy-2, 3-pentanedione a High-flux Reaction?

We were interested in the Almaas *et al*. report which suggests that the biochemical activity of metabolism is dominated by a few high-flux backbone reactions which are embedded in a network of mostly small-flux reactions (6). They reported that only high-flux reactions go through noticeable flux changes while small-flux reactions undergo small shifts. Based on this, we speculated there may be hidden high-flux reactions among the AI-2 synthesis pathways. As stated above and confirmed by experiment and simulation, the increase in transcription and/or translation of *luxS* and *pfs*, cannot enhance AI-2 production significantly. Further, a dramatic increase, more than 200-fold, in upstream precursor, SAM, only stimulated an approximate 60% AI-2 increase (203).

This turned our attention to post LuxS processing (the correct cyclization of DPD, (178)) which is reported to be a result of mass action kinetics as opposed to an enzyme or chaperone-mediated event. We wonder whether this conversion, putatively in the cell cytoplasm, could proceed without any biological assistance. After many efforts including our own, biologically produced AI-2 has never been isolated without further biological assistance such as binding to a cognate receptor (39, 171, 178, 232,

233). Similarly pure DPD has also not been reported, instead "pure" DPD is a mixture of DPD together with its two anomers at their low concentration (171). The mechanism by which AI-2 is formed from its precursor, DPD, remains enigmatic in *E. coli*. Hence, we predicted that the reaction from DPD to AI-2 potentially serves as a hidden high-flux reaction in the AI-2 quorum sensing network.

During our "fit" simulations, the AI-2 synthesis rate increased significantly with the growth of cells. This rate constant represents the net reaction rate from DPD to AI-2; our results clearly indicated that the reaction from DPD to AI-2 has a strong impact on AI-2 level. Furthermore, mechanistically, DPD is putatively the principle molecule from which all bacterial AI-2 is derived (55, 178, 232). Because of the apparent impact of this reaction on AI-2 level, we performed additional simulations (Fig. 2-9) to differentiate potential mechanisms that contribute to this pathway. First, we intentionally reduced the AI-2 synthesis rate constant, k'_{synGlc}, to gauge its importance on AI-2 formation from DPD in the case of glucose-mediated flux increases and Pfs/LuxS synthase mRNA changes (DPD_sim1, Fig. 2-9A). This reduced synthesis rate was ~3-fold lower than the "optimized" AI-2 synthesis rate (k_{synGlc}) in the earlier glucose simulations (Glc_sim1, Glc_sim2 in Fig. 2-8), but was maintained ~3-fold higher than the initial simulations (e.g., GlcFlx_sim in Fig. 2-7). The resultant AI-2 level was much lower than our observations, as we expected. This case represents a logical

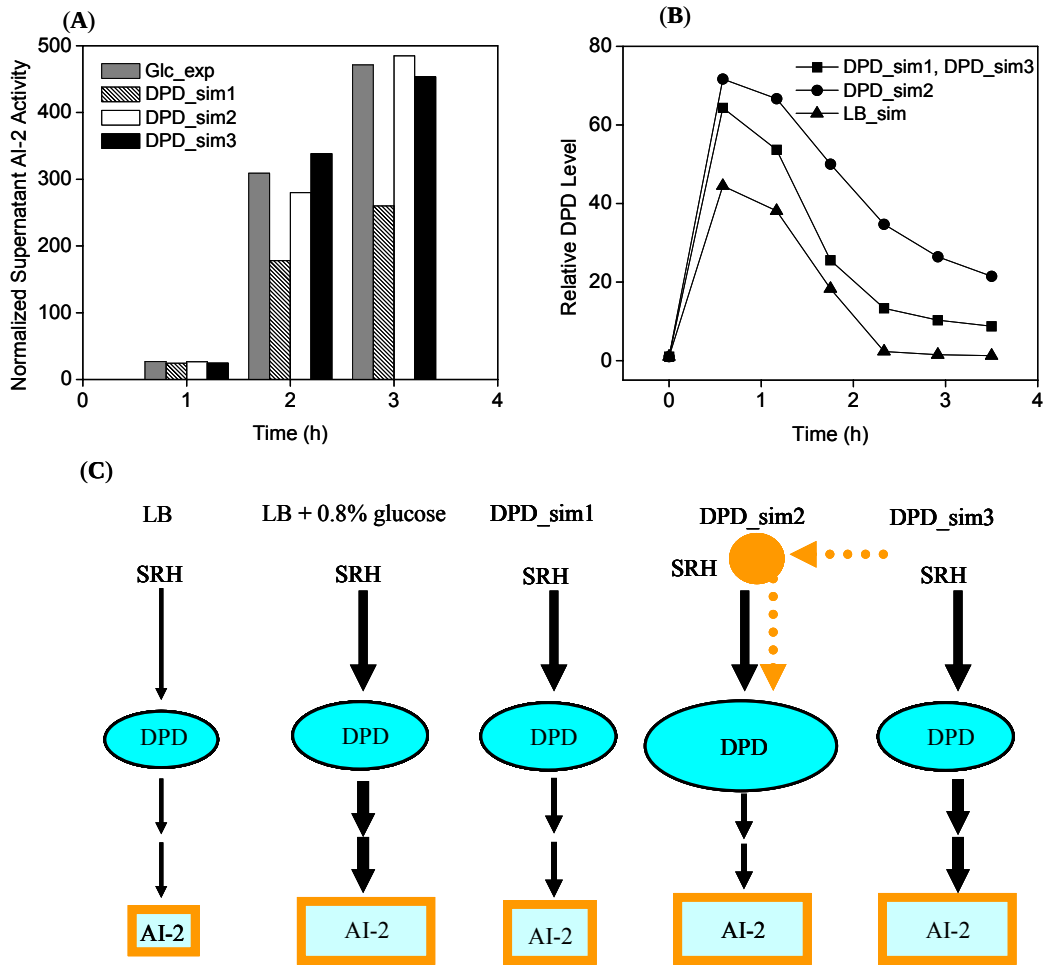

Figure 2-9 Modulating flux from DPD to AI-2 significantly affects AI-2 formation

(A, B) "DPD_sim1" denotes base model for DPD and a low AI-2 synthesis rate, k'_{synGlc}. "DPD_sim2" denotes artificially high DPD level with low AI-2 synthesis rate, k'_{synGlc} (this is case for high flux through DPD to AI-2). "DPD_sim3" denotes a normal DPD level with "optimized" AI-2 synthesis rate k_{synGlc}. "Glc_exp" denotes experimental data with glucose present; "LB_sim" denotes simulation results for base case in LB media. **(C)** Schematic of AI-2 synthesis from Pfs product, SRH. The relative areas of DPD and AI-2 represent, but are not scaled to their respective quantities. Dashed arrows represent unknown pathways. Relative DPD level was obtained from the simulated DPD molecule at time t divided by the initial DPD molecule at initial time t_0.

extension of our experimental findings, and is included to represent an intermediate level of enhanced reaction (Fig. 2-9A, Table 2-7).

Table 2-7 AI-2 synthesis rate constant comparison under simulations with different DPD levels

Growth phase		Synthesis rate in exponential phase (min^{-1}) (k_{synGlc}, k'_{synGlc})					Uptake rate in Stationary phase (min^{-1})			
Time/min		35	35	35	35	35	35	70	140	140
Run #		1	2	3	4	5	6	7	8	9
DPD_sim1	k'_{synGlc}	0.0012	0.0012	0.015	0.015	0.015	0.015	0.006	0.006	0.006
DPD_sim2	k'_{synGlc}	0.0012	0.0012	0.015	0.015	0.015	0.015	0.006	0.006	0.006
DPD_sim3	k_{synGlc}	0.0012	0.0012	0.05	0.05	0.05	0.05	0.006	0.006	0.006

Note: DPD_sim3 is the duplicate of previous Glc_sim1

Second, "DPD_sim2" was carried out by maintaining a ~20% higher DPD concentration than the previous cases, but with the same AI-2 synthesis rate constant k'_{synGlc} as in DPD_sim1. In Mobius, this is accomplished by redefining the input function of DPD tokens so that upon transition or "firing", the number of DPD tokens was not reduced by 1 and was instead, unchanged. This case represents a situation where other reactions produce DPD from as yet unidentified pathways (indicated by a side entry reaction in DPD_sim2 of Fig. 2-9C). The simulated results agreed well with our experimental data.

Third, "DPD_sim3" (same as Glc_sim1 in Fig. 2-8), was performed under the original DPD configuration with the "optimized" synthesis rate constant, k_{synGlc}. This simulation represents the situation where the rate constant from DPD to AI-2 was increased 40-fold over time (indicated by the thick arrow in Fig. 2-9C). As noted above, the simulations fit the data well.

The AI-2 synthesis rates for all three simulations are listed in Table 2-7. The DPD levels (relative to the initial tokens) under these three different conditions are depicted in Fig. 2-9B along with the base LB case. An initial rapid transient was observed in which the +glucose cases reached a significantly higher level. The ~3-fold increase in AI-2 synthesis rate constant (k'_{synGlc}) coupled with an artificially increased DPD level (DPD_sim2) resulted in a close fit with the experimental data. An additional 3-fold increase in the AI-2 synthesis rate constant, k_{synGlc}, coupled with the original DPD conditions also resulted in a good fit of the experimental data (DPD_sim3).

Readily apparent from these simulations is that AI-2 production can be made to match experiments either by elevating the intracellular DPD level or by increasing the AI-2 synthesis rate constant from DPD. Our simulations are consistent with either an alternative source of DPD, or an enhanced reaction rate from DPD, both of which served to explain the increased AI-2 level in the presence of glucose.

In total, our simulations suggest that in order to accurately simulate the AI-2 level in the extracellular medium, the reaction from DPD to AI-2 must increase in time; and in the presence of glucose, must increase an additional 10-fold beyond the base case. Or alternatively, the reaction rate must increase ~3-fold in concert with a significantly increased level of intracellular DPD. All of these scenarios suggest the reaction from DPD may be a high flux reaction that varies significantly in rate.

Experiments demonstrating existence of alternative AI-2 synthesis pathways

In order to probe this hypothesis experimentally, we turned to the substrates and byproducts of this two-enzyme AI-2 synthesis system. In particular, we considered the potentially broad substrate specificity of Pfs (it participates in both

reaction pathways, Fig. 2-1). We incubated soluble cell extracts and imidazole eluted enzyme fractions of NC13 (a *pfs* null mutant) and DH5α (a *luxS* frameshift mutant) with and without the overexpression of His-Pfs and His-LuxS, respectively, with adenosine. Then, we assayed for BB170-responsive autoinducer AI-2 activity (Fig. 2-10) (experiments were carried by Yoshi Hashimoto).

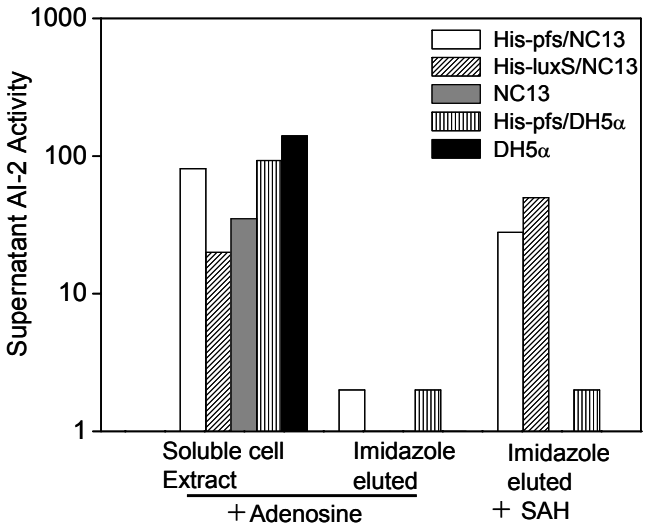

Figure 2-10 AI-2 produced from reactions with substrate adenosine and SAH

V. harveyi responsive autoinducer activity was measured after reaction of (1) adenosine with soluble extracts of cells over-expressing His-Pfs or His-luxS or imidazole eluted fractions of purified His-pfs or His-luxS, and (2) reaction of SAH with purified His-Pfs or His-LuxS. Strains NC13 and DH5α are Pfs and LuxS mutants, respectively.

Interestingly, all reactions of soluble cell extracts incubated with adenosine were found to induce BB170 cells to produce luminescence, irrespective of the absence of His-Pfs or His-LuxS. Further, imidazole eluted fractions of Co^{2+} resin immobilized His-Pfs or His-LuxS induced no or negligible amounts of luminescence when reacted with adenosine (positive controls with SAH showed significant AI-2 production). Reaction of soluble cell extracts with Co^{2+} immobilized enzymes but without adenosine induced negligible luminescence and moreover, adenosine itself showed no independent autoinducer activity on BB170 cells (data not shown here). HPLC analysis revealed no reaction of adenosine with either purified Pfs or LuxS (data not shown here).

Because AI-2 activity is made from cell extracts in the absence of Pfs in one case and LuxS in the other and because the purified enzyme fractions yield no autoinducer from adenosine, we conclude that adenosine is not a substrate for either enzyme. Instead, other enzymes or precursors in soluble cell extracts are likely responsible for converting adenosine to a BB170 responsive autoinducer.

In further studies of *in vitro* AI-2 synthesis, we found that LuxS could act on SAH directly, producing AI-2 activity (Hashimoto *et al*, in preparation). This was not revealed *in vivo* as conditioned medium from *pfs* null mutants were devoid of AI-2. Nevertheless, several preparations of LuxS were shown to convert SAH to AI-2 activity. We note that eukaryotes convert SAH to adenosine and homocysteine via SAH hydrolase in one step. While the products of LuxS mediated SAH degradation do not include adenosine, the potential for enzymatic cross reactivity with SAH was an interesting finding. Thus, we speculated that *E. coli* may convert adenosine to AI-2

via a non-LuxS pathway. Interestingly, an alternative pathway for DPD and AI-2 formation was found in tomato, where DPD was formed from D-ribulose-5-phosphate spontaneously. D-ribulose-5-phosphate was synthesized from D-ribose-5-phosphate and the enzyme is responsible for this conversion is ribose-5-phosphate isomerase (Rpi) (104, 113). In related work, LuxS independent AI-2 formation was reported from a sugar phosphate, ribulose-5-phosphate, which exhibited stronger induction of the AI-2 specific reporter strain than a spontaneously formed product 4-hydroxy-5-methyl-furanone (MHF) from DPD (121, 264). In *E. coli*, adenosine can be salvaged to ribose-1-phosphate through pentose phosphate metabolism, while ribose-1-phosphate can be converted to ribose-5-phosphate by phosphopentomutase, then ribose-5-phosphate can be isomerized to ribulose-5-phosphate (245). The existence of AI-2 from reaction of adenosine with cellular extracts from either *luxS* or *pfs* mutant may then be the result of a series of reactions of adenosine salvation through ribose metabolism. The reconstruction of this pathway *in vitro* is currently underway.

These experimental findings demonstrate that alternative pathways for autoinducer AI-2 formation exist and our simulation results suggest their rates are dependent on glucose. It is uncertain whether all these alternative pathways are related to DPD, whose autocyclization is putatively responsible for AI-2 formation (39, 178, 227). We favor the existence of DPD-related alternative pathways for AI-2 formation because (1) chemically-synthesized DPD was shown to be a strong inducer of AI-2 activity (55, 171) and (2) all the identified autoinducers were shown derived from DPD (178, 232).

In summary, these reports indicate alternative pathways to AI-2 other than those well-

documented exist, among which ribose sugar phosphates may be involved. We suggest that the dramatic AI-2 increase in the presence of glucose may be attributed to the prevalence of sugar phosphates in cells grown with glucose or to other ill-defined pathways in *E. coli*.

Discussions

An SPN model was employed to simulate AI-2 quorum-sensing circuit in *E. coli*. Simulation results agreed well with experimental data, particularly for the case of cells grown in LB media without glucose. The appearance and disappearance of AI-2 in the growth medium was directly calculated based on the known biochemical pathways. The mRNA levels of two important AI-2 synthases (Pfs and LuxS) were accurately depicted. Moreover, the SPN model predicted both the relative increase in synthase level as well as the relative insensitivity of AI-2 due to this perturbation. It is also noteworthy that the variances calculated by the SPN were similar to the experimental errors associated with several of our measurements (e.g., mRNA levels, LuxS, Pfs levels). By representing this network in the Mobius simulation environment, one can with relative ease add additional structure and complexity, in order to generate testable hypotheses regarding the predicted outcomes.

As an example, we speculated that increased metabolic flux from the addition of glucose to the growth media would be required to enhance AI-2 production (additional synthases would be insufficient). This was validated by the simulation results, where a 50% increase in flux resulted in ~35% AI-2 production (Fig. 2-8). More importantly, our simulations led to an hypothesis that a significant increase in

AI-2 production from cells grown with glucose may have resulted from unrevealed alternative pathways involving compounds such as sugar phosphates or other unknown regulators modulating the flux to AI-2 (247, 264). In separate experimental tests using cell extracts, we confirmed that adenosine can be converted to AI-2 from both *pfs* and *luxS* mutants, demonstrating for the first time a biological route to AI-2 from adenosine. It is likely, however, this particular pathway is masked *in vivo* as the addition of adenosine to wt cells does not stimulate AI-2 production (not shown). Our results would suggest that the presence of glucose instead alters the relative flux between these pathways.

We also showed that the level of DPD plays an important role in AI-2 formation. This is consistent with recent reports indicating that DPD is the core molecule for AI-2 formation (171, 232, 233). Our simulations showed that AI-2 production can be effectively influenced by modulating the flux from DPD to AI-2, which can be achieved by increasing the concentration of DPD, or by enhancing the AI-2 synthesis rate constant. However, we note DPD is reportedly highly reactive and unstable (171, 286). Therefore, we believe it is unrealistic that a cell can maintain a high DPD level without chaperones or other compartmentalization moieties for enabling stimulated AI-2 synthesis. It has been demonstrated *in vitro* that AI-2 can be derived from DPD and its two ring-closed equilibrium anomers without enzyme catalysis, suggesting that the species specificity is derived at the level of the cognate receptor (171, 232, 233). In the absence of a DPD-specific efflux transporter, it is likely that DPD undergoes intramolecular nucleophilic attack by the hydroxyl group on the carbonyl carbon *in vivo*, producing five-membered cyclic furanose anomers.

These two anomers go through mutarotation, like other cyclic sugar anomers, and the equilibrium between these two anomers can be shifted due to addition of the boric acid, which can stimulate the production of *V. harveyi* AI-2 anomer and repress the release of the *S. typhimurium* AI-2 anomer (178).

Early in the 1960s, Pigman and Isbell reported that ring closure reactions from unstable acyclic chain forms are extremely rapid with reaction rate constants as high as is 10^2 per minute (202). They also noted that the maximum mutarotation rate between the two cyclic anomers is only about 10^{-2} per minute. At the same time, they noted that if there are no factors other than water to facilitate anomer mutarotation, the reaction rate is very slow, of the order 10^{-3} per minute (128). They further pointed out that this slow mutarotation rate can be increased by factors such as acids or bases. Therefore, we speculated that the ring-closure reaction (from DPD to cyclic AI-2 precursors) is a fast reaction while the mutarotation rate of different cyclic AI-2 anomers is the slow step for forming specific quorum-sensing AI-2 signal. Our initial AI-2 synthesis rate was based on a slow sugar cyclic anomers' mutarotation rate under water's catalysis, which is in the range of the reported literature data. During the simulations with glucose, we increased the initial AI-2 synthesis rate to match experimental data. However, according to the current knowledge of the AI-2 synthesis process, the conversion of DPD to AI-2 is determined exclusively by mass action kinetics at a presumably constant temperature, pressure, pH, etc. Hence, it is infeasible that the AI-2 reaction rate from DPD, as described here, will increase so dramatically unless the concentration of DPD within the cell increases concomitantly, which is seemingly also infeasible.

In order to rectify these discrepancies, it is logical that other enzyme or chaperone mediated activities interact with the DPD → AI-2 reaction or other pathways lead to a substantial (~2-3 fold) increase in flux to DPD within the cell. Hauck *et al*. already demonstrated the existence of an alternative pathway to AI-2 and Tavender *et al*. showed that ribulose-5-phosphate can strongly induce the bioluminescence of AI-2 specific response reporter (113, 264). Adenosine can be shunted to ribulose-5-phosphate through pentose phosphate metabolism, therefore we suspect that ribose sugar phosphates may be possible candidates for conversion to AI-2. Independently, we measured transcript levels of the enzymes involved in the oxidative pentose phosphate pathway (catalyzing reactions from glucose-6-phosphate to ribulose-5-phosphate) and they were observed to increase about 1.4 to 2.1 fold due to the presence of glucose (in DNA microarray experiments not shown here; Wang *et al.*, in preparation). Increased activity of these enzymes may yield more ribulose-5-phosphate, a putative precursor for AI-2 (113, 264).

It is particularly noteworthy that there are two different structures of AI-2 reported from the same precursor, DPD (39, 178) in two different biological systems. If there is more than one reaction for producing or consuming one metabolite, it is more likely that one reaction dominates (6). Based on this theory, one autoinducer structure should be favored. Bassler and co-workers have already demonstrated this by showing that the AI-2 structure in *Vibrio harveyi* is distinct from that in *Salmonella typhimurium*, where boric acid can shift the direction/equilibrium of these two different structure signal molecules (178). It is not unreasonable to suggest that under different biological contexts (microbe, microenvironment, etc.), the pathways

for the formation of AI-2 are different. This is corroborated by our calculations demonstrating that the AI-2 synthesis rates in the absence and presence of glucose are different and change over time. One might even expect that the resultant AI-2 structure varies as growth condition changes. Analogously, we have already demonstrated that genes affected by *luxS* mutation vary with growth condition, such as cell density or glucose addition (277).

Questions such as these arise, and can be put into an experimental context, upon the examination of model simulations relative to experimental observations. The use of SPN in Mobius environment makes the implementation of a model easier than using other programming languages, there is no need to write specific code for each model. This makes it easy to replicate, modify or extend a particular model (99) so that a large system can be decomposed into several small systems which can then be reconstituted into more complex systems of larger scale. Indeed, our current model was originally comprised of an AI-2 synthesis model only. This makes it possible to achieve an integrated understanding of the hierarchical nature of quorum signaling regulatory cascades. For different layers of genetic pathways, from available biological information, we can construct models as we did in this study, then modify and integrate them for a global model based on experimental validation.

Acknowledgements

We thank B. L. Bassler, H. Aiba, R. Kolter, A. Hochschild, L. I. Rothfield, and M. Berlyn for generously providing strains and plasmids used in the study. We are very grateful to the wonderful discussions and suggestions from Daniel Mitchell, Stephen Ramsey about SBML. We are grateful to the proofreading from J. March. This work

was supported by the National Science Foundation (Grants BES-0124401, BES-0222687).

Chapter 3: Transcriptional Analysis of *lsrR* and *lsrK*

Abstract

Currently, except the *lsrACDBFG* operon, no other genes are identified responsive to the AI-2/phospho-AI-2 mediated quorum sensing regulations. LsrR was suggested as a quorum sensing uptake repressor and LsrK was revealed to phosphorylate AI-2 in *Salmonella*. Similar functions have been suggested for these two genes in *E. coli* due to the homology. Therefore, the possibility was tested with an *lsrR* promoter *lacZ* fusion reporter *lsrR*-lacZ, and an *lsrK* promoter lacZ fusion reporter *lsrK*-lacZ. From these fusion reporters' analysis, *lsrR* was found subject to negative regulation of *lsr* and *lsrR,* and positive regulation of cyclic AMP Receptor Protein (CRP) and *luxS, lsrK* genes. However, *lsrK* transcription was only subject to catabolite repression but not other quorum sensing regulatory genes. A reverse transcriptase (RT) PCR analysis discovered the existence of a monocistronic mRNA spanning the whole coding region of *lsrR* and *lsrK*. This demonstrated that *lsrR* and *lsrK* belong to the same operon and that *lsrK* regulated additionally by *lsrK* promoter except *lsrR* promoter. In order to further characterize the regulations associated with LsrR repressor, recombinant LsrR protein was expressed in *lsr*-lacZ fusion reporter strains, which resulted in reduced *lsr* expression. This recombinant protein was expressed in *lsrR* mutants and purified for further gel-motility shift analysis of the interactions between LsrR protein and its operator DNAs, including *lsr*, *lsrR* promoter. These investigations undoubtley expanded the recently identified AI-2 uptake network and broadened the *E. coli* quorum sensing regulations.

Introduction

In *E. coli*, extracellular AI-2 peaks during the mid exponential phase and rapidly decreases during the entry of stationary phase. At the same time, LuxS protein does not decreases correspondingly (109, 293). The disappearance of extracellular AI-2 activity in *E. coli* and *S. typhimurium* was due to the importation of an ATP-binding cassette (ABC) transporter named the *luxS*-regulated (Lsr) transporter(260, 276, 293). Recently, this AI-2 uptake regulatory network, including a transporter Lsr, its putative repressor LsrR and kinase LsrK have been partially identified in *E. coli* (276).

The uptake of extracellular AI-2 is subject to cAMP-CRP regulations in *E. coli* and *S. typhimurium* (260, 276). Specifically, CRP protein was demonstrated binding to a cAMP-CRP binding site located upstream of *lsr* promoter in *E. coli* (276). AI-2 uptake was also reported being repressed in a *glpD* mutant, which encodes glycerol-3-phosphate (G3P) dehydrogenase. G3P, involving in glycerol and G3P metabolism, accumulated in the *glpD* mutant and then repressed *lsr* transcription through catabolite repression (293). A reduced transcription of *lsr* promoter of *S. typhimurium* was revealed in *cya* and *pstI* mutants, wherein these two genes indirectly affect catabolite repression. Besides that, the uptake of AI-2 is also controlled by the expression of *lsr* operon's repressor LsrR in *E. coli* and *S. typhimurium* (260, 276, 293) A kinase, LsrK in *S. typhimurium* can phosphorylate AI-2 into phospho-AI-2 and the phospho-AI-2 has been proposed as the inducer responsible for derepressing LsrR's repression on the *lsr* operon (260). Similar mechanism probably presented in *E. coli* as well (276, 293). DHAP (dihydroxy-acetone phosphate) or its derivative repressed *lsr* transcription by preventing the binding of phospho-AI-2 to LsrR (293).

In *S. typhimurium*, LsrF and LsrG are involved in modifying and processing phospho-AI-2 (260). Xavier *et al.* suggested that one of the modification products from phospho-AI-2 probably is DHAP because pentose phosphates are often converted to DHAP for further metabolism (293).

In order to further characterize the regulatory mechanims associated with *lsrR*, *lsrK* in *E. coli* quorum sensing uptake system, we constructed *lsrR*-lacZ, *lsrK*-lacZ fusion reporter to study the transcriptional regulations associated with these two genes. The transcriptional analyses revealed that *lsrR* is subject to catabolite repression and negative regulation of LsrR, while subject to positive regulation of *luxS* and *lsrK*. However, *lsrK* transcription is only positively regulated by cAMP-CRP. The existence of monocistronic transcript among *lsrR* and *lsrK* coding region revealed that these two genes belong to the same operon, named *lsrRK* operon. Therefore, *lsrK* transcription is regulated by *lsrR* promoter, additionally mediated by *lsrK* promoter. LsrR overexpression in an *lsr*-lacZ reporter strain significantly repressed *lsr* transcription.

Materials and Methods

Bacterial strains and growth conditions. The bacterial strains and plasmids used in this study are listed in Table 3-1. *E. coli* K-12 strain W3110 (F^-, λ^-, in(*rrn*D-*rrn*E)) was obtained from Genetic Stock Center (New Haven, Connecticut). Cultures of *E. coli* (wild type and different mutants) that had been grown overnight in LB or LB plus 0.8% glucose were diluted to OD_{600} about 0.03 in LB or LB plus 0.8% glucose. The cultures were then incubated at 30°C with shaking at 250 rpm in 50 ml flasks.

Table 3-1 Bacterial strains and plasmids used in this study

Strain/plasmid	Relevant genotype and property	Source or reference
Strains		
E. coli		
W3110	Wild type	Laboratory stock
LW1	W3110 Δ*crp*::Kan	Laboratory stock
LW5	W3110 Δ(*lsrACDBFG*)::Kan	Laboratory stock
LW6	W3110 Δ*lsrR*::Kan	Laboratory stock
LW10	W3110 Δ*lsrK*::Kan	Laboratory stock
HT28	W3110 Δ*cya*::Kan	(142)
ZK126	W3110 Δ*lacU*169 tna-2	(45)
ZK1000	ZK126 Δ*rpoS*::Kan	(24)
LW2	ZK126 Δ*crp*::Kan	Laboratory stock
LW7	ZK126 Δ*luxS*::Kan	Laboratory stock
LW8	ZK126 Δ*lsrR*::Kan	Laboratory stock
LW9	ZK126 Δ(*lsrACDBFG*)::Kan	Laboratory stock
LW11	ZK126 Δ*lsrK*::Kan	Laboratory stock
DH5α	*recA1 supE44 endA1 hsdR17 gyrA96 relA1 thiΔ (lac-proAB)* F' [*traD36 proAB+ lacI*^{q} *lacZΔM15*]	Invitrogen
V. harveyi		
BB152	BB120 *luxL*::Tn5 (AI-1-, AI-2+)	(257)
BB170	BB120 *luxN*::Tn5 (sensor 1- ,sensor 2+)	(15)
Plasmids		
pFZY1	galK'-lacZYA transcriptional fusion vector, Ap^r	(147)
pLsrR-BAD	pBAD202D derivative, containing *lsrR* coding sequence, Kan^r	This study

Plasmid construction. The plasmids used in this study are listed in Table 3-1, and were generated using standard procedures (221). Restriction enzymes, T4 DNA ligase and Vent DNA polymerase were used as specified by the manufacturer (New England Biolabs, Beverly, MA). *E. coli* W3110 chromosomal DNA preparation was performed using the Qiagen Dneasy Tissue Kit (Qiagen, Valencia, CA). Extractions of DNA from agarose gels were performed using the Qiagen QIAEX II Gel

Extraction Kit. Oligonucleotides were from Integrated DNA Technologies (Coralville, IA). DNA sequencing was performed at the DNA core facility of the Center of Biosystems Research (University of Maryland Biotechnology Institute). All constructs made by PCR were sequenced to verify their integrity.

Plasmid pFZY1 is a mini-F derivative (average copy number, 1 to 2 per cell) with a polycloning site upstream of a promoterless *galK'-lacZYA* reporter segment (147). To create pJLlsrR, the *lsrR* promoter region (-340 to +59 relative to the start codon of *lsrR* (b1512)) was amplified by PCR using primers lsrRpF and lsrRpR (Table 3-2). The purified PCR product was digested with EcoRI-BamHI, and was inserted into EcoRI-BamHI digested pFZY1. To create pJLlsrK, the *lsrK* promoter region (-367 to +53 relative to the start codon of *lsrK* (b1511)) was amplified by PCR using primers lsrKpFn1 and lsrKpRn2 (Table 3-2). The purified PCR product was digested with EcoRI-BamHI, and was inserted into EcoRI-BamHI digested pFZY1.

Plasmid pBAD202D, with a topoismoerase I and a 3' single-stranded overhang, can directionally clone the blunt PCR product in the needed orientation (Invitrogen). To create pLsrR-BAD, the entire *lsrR* coding region was amplified by PCR using primers lsrRpBADF1 and lsr-pBADR1 (Table 3-2). The purified PCR product was inserted into pBAD202D.

RT-PCR. cDNA was synthesized from total RNA and random hexamers using the SuperScriptTM III First-Strand Synthesis System for Reverse Transcriptase(RT)-PCR (Invitrogen) according to the manufacturer's instructions. Regular PCR was then used

to check existence of the *lsrRK* operon, and data was presented from reactions using 22 amplification cycles. Primers were designed and purchased from Integrated DNA Technologies (Coralville, IA).

Table 3-2 Primers used in this study

Name	Sequence	Relevant description
lsrRpF	CCGGAATTCTCGATGCCTTTCAG GACATTG	Upstream primer for cloning *lsrR* promoter
lsrRpR	CTCGGATCCGCGACCTGTTCTTCT TCACACATT	Downstream primer for cloning *lsrR* promoter
lsrKpFn1	CCGGAATTCTCGCTCCGGTTATA TCAGCCAGGGCGAACA	Upstream primer for cloning *lsrK* promoter
lsrKpRn2	CTCGGATCCTCCAGCGCCATCAG GTAGTACTTT	Downstream primer for cloning *lsrK* promoter
lsrRpBADF1	CACCATGACAATC AACG ATTC GGCA	Upstream primer for cloning *lsrR* sequence
lsrRpBADR1	TTAACTACGTAAAATCGCCGCTG CTGT	Downstream primer for cloning *lsrR* sequence
lsrRbF	AATTCATTCTTCACTTTGAACAT ATTTAAATCTTTAATGCAATTGT TCAGTTCT	Upstream sequence for annealing *lsrR* promoter for binding with LsrR protein
lsrRbR	AGAACTGAACAATTGCATTAAAG ATTTAAATATGTTCAAAGTGAAG AATGAATT	Downstream sequence for annealing *lsrR* promoter for binding with LsrR protein
lsrbF	GGTTATGAACAAATTAAAAGCAG AAATACATTTGTTCAAAACTCAC CTGCAAAACTGAACGGGGGAAA T	Upstream sequence for annealing *lsr* promoter for binding with LsrR protein
lsrRbR	ATTTCCCCCGTTCAGTTTTGCAGG TGAGTTTTGAACAAATGTATTTCT GCTTTTAATTTGTTCATAACC	Downstream sequence for annealing *lsr* promoter for binding with LsrR protein
lsrK3	AATGTGCCGGTTTCTTTGAC	Primer for RT-PCR of *lsrR-lsrK*
lsrR3	TTATATCAGCCAGGGCGAAC	Primer for RT-PCR of *lsrR-lsrK*

β-galactosidase assays. Cultures of *E. coli* were grown overnight in LB, diluted 100-fold into fresh LB and grown to mid-exponential phase, then diluted into different mediums with OD_{600} around 0.03. The cultures were incubated at 30°C with shaking at 250 rpm in flasks. Samples were removed at regular intervals for determination of OD_{600} and β-galactosidase activity. Specific activity of β-galactosidase is expressed as Miller units (175).

Expression and purification of the LsrR repressor protein. *E. coli* strain DH5α bearing pLsrR-BAD was grown LB medium. After the optical density at 600nm reached 0.4~0.5, the culture was induced with 0.2% arabinose for 6 hour. Cells were harvested by centrifugation and stored at −80°C. All purification procedures were performed at 4°C. The cells were resuspended in PBS buffer with 10 mM immidazole (pH 7.4,) and disrupted by sonication on ice, and cell debris was removed by centrifugation. The solution was loaded nickel Chelating Sepharose™ High Performa column that had been equilibrated in equilibrium buffer (20mM PO_4^{3-}, 250mM NaCl, 10 mM immidazole, pH 7.4). Ten column volumes of equilibrium buffer was allowed to flow through the column, and then 5 column volumes of washing buffer (20mM PO_4^{3-}, 250mM NaCl, 10 mM immidazole concentration, pH 7.4) were allowed to flow through the column. LsrR was eluted using a different imidazole gradient from 20 to 300 mM in washing buffer. The eluted protein samples were dialyzed in PBS buffer.and frozen at −80°C in 50-µl aliquots. The purified protein was checked by SDS-PAGE and western blot by anti-Thio (Invitrogen). Approximately 10 mg of LsrR was purified from 1 liter cell culture.

Similarly DH5α bearing pBAD (no *lsrR* gene insertion) was grown LB medium. LsrR null protein was purified the same procedure as stated above, which was used as a control during Gel motility shift assay.

Gel motility shift assay. The 69 bp DNA fragments containing *lsr* promoter and 70 bp DNA fragments containing *lsrR* promoter regions were synthesized by Integrated DNA Technologies (Coralville, IA)(Table 3-2). A digoxygenin (DIG) gel shift kit

(Boehringer Mannheim) was used for labeling of DNA fragments and detection of signals according to the manufacturer's instructions. Binding reactions were performed by incubating the labeled DNA fragments with various amount of purified LsrR in 20 μl of binding buffer (10 mM Tris-HCl [pH8.0], 50 mM KCl, 1 mM EDTA, 1 mM dithiothreitol, 50 μg ml^{-1} bovine serum albumin, 15 μg ml^{-1} sonicated salmon sperm DNA). Following incubation at 37°C for 10 min, 5 μl of gel loading buffer (0.25 x TBE, 60%; glycerol, 40%; bromphenol, 0.2% [w/v]) was added and mixtures were electrophoresed in a 6% native polyacrylamide gel in 0.5 x TBE buffer (45 mM Tris-borate, 1 mM EDTA, pH 8.0). DNA bands were detected according to the manufacturer's instructions.

Result

Transcriptional regulation of *lsrR* by LsrR and CRP

Previous microarray analysis demonstrated that *lsrR* expression is induced by *luxS* gene and validated by quantitive RT-PCR (277). *Lsr* operon is also induced by *luxS* which suggest that the repression of LsrR on *lsr* regulon released or decreased due to the presence of phospho-AI-2. To investigate the control of *lsrR* transcription in greater detail, we constructed a *lacZ* fusion plasmid containing the *lsrR* promoter region and checked its expression levels in different mutant strains and growth conditions (Fig. 3-1). The overall regulatory pattern of the *lsrR* gene is similar to that of the *lsr* operon (276). When the wild type ZK126 cells (*lsrR-lacZ*) were grown in LB medium, transcription from the *lsrR* promoter remained low until the cells entered the stationary phase. Deletion of *lsrR* significantly increased *lsrR* expression,

indicating that the *lsrR* transcription was self-repressed. Deletion of either *luxS* or *lsrK* dramatically reduced the *lsrR* expression because there is no AI-2/phospho-AI-2 available in these two mutants (260). Deletion of the *lsrACDBFG* operon increased the *lsrR* transcription even with slower AI-2 importation, which suggested the existence of alternative AI-2 importer and possible similar phospho-AI-2 degradation enzymes (LsrF and LsrG) (260, 276). The addition of glucose in LB medium significantly reduced *lsrR* transcription, and the deletion of the *crp* gene resulted in similar effects on *lsrR* expression as the addition of glucose (Fig. 3-1). These results suggested that *lsrR* expression was subject to catabolite repression, and CRP was needed for stimulation of the *lsrR* transcription. In our previous research, a CRP binding site (CRP I) located upstream of the *lsr* promoter region was identified, which is necessary for activation of the *lsr* operon (276). Examination of the intergenic region between *lsrR* and *lsr* operon, which are transcribed divergently, revealed another CRP binding site (CRP II), which has a typical 6-bp spacer between two conserved motifs. Gel mobility shift assay (Carried by Liang Wang) results demonstrated that cAMP-CRP binds to a 46 bp DNA fragment in the intergenic region containing this site (277). CRP did not bind the identical DNA fragment with substitutions in four base pairs of one of the CRP-binding motifs. These positively confirm CRP binding capability to the *lsrR* regulatory region. Whether the two CRP binding sites are independent or cooperate in stimulation of transcription of *lsrR* and the *lsr* operon needs further investigation, however, these results clearly indicate that the promoters of *lsrR* and the *lsr* operon are both subject to LsrR repression and CRP activation.

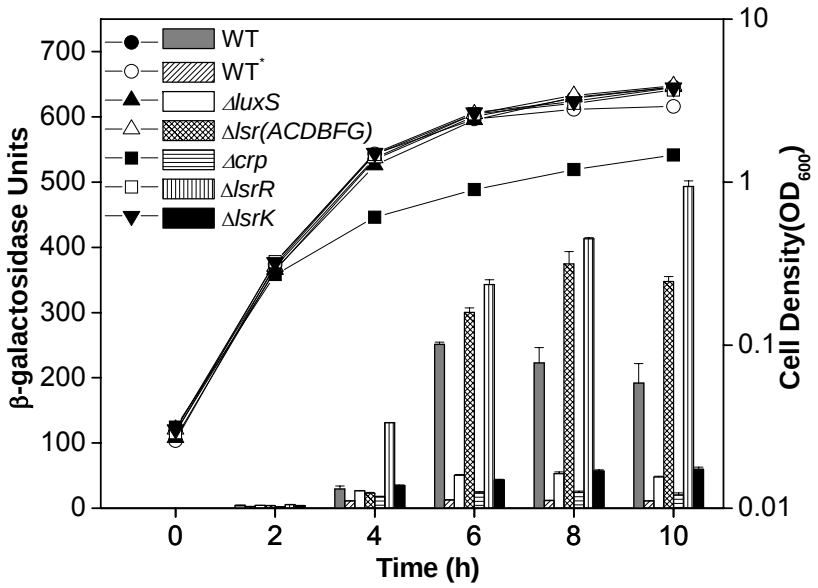

Figure 3-1 Transcriptional regulation of *lsrR* expression

Transcriptional regulation of *lsrR* expression. *E. coli* ZK126 (wild type) and strains containing deletion of *crp*, *luxS*, *lsrK*, *lsrR*, and *lsrACDBFG* carry plasmid pJLlsrR (*lsrR-lacZ*). All strains were grown in LB medium except for ZK126 (WT*), which was grown in LB plus 0.8% glucose. At different time points during cell growth, aliquots were collected for measurement of the OD_{600} (circles, triangles, and squares) and ß-galactosidase activity (bars).

Disrupt of *rpoS* also increased the *lsrR*-lacZ transcription (Fig 3-2), which means quorum sensing uptake repressor LsrR probably interacting with *rpoS* to globally mediate cellular phenotype and processes.

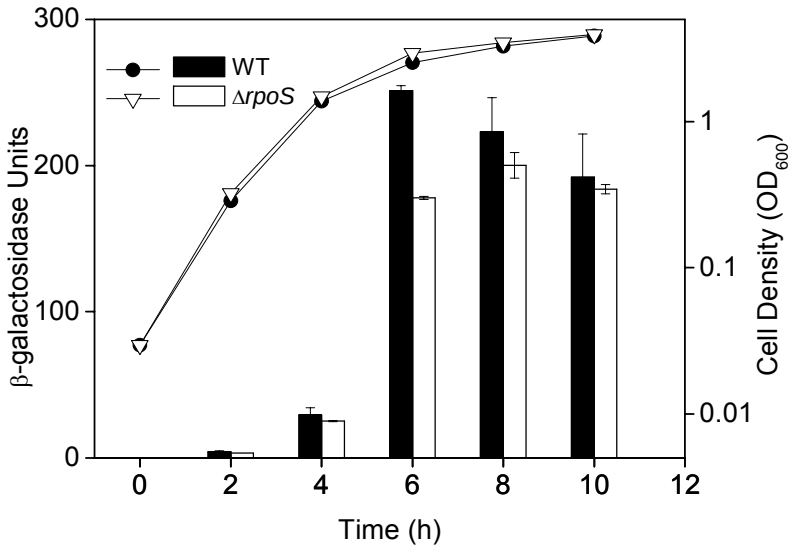

Figure 3-2 Deletion of *rpoS* increase *lsrR* expression

***lsrK* and *lsrR* belong to the same operon**

Microarray and quantitive RT-PCR results showed that *lsrK* expression was increased in the presence of *luxS*. This is consistent with its role as a kinase that phosphorylates uptaken AI-2 to phospho-AI-2, which has been suggested as an inducer for derepress *lsrR* meidations. To confirm regulation of *lsrK* expression, we constructed another *lacZ* fusion plasmid with the *lsrK* promoter region (-367 to +53 relative to the start codon of *lsrK*). Surprisingly, deletion of *luxS*, *lsrR*, *lsrK*, or *lsr* operon, did not affect *lsrK* expression compared to the wild type (Fig. 3-3). In addition, the β-galactosidase activities for the *lsrK-lacZ* fusion were more than 20-fold lower than those of the *lsrR-lacZ* fusion (Fig. 3-1, 3-3). However, similar hybridization signals for *lsrK* and *lsrR* in the wild type cells during the microarray experiments were observed (277).

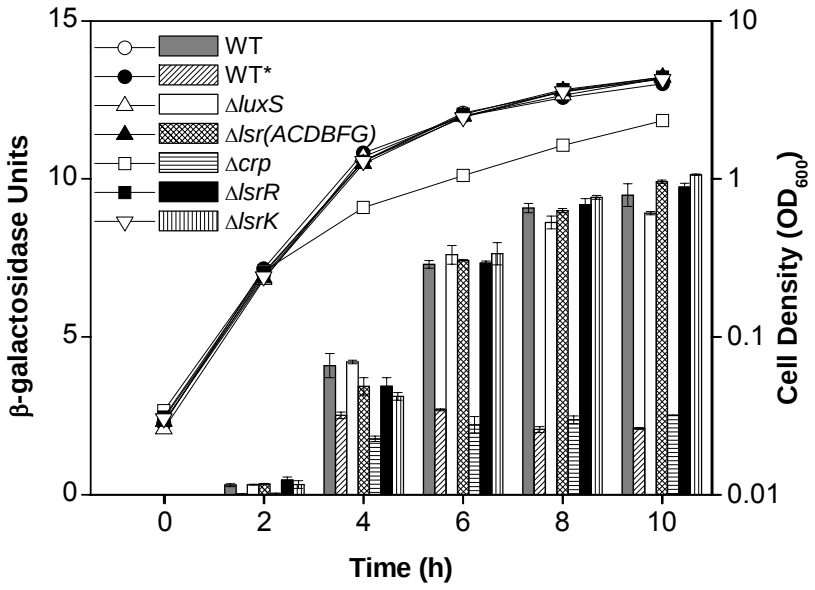

Figure 3-3 Transcriptional regulation of *lsrK* expression

E. coli ZK126 (wild type) and strains containing deletions of *crp*, *luxS*, *lsrK*, *lsrR*, and *lsrACDBFG* carry plasmid pJLlsrK (*lsrK-lacZ*). All strains were grown in LB medium except ZK126 (WT*), which was grown in LB plus 0.8% glucose. At different time points during cell growth, aliquots were collected for measurement of the OD_{600} (circles, triangles, and squares) and ß-galactosidase activity (bars).

Further, it was also found that the *luxS* mutant cells had *lsrK* hybridization signals that were much lower than that for *lsrR* (data not shown). Therefore, we speculated that *lsrK* could be transcribed together with *lsrR* under control of *lsrR* promoter. To test this idea (*lsrRK* operon), a regular RT-PCR was performed (differential display, experiments carried by John March) (Fig 3-4) and there is a monocistronic transcript spanning the coding sequences of both *lsrR* and *lsrK* (277).

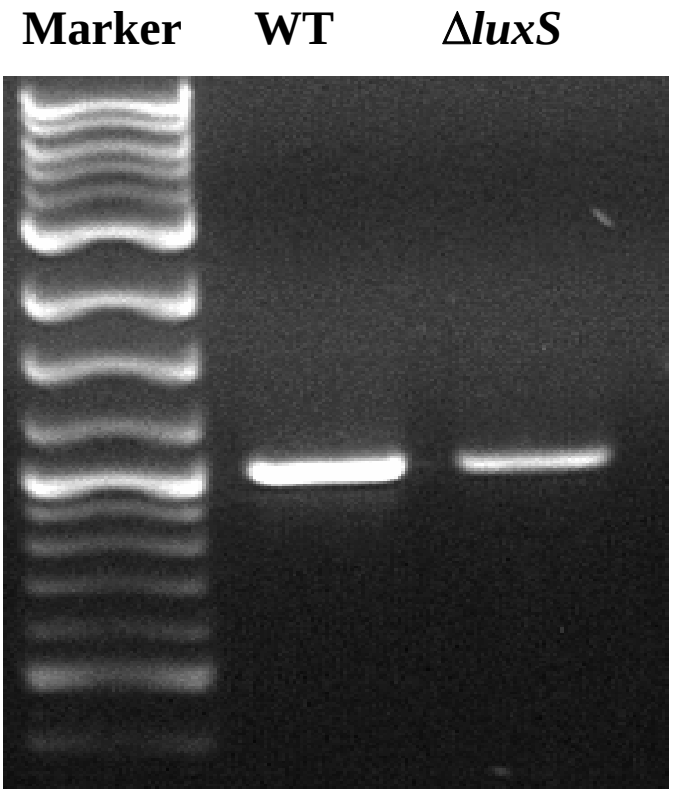

Figure 3-4 Transcriptional analysis for *lsrRK* operon
The agarose gel was run to show DNA fragments obtained from RT-PCR of total RNA prepared from the OD 2.4 cell cultures of the wild type (WT) and the Δ*luxS* mutant grown in LB. Specific primers were used to amplify the fragments that span coding sequences of the *lsrR-lsrK* genes. The 2-log DNA ladder (New England BioLabs) was used.

Also the addition of glucose (0.8%) to the growth medium or deletion of *crp* gene reduced transcription of the *lsrK-lacZ* fusion (Fig. 3-3), which suggests the additional catabolite repression control of *lsrK* by CRP. The detailed molecular interactions between *lsrK* promoter and CRP await further studies.

Overexpression of *lsrR* represses in vivo *lsr* transcription

Quorum sensing signal repressor to regulate gene expression is commonly existed. For examples, LuxR type protein binding with AI-1 signals to mediate gene expression including bioluminescence induction (90). Numerous researches have also demonstrated that quorum sensing regulators mediate many cellular phenotypes and morphologies (52, 105, 117): quorum sensing regulator LuxR was reported to regulate type III secretion in *V. harveyi* (117); HapR of *V. cholerea* represses virulence cascade and biofilm-related genes and activates protease production at high cell densities (105, 130, 148); VirR mutation in *Erwinia carotovora* ssp. *atroseptica* (*Eca)* completely restores virulence factor production to an *Eca* mutant (29).

In order to further discover the regulations and interactions associated with LsrR repressor, we overexpressed this protein in an *lsr*-lacZ reporter system. Consistent with our previous results, the overexpression of *lsrR* resulted in down-regulation of *lsr* transcription (Fig 3-5). This demonstrated that LsrR represses *lsr* transcription significantly. Therefore a thioredoxin-tagged LsrR protein was expressed and purified to investigate the binding of LsrR with *lsr* promoter. Purified pools was checked on sodium dodecyl sulfate-polyacrylamide gel electrophoresis (SDS-PAGE) and detected by Anti-Thio, results are shown in Fig 3-6. LsrR started to elute from the column at the 20 mM immidazole concentration, which probably because the thioredoxin tag only has two modified His residue for binding. Maybe a His-tagged recombinant LsrR protein will help to solve this problem and provide higher purity protein.

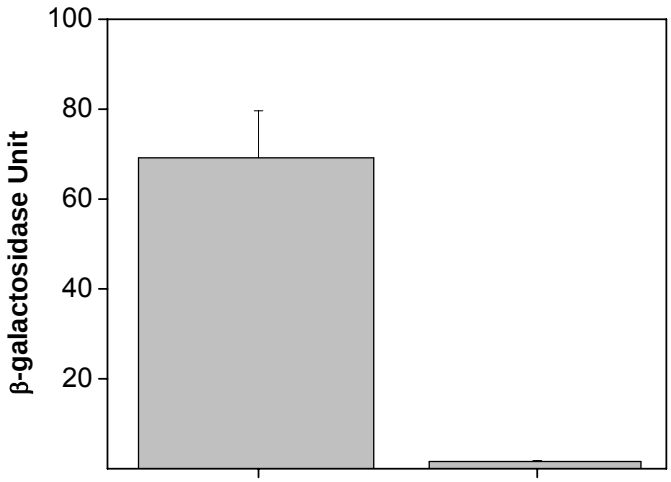

Figure 3-5 LsrR overexpression represses *lsr* transcription
Measured b-galactosidase unit for *lsr*-lacZ fusion reporter in ZK126 *lsrR* mutant without or with *lsrR* expression.

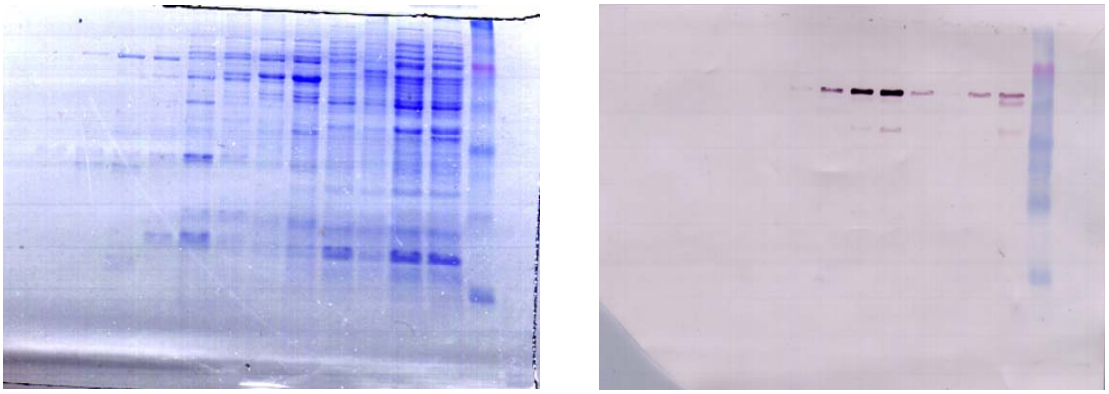

Figure 3-6 LsrR purification and detection by Comassie stain and Western blot

Lanes from right to left: lane 1 Marker, lane 2, cell lycate, lane 3 supernatant of cell lycate, lane 4 flow through, lane 5, 10 mM imidazole washing buffer, lane 6-lane 13, 20mM,30,40,50,60,100,150,300 mM imidazole eluted protein pools.

(**A**)

(**B**)

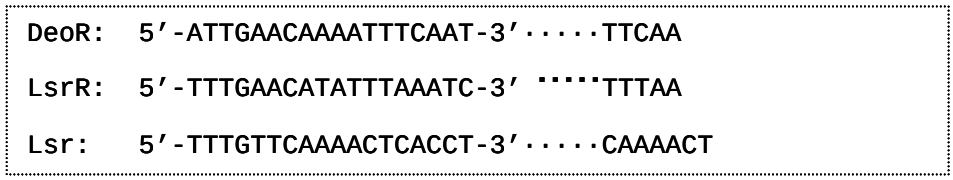

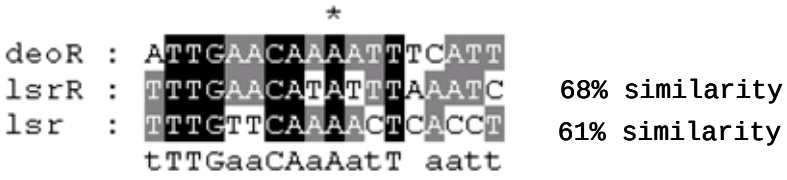

Figure 3-7 Determination of LsrR binding site on *lsr*, *lsrR* promoter

The intergenic region sequence between *lsrR* and *lsr* operon was analyzed by RegulonDB for possible promoter region for both gene. Then similarity analysis against DoeR binding site was carried out since LsrR in *E. coli* and DeoR in *B. subtilis* because both proteins belong to the same SorC protein family (295). Two similar binding sites were found from the intergenic region (Fig 3-7). Through sequence similarity analysis with DeoR binding site, a 69 bp DNA sequence located from -69 to -1 (according to *lsr* translational initiation codon) was used to react with purified LsrR protein. Another 54 bp long predicted promoter region (-1 to -54, according to *lsrR* translational initiation codon) also reacted with purified LsrR protein. Since LsrR was found self-repressed, we also carried the same gel-motility shift assay for *lsrR* promoter sequence. However, we could not see evident shift (Fig 3-7). Different protein concentration was tested but no evident shift either (Data not shown here). This is probably because the binding of LsrR with *lsr* promoter needs help from some other molecules. CRP probably a good candidate since both promoters need the activation of CRP protein to initiate the transcription (276, 277), it is possible that two activator site mediate the formation of probable DNA loops to cooperate with its repressor protein LsrR. Therefore, we are going to utilize the CRP protein as our positive control for LsrR-*lsr* promoter binding assay: the whole intergenic region will be PCR out and reacted with CRP protein (positive control) and then purified LsrR protein will be added and multi-band shift are expected. Another possible candidate for helping binding probably some AI-2 anomers or processed AI-2 since dRib-5-P was demonstrated as an inter inducer cooperating the binding between DeoR and its DNA operator (299). If this is the case, the binding assay will

be more complicated to test. I*n vitro* synthesized AI-2 might be helpful for this binding assay.

Discussions

Investigations of *lsrR*-lacZ, *lsrK*-lacZ fusion reporters in different mutants elucidated the interactions between *lsrR*, *lsrK* and their associated transporter *lsr* operon, AI-2 synthase gene *luxS* and catabolite repression gene *crp* , which expanded the uptake regulatory network from our previous research (276): LsrR is subject to the induction of *luxS* and *lsrK*, and the repression of itself and *crp*. LsrR repression effect was also validated by its *in trans* expression under *lsrR* mutant, where *lsr* transcription was significantly repressed due to the expression of LsrR protein (detected by Anti-Thio). LsrR protein was then expressed and purified for *in vitro* analysis of LsrR's function. The modified Thio-redoxin tagged protein did not lead to higher purity protein, maybe a common His tag will help solve this problem and provide more pure LsrR protein. The direct binding of LsrR repressor with its DNA operators was characterized by DNA gel motility shift assay. Even though we did not find evident shift from current work, hopefully the refined binding assay will point us to the right directions.

Since *lsrR*, *lsrK* regulate for AI-2 uptake together with lsr operon, it will be interesting whether this uptake regulatory network affect other cellular phenotypes and morphologies related to quorum sensing process. This will be discussed in the following chapter.

Chapter 4: Quorum Signal AI-2 Uptake Regulators in *Escherichia coli* Affects Biofilm Architecture and sRNA Regulations

Abstract

Recently, the AI-2 uptake regulatory network, comprised of a transporter Lsr, its repressor LsrR and cognate kinase LsrK, was identified in *E. coli*. This regulatory network has been shown to be an integral part of the AI-2 quorum-sensing cascade. This complex regulatory network involving transport and subsequent processing of quorum signal, via LsrR- and LsrK- mediated regulation, may have an impact on other cellular functions. The elucidation of these underlying mechanisms will provide valuable insight into the quorum sensing behavior of *E. coli*.

In this study, we characterized the physiological changes due to the genomic deletion of *lsrR*, *lsrK*. We discovered that many genes were co-regulated by *lsrK* and *lsrR* but in a distinctly different manner than the *lsr* operon (where LsrR serves as a repressor that is derepressed by the binding of phospho-AI-2 to the LsrR protein). Additionally, we found that both the quantity and architecture of biofilms were regulated by this distinct mechanism, as *lsrK* and *lsrR* knockouts behave identically. Similar biofilm architectures probably resulted from the concerted response of a set of genes including *flu* and *wza*. We also found lots of genes regulated either by *lsrR* or *lsrK*, where the specific mechanisms still await further investigations. Interestingly we also observed several small RNA regulators involved with quorum sensing cascade, including a global regulator DsrA. This suggests that *E. coli* quorum sensing signal probably utilizes small RNA to fine-tune cellular phenotype as observed in other bacterial systems.

Introduction

Bacteria communicate with each other through small 'hormone-like' organic molecules referred to as autoinducers. Autoinducer-based bacterial cell-to-cell communication enabling population-based multicellularity has been termed quorum sensing (90). Cellular functions controlled by quorum sensing are varied and reflect the needs of a particular bacterial species for inhabiting a given niche (34, 140, 272).

Quorum sensing in *Escherichia coli* and *Salmonella* has been a topic of great interest and different intercellular signaling systems have been identified: that mediated by LuxR homolog, SdiA; the LuxS/AI-2 system; an AI-3 system; and a signaling system mediated by indole (5, 54, 124, 237, 247, 275). Among these, the LuxS/AI-2 system possesses the unique feature of endowing cell population-dependent behavior while interacting with central metabolism through the intracellular activated methyl cycle (272, 287). Therefore, it has the potential to influence both gene regulation and bacterial fitness.

AI-2's function has been studied using *luxS* mutants and by adding conditioned medium or *in vitro* synthesized AI-2 to bacterial cultures. It is noteworthy that the *luxS* transcription profile is not synchronous with the accumulation profile of extracellular AI-2 in bacterial supernatants (18, 109, 293). In *E. coli*, extracellular AI-2 activity peaks during the mid exponential phase and rapidly decreases during entry into the stationary phase. A corresponding decrease LuxS protein levels is not observed (109, 293). The disappearance of extracellular AI-2 activity in *E. coli* and *S. typhimurium* is due to its uptake, carried out by its import through an ATP-binding cassette (ABC) transporter named the *luxS*-regulated (Lsr)

transporter (260, 276, 293). The transporter proteins are part of the *lsr* operon, which is regulated by two genes, *lsrK* and *lsrR*, located immediately upstream and divergently transcribed in its own *lsrRK* operon (277). Cytoplasmic kinase, LsrK, phosphorylates AI-2 into an activated molecule that is suggested to bind and de-repress the *lsr* repressor LsrR. LsrF and LsrG, located downstream of the Lsr transporter, were found to process and degrade phospho-AI-2. An analogous network has been proposed in *E. coli* based on gene sequence similarity (260, 261), and is now partially elucidated (276, 293) (Fig. 4-1).

Because of their role in regulating the AI-2 signaling molecule, LsrR and LsrK are among the first positively identified quorum sensing regulators in *E. coli* (54, 277, 293). Previous research has demonstrated that quorum sensing regulators mediate many cellular phenotypes and morphologies (52, 105, 117): HapR of *V. cholerea* represses virulence cascade and biofilm-related genes and activates protease production at high cell densities (105, 130, 148). The deletion of *hapR* results in increased expression of virulence regulator, AphA, and biofilm formation (105, 148); *V. harveyi* quorum sensing regulator LuxR was also reported to regulate type III secretion (117); VirR mutation in *Erwinia carotovora* ssp. *atroseptica* (*Eca)* completely restores virulence factor production to an *Eca* mutant (29).

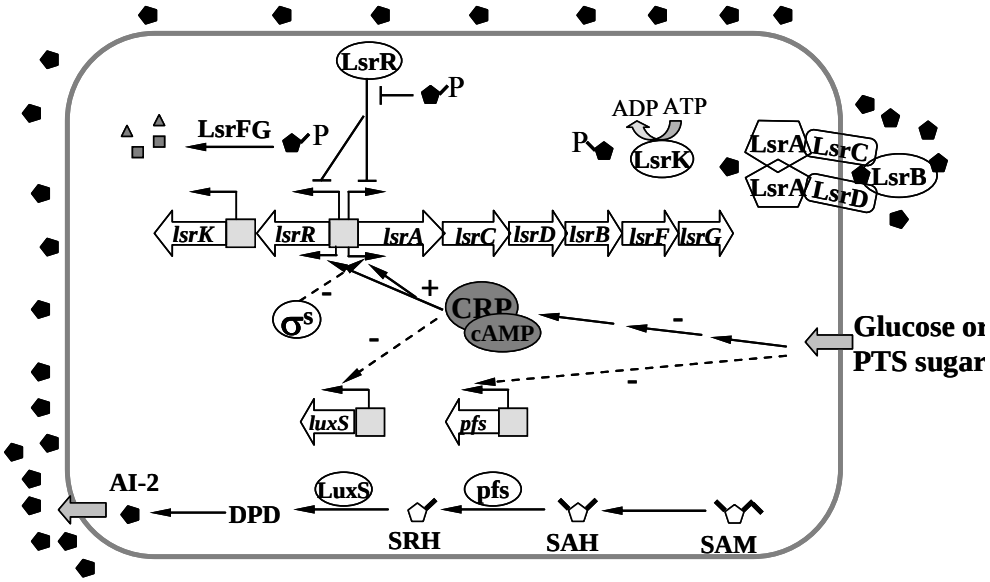

Figure 4-1 Regulation of AI-2 uptake network
(Adapted from Wang *et al.* 2005, J Bact (187):8350-8360)

While it is well known that AI-2 uptake is an integral part of the quorum-sensing network, it remains intriguing that AI-2 signaling bacteria actively transport its QS autoinducer – in many other systems the signal molecule is freely diffused or binds a cognate receptor. It is possible that bacteria import and internalize AI-2 to terminate extracellular AI-2-dependent cellular responses and alternatively trigger cytoplasmic AI-2-dependent gene expression. The physiological functions associated with either extracellular or cytoplasmic AI-2 can be understood using *lsrK* and *lsrR* mutants. In *lsrK* mutants, the Lsr transporter expression is always repressed and AI-2

remains in supernatant (extracellular AI-2) (276). In *lsrR* mutants, the Lsr transporter is constantly expressed and extracellular AI-2 is continuously imported into the cell (cytoplasmic AI-2). The elucidation of *lsrR*, *lsrK* or *lsrRK* operon regulated genes and physiologies will provide valuable information for *E. coli* quorum sensing system and suggest new targets for controlling quorum sensing behaviors.

In order to elucidate the genes controlled by quorum sensing regulator, LsrR, and its kinase, LsrK, in *E. coli*, we carried out genome wide transcriptome analyses of *lsrR* and *lsrK* mutants relative to the isogenic parent strain W3110. We further evaluated physiological changes (biofilm formation, motility etc) resulting from the mutations. We found *lsrR* and *lsrK* serve as global regulators of gene expression and affect biofilm architecture through the coordinate regulation of biofilm-related genes, such as *wza* (responsible for colanic acid), and the autoaggregation gene, *flu*. For the first time, small riboregulators were shown to interact with quorum sensing regulators *lsrR, lsrK* in *E. coli*. While many important genes were found regulated by *lsrR* and *lsrK*, those associated with host invasion, stress responses and foreign DNA were most prevalent. Finally, and perhaps most importantly, our analysis suggests that *lsrR* and *lsrK* (or more specifically LsrR and AI-2) operate in tandem, which is the inverse of their role in regulating AI-2 uptake. We believe the sheds light on the widely-discussed differences between AI-2 as a metabolic by-product and as a QS signaling molecule (277, 287).

Materials and Methods

Bacterial strains and growth conditions *E. coli* K-12 strain W3110 (F^-, λ^-, in (*rrn*D-*rrn*E)) was obtained from the Genetic Stock Center (New Haven, Connecticut). Details of its kanamycin resistant isogenic mutants W3110 Δ*lsrR, W3110* Δ*lsrK* used in this study are described elsewhere (276). Luria-Bertani broth (LB) contains 5 g L^{-1} yeast extract (Difco), 10 g L^{-1} bacto tryptone (Difco), and 10 g L^{-1} NaCl. Overnight cultures of *E. coli* (wild type and Δ*lsrR*, Δ*lsrK* mutants) in LB, were diluted to an OD_{600} of ~0.03 in LB and subsequently incubated at 30°C and 250 rpm in 50 ml shake flasks. When the cultures reached the appropriate OD_{600} (2.4), the cells were harvested for RNA extraction.

RNA isolation Total RNA was isolated using RNeasy Mini Kits (Qiagen Inc., Valencia, CA) according to the manufacturer's instructions. RNAprotect Bacteria Reagent (containing tetradecyltrimethylammonium bromide) (Qiagen Inc., Valencia, CA) was added to the cultures to stabilize the RNA before isolation. The RNase-Free DNase Set (Qiagen Inc., Valencia, CA) was used for on-column DNase digestion to remove residual DNA during RNA purification. Finally, the RNA was eluted with nuclease-free water.

cDNA synthesis and labeling cDNA was synthesized and labeled according to the manufacturer's suggestions for the Affymetrix *E. coli* Antisense Genome Array (Affymetrix Inc., Santa Clara, CA). Briefly, in 60 µl of reaction mixture, 10 µg of total RNA was used for cDNA synthesis using random primers (12.5 ng/µl) and SuperScript II reverse transcriptase (25 U/µl) (both from Invitrogen Corp., Carlsbad, CA). RNA was removed by addition of 20 µl of 1N NaOH and incubation at 65°C for

30 minutes. cDNA was purified with Qiaquick PCR Purification Kit (Qiagen Inc., Valencia, CA), then fragmented using DNase I (0.6 U/μg of DNA) (Amersham Pharmacia Biotech, Piscataway, NJ) at 37°C for 10 minutes. The Enzo BioArray Terminal Labeling Kit with Biotin-ddUTP (Affymetrix Inc., Santa Clara, CA) was used to label the 3' termini of the fragmented cDNA by terminal deoxynucleotide transferase. A gel–shift assay with NeutrAvidin (Pierce Biotechnology, Inc. Rockford, IL) was performed to estimate the labeling efficiency based on the instructions from Affymetrix.

Microarray hybridization, washing and scanning The hybridization solution mix was made with the labeled cDNA according to the manufacturer's instructions (Affymetrix Inc., Santa Clara, CA), and the mixture was hybridized to the *E. coli* Antisense Genome Arrays at 45°C for 16 hours. A GeneChip Fluidics Station (Affymetrix Inc., Santa Clara, CA) was used to automate the washing and staining of the arrays. Sequentially, the arrays were stained with ImmunoPure streptavidin (Pierce Biotechnology, Inc., Rockford, IL), Anti-streptavidin goat antibody (Vector Laboratories Inc., Burlingame, CA), and R-Phycoerythrin streptavidin (Molecular probes Inc., Eugene, OR). Finally, the probe arrays were scanned using the Affymetrix GeneArray scanner.

Data analysis Microarray Data was analyzed with the Affymetrix Microarray Suite Software 5.1 (Affymetrix Inc., Santa Clara, CA) and a four-comparison survival method (40). The fluorescence of each array was normalized by scaling total chip fluorescence intensities to a common value of 500. For each growth condition, two independent experimental cell cultures (wild type) were compared with two

independent control groups (Δ*lsrR* or Δ*lsrK* mutant) and four comparisons were made. The fold change for each gene was calculated as division of signal intensity for these two mutants by the signal intensity for the wild type respectively. The reported value for the fold change is the average of the four comparisons. Genes with consistent increase or decrease in all comparisons were determined and used for the analysis. However, the induced genes with absent calls of the array signal in the experimental groups, and the repressed genes with absent calls of the array signal in the control groups were eliminated for the analysis. The determination of gene functional categories was based on the *E. coli* K12-MG1655 role category database from TIGR (http://www.tigr.org/tigr-scripts/CMR2/gene_table.spl?db=ntec01).

Motility assays The media used for the motility swimming assay is tryptone broth (10 g L^{-1} tryptone (Difco), 5 g L^{-1} NaCl) that contained 0.3% Difco agar. Cultures of *E. coli* were grown overnight in liquid tryptone broth, diluted 100-fold into the same fresh medium and grown to mid-exponential phase, to an optical density (OD_{600}) of 0.9~1.1. Swim plates were inoculated at the center with 5 μl of cell culture, and incubated at 30°C in a humid environment for 25 hour. The motility halos were measured and 6 to 10 plates were used to compare motility between strains.

Biofilm and time course assays. The biofilm assays were performed as described previously (205) with slight modification. *E. coli* cells were grown in polystyrene tubes in LB with at 30 °C without shaking for 24 h, and subcultured at a 1:100 dilution into different media: LB, LB and glucose, glycerol minimal, glucose minimal, glycerol minimal with Casamino Acids (CAA), glucose minimal with CAA,

or minimal medium with CAA. CAA was used at 5% (w/v). These cultures were grown for 24 h at 30 °C without shaking and then rinsed with distilled water and stained with 1.0% crystal violet. After 20 min, the tubes were rinsed. The biofilm-associated crystal violet was solubilized by dimethyl sulfoxide, and the OD_{570} of the suspension was measured.

For the biofilm time course analysis, cell cultures were grown as above but only inoculated in LB medium in triplicate and allowed to incubate for times varying from 0 h to 32 h grown at 30 °C without shaking. At different time points, the biofilm was estimated by the crystal violet method stated as above.

SEM (Scanning Electron Microscopy) Images for late exponential phase broth culture cells were taken. For this, cells were collected and gently washed three times with Millonig's phosphate buffer (pH 7.3, centrifugation by 2000g for 10 min) and fixed with 2 % glutaraldehyde (1hr at room temperature and 9 hr at 4 ˚C). Cells were collected with 0.2 µl filters and then residual glutaraldehyde was washed out with Millonig's phosphate buffer three times before cells were further fixed in 1% OsO_4. The filters were then dehydrated with ethanol (70 %, 95 % and 100 %) continuously. The filters were fully dehydrated with Denton Vacuum freezer (Denton DCP-1 critical point dryer) and coated with Ag-Pd (Denton DV 502/503 vacuum evaporator). Coated filters were examined under the electron microscopy. This process was performed in the Biological Ultrastructure Laboratory at the University of Maryland, College Park.

Real-Time RT-PCR cDNA was synthesized from total RNA and random hexamers using the SuperScript™ III First-Strand Synthesis System for RT-PCR (Invitrogen)

according to the manufacturer's instructions. Primers were designed and purchased from Integrated DNA Technologies (Coralville, IA). Regular PCR was used to check the uniqueness of the primers before using the cDNA for quantification PCR. Real-time RT-PCR was performed in 50 μl of reaction mixture containing the Platinum SYBR Green qPCR Supermix UDG (Invitrogen), 0.2 μM of primers, and cDNA (50°C, 2 min; 95°C, 2 min; 95°C, 15 s, 40 cycles; 60°C, 1 min). The reaction and detection of dye-labeled PCR products were performed with an Applied Biosystems 7300 Real-Time PCR System (Appled Biosystems). *16S rRNA* was used as the normalizing gene for all reactions since its transcript levels were not significantly different between the wild type and the mutants (data not shown).

Autoaggregation assay The autoaggregation assays were performed as described previously (111) with slight modification. Overnight cultures were adjusted to the same optical densities and 10ml of each culture was placed in a 15 ml falcon tube and kept on ice. At each time point, 100 μl samples were taken from each tube, ~1 cm from the top, and transferred to new tubes containing 1 ml 0.9% NaCl for measuring optical density.

Flow cell biofilm experiments and image analysis. *E. coli* K12 W3110 that expresses constitutively the green fluorescent protein (GFP) via pCM18 was streaked on LB erythromycin (300 μg/mL) agar plates and was grown in the same medium overnight. *E. coli* K12 W3110 ΔlsrK:Kan^r/pCM18 and *E. coli* K12 W3110 ΔlsrR:Kan^r/pCM18 were streaked on LB erythromycin (300 μg/mL) and kanamycin (50 μg/mL) agar plates and were grown overnight in the same medium. Overnight cultures were diluted into LB and erythromycin (300 μg/mL) to have an OD_{600} of 0.05. The flow

cell was inoculated for two hours at 30^{o}C with 200 mL of these cells, then fresh medium was added at 10 mL/hr flow rate for 49 hours. The number of cells in the culture after two hours of inoculation was 1.4 ~3.2 x 10^{5} cells/mL. For the wild type strain, biofilm formation was not significant at 24 hr, so only 49 hour images were taken for all three strains. GFP was visualized by exciting with an Ar laser at 488 nm (emission 510 – 530 nm) using a TCS SP5 scanning confocal laser microscope with a 63x HCX PL FLUOTAR L dry objective with correction collar and numerical aperture of 0.7 (Leica Microsystems, Mannheim, Germany). Color confocal flow cell images were converted to gray scale using Image Converter (Neomesh Microsystems, Wainuiomata, Wellington, New Zealand). Biomass, substratum coverage, surface roughness, and mean thickness were determined using COMSTAT image-processing software (22) written as a script in Matlab 5.1 (The MathWorks) and equipped with the Image Processing Toolbox. Thresholding was fixed for all image stacks. At each time point, nine different positions were chosen for microscope analysis and 225 images were processed for each time point. Values are means of data from the different positions at the same time point, and standard deviations were calculated based on these mean values for each position. Simulated three-dimensional images were obtained using IMARIS (BITplane, Zurich, Switzerland). Twenty-five pictures were processed for each three-dimensional image.

Results

Deletion of the E. coli W3110 *lsrR, lsrK* gene does not affect growth or motility but biofilm architecture.

We observed neither *lsrR* nor *lsrK* growth rate dependency when grown in Luria-Bertani (LB) medium (Fig. 4-2 A). We did find a slight difference in cell motility between the mutants and the wild type, as measured using 0.3% agar on tryptone broth. The mutants were similar to each other and slightly more motile than the parent strain (Fig 4-2 B). No significant differences in biofilm formation were observed between the wild type, Δ*lsrR,* and Δ*lsrK* when supported in LB (or with glucose) or various minimal media containing Casamino Acids or in minimal media without Casamino Acids (see Materials and Methods) (Fig.4-3A). Finally, we tested biofilm formation of all three strains in LB media (see Materials and Methods) as a function of time. Prior to 24 hours, no significant differences were observed between the wild type and the Δ*lsrR*, Δ*lsrK* mutants. After about 30 hours, both mutants formed more biofilm than the wild type (Fig. 4-3B). Based on this interesting observation, we utilized scanning electron microscopy to visualize the morphology of the biofilms and found out that W3110 Δ*lsrR*, Δ*lsrK* formed different biofilm structures than the wild type: an extracellular matrix was observed on the surface of both mutants but not on the wild type (Fig. 4-4). In order to discover genes associated with these motility and biofilm phenotypes, seemingly oppositely signaled than in *V. cholerae*, we carried out a transcriptome analysis of *lsrR*, *lsrK* mutants against their isogenic parent and a flow cell analysis for understanding holistically, the biofilm formation (see below).

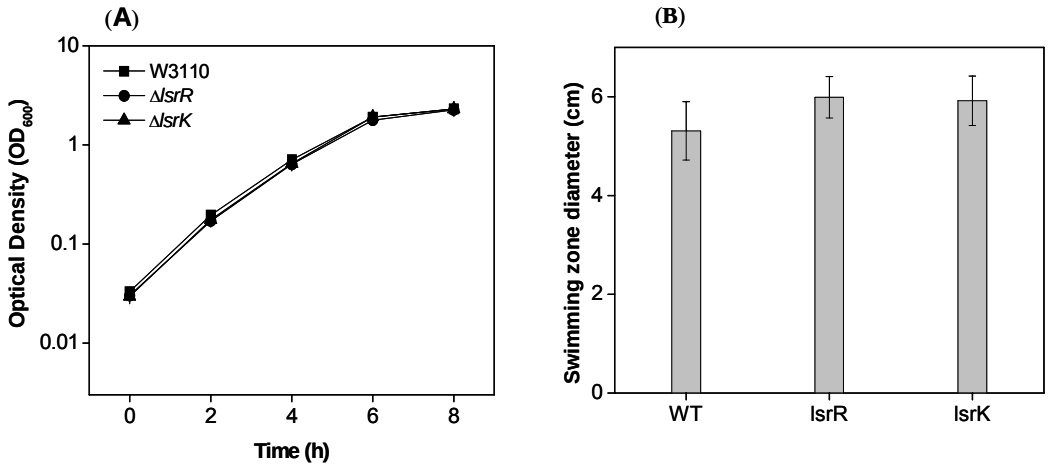

Figure 4-2 Genomic deletion of *lsrR, lsrK* does not affect growth, motility

(A) Growth curve of W3110 and W3110 Δ*lsrR*, Δ*lsrK*. Overnight cultures were diluted 1:100 in LB and grown to the mid-exponential phase, then diluted again into fresh LB at an OD_{600} of 0.03. At different time points, aliquots were collected for measurement of OD_{600}. (B) Motility assay of W3110 and W3110 Δ*lsrR*, Δ*lsrK*.

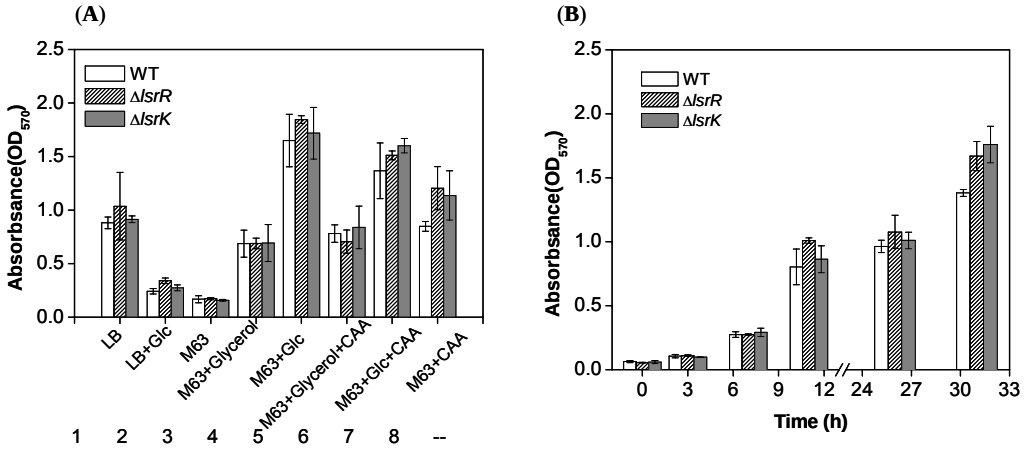

Figure 4-3 Crystal violet estimation of biofilm formation

(A) Biofilm assay in 8 different media, CAA means 0.5% casamino acid, "Glc" represents 0.8% glucose. (B) Time course biofilm assay in LB medium. WT represents W3110.

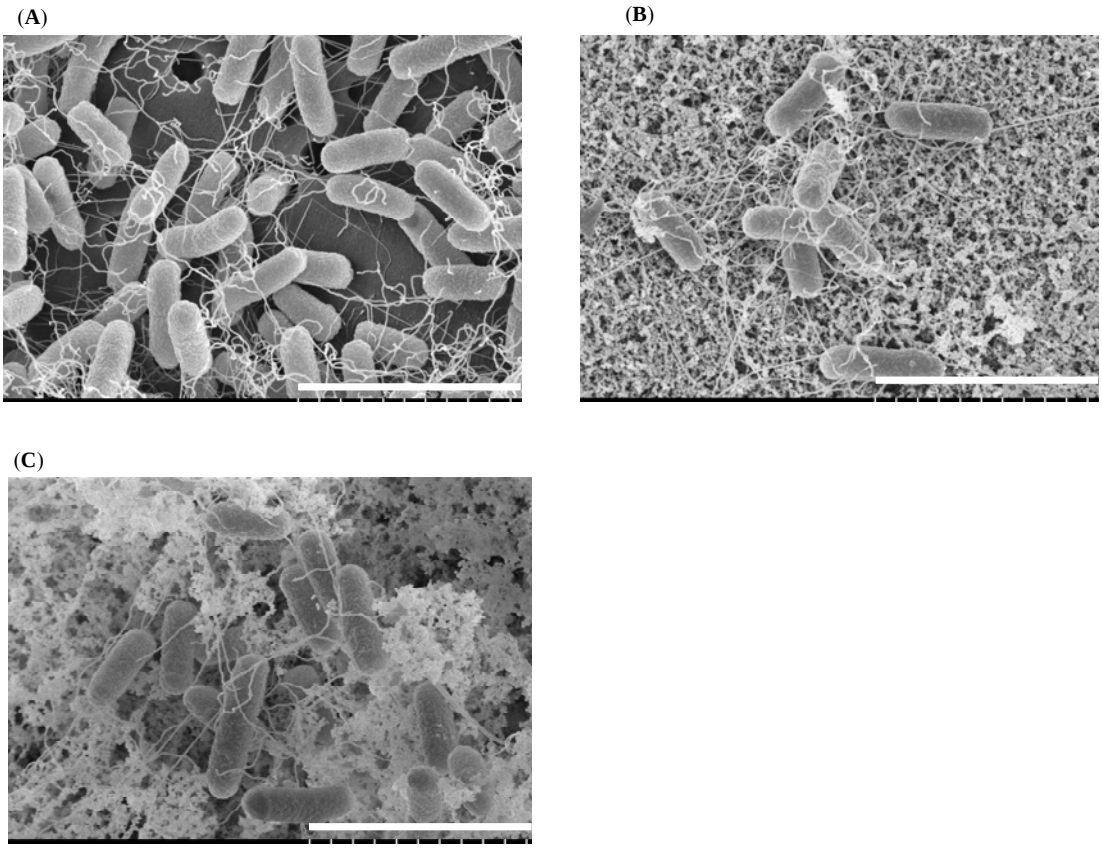

Figure 4-4 Biofilm structure from Scanning Electron Microscope
(A) wild type W3110, (B) isogenic *lsrR* mutant, (C) isogenic *lsrK* mutant. Scale bar: 4 μm.

Genomic transcriptional analyses of the *lsrR, lsrK* mutations.

Using DNA microarrays, we compared the genomic transcript levels of the wild type and Δ*lsrR*, Δ*lsrK* of *E. coli* W3110 respectively. Cells were grown in LB medium (without glucose) to an OD_{600} of 2.4±0.1 (early stationary phase). Under this growth condition, extracellular AI-2 in cultures of wild type cells is partially

transported back into the cells, nearly completely depleted from Δ*lsrR* mutants, and retained at near peak levels in Δ*lsrK* mutants (276). To verify our microarray data, we performed real-time RT-PCR on a selected number of the identified *lsrR-, lsrK*-regulated genes. Fig.4-5 shows that there was a strong positive correlation ($r^2 = 0.98$ for *lsrR* mutants and $r^2 = 0.96$ for *lsrK* mutants) between the two techniques.

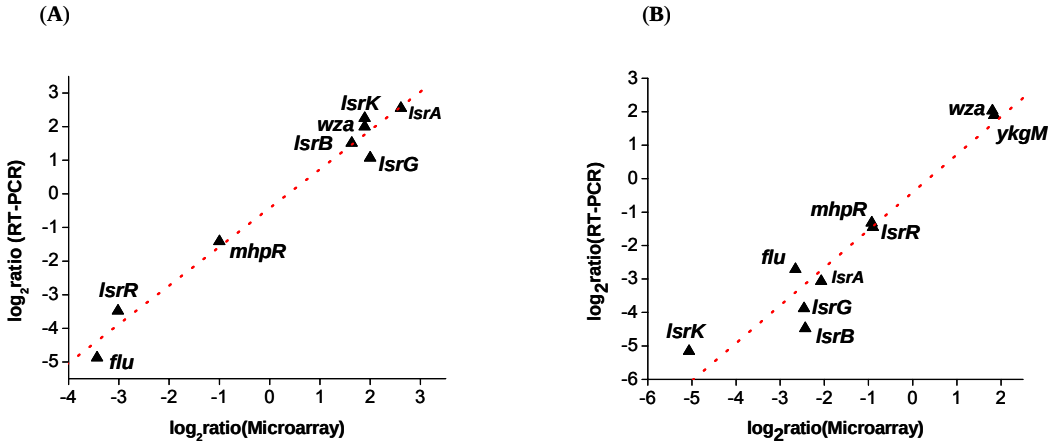

Figure 4-5 Correlation of microarray and Real Time PCR
The differences in expression of eight *lsrR*-controlled genes and 9 *lsrK*-controlled were log2 transformed and plotted against each other, microarray versus real-time RT-PCR. (A) is for W3110 Δ*lsrR*, (B) is for w3110 Δ*lsrK*

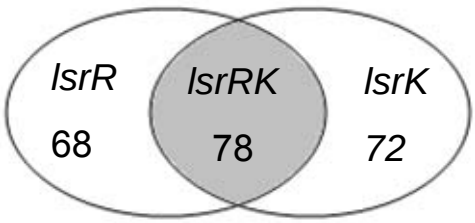

Figure 4-6 Three different groups gene regulated by *lsrR* and *lsrK*

Table 4-1 Genes co-regulated by *lsrR, lsrK*

B. no	gene	Gene product[a]	Fold change	
			Δ*lsrR*/WT	Δ*lsrK*/WT
Divergently regulated genes				
b0564	*appY*	regulatory protein affecting appA and other genes	-2.2	2.6
b1511	*lsrK*	putative kinase	3.7	-33.5
b1513	*lsrA*	putative ATP-binding component of a transport system	6.1	-4.2
b1514	*lsrC*	putative transport system permease protein	2.5	-2.0
b1515	*lsrD*	putative transport system permease protein	3.0	-3.2
b1516	*lsrB*	putative LACI-type transcriptional regulator	3.1	-5.4
b1517	*lsrF*	orf, hypothetical protein	3.1	-2.9
b1518	*lsrG*	orf, hypothetical protein	4.0	-5.5
b1519	*tam*	putative enzyme	2.1	-2.0
Co-regulated genes				
b1512	*lsrR*	putative transcriptional regulator, sorC family	-8.1	-2.0
b0218	*yafU*	orf, hypothetical protein	3.0	4.2
b0296	*ykgM*	putative ribosomal protein	3.2	3.6
b0326	*yahL*	orf, hypothetical protein	2.9	2.5
b0327	*yahM*	orf, hypothetical protein	3.2	2.2
b0334	*prpD*	orf, hypothetical protein	-2.0	-2.2
b0346	*mhpR*	transcriptional regulator for mhp operon	-2.0	-2.1
b0450	*glnK*	nitrogen regulatory protein P-II 2	4.4	3.6
b0451	*amtB*	probable ammonium transporter	2.3	2.2
b0521	*arcC*	putative carbamate kinase	-2.5	-2.6
b0527	*ybcI*	orf, hypothetical protein	2.0	2.6
b0685	*ybfE*	orf, hypothetical protein	2.4	2.4
b0718	*ybgQ*	putative outer membrane protein	2.0	2.4
b0787	*ybhM*	orf, hypothetical protein	4.2	2.9
b0939	*ycbR*	putative chaperone	2.5	2.1
b1031	*ycdV*	putative ribosomal protein	-2.0	-3.4
b1137	*ymfD*	orf, hypothetical protein	2.6	2.7
b1140	*intE*	prophage e14 integrase	2.3	2.2
b1160	*ycgW*	orf, hypothetical protein	2.0	3.2
b1161	*ycgX*	orf, hypothetical protein	4.6	4.1
b1196	*ycgY*	orf, hypothetical protein	2.0	2.7
b1450		orf, hypothetical protein	6.6	2.4
b1454		putative transferase	2.4	2.5
b1555		orf, hypothetical protein	2.0	2.0
b1558	*cspF*	cold shock protein	3.0	3.9
b1571	*ydfA*	orf, hypothetical protein	4.1	3.5
b1575	*dicB*	inhibition of cell division	2.2	2.3
b1625		orf, hypothetical protein	3.1	3.7
b1697	*ydiQ*	putative transport protein	2.0	2.1
b1796	*yoaG*	orf, hypothetical protein	4.8	2.2
b1798	*yeaS*	orf, hypothetical protein	2.2	2.2
b1954	*dsrA*	Regulatory RNA; positive regulation of promoters sensitive to HNS negative regulation	3.6	4.4
b2000	*flu*	outer membrane fluffing protein, similar to adhesin	-10.8	-6.3

Table 4-1 continued

b2001		orf, hypothetical protein	-5.2	-3.5
b2014	*yeeF*	putative amino acid/amine transport protein	-3.1	-2.2
b2020	*hisD*	L-histidinal:NAD+ oxidoreductase; L-histidinol:NAD+ oxidoreductase	-2.1	-2.0
b2062	*wza*	putative polysaccharide export protein	3.7	3.5
b2110	*yehC*	putative chaperone	2.5	2.3
b2274		orf, hypothetical protein	3.7	3.5
b2312	*purF*	amidophosphoribosyltransferase = PRPP amidotransferase	-2.0	-2.0
b2483	*hyfC*	hydrogenase 4 membrane subunit	2.3	2.5
b2629	*yfjM*	orf, hypothetical protein	4.7	4.0
b2734	*pphB*	protein phosphatase 2	2.8	2.6
b2832		putative transport protein	3.9	3.4
b2848	*yqeJ*	orf, hypothetical protein	3.8	3.7
b2850	*ygeF*	orf, hypothetical protein	3.6	2.0
b2854		orf, hypothetical protein	2.3	2.0
b3109	*yhaN*	orf, hypothetical protein	2.0	2.0
b3118	*tdcA*	transcriptional activator of tdc operon	2.2	2.5
b3120	*yhaB*	orf, hypothetical protein	4.0	3.6
b3136	*agaS*	putative tagatose-6-phosphate aldose/ketose isomerase	2.8	3.5
b3264	*envR*	putative transcriptional regulator	2.8	2.5
b3324	*yheE*	putative general secretion pathway for protein export (GSP)	2.4	2.1
b3484	*yhhI*	putative receptor	3.2	2.5
b3490	*yhiL*	orf, hypothetical protein	2.3	3.8
b3507	*yhiF*	orf, hypothetical protein	3.3	5.2
b3512	*yhiE*	orf, hypothetical protein	3.3	5.1
b3578	*yiaN*	putative membrane protein	2.4	2.0
b3587	*yiaW*	orf, hypothetical protein	2.5	2.6
b3595	*yibJ*	orf, hypothetical protein	2.2	2.5
b3596	*yibG*	orf, hypothetical protein	2.1	2.6
b3817	*yigF*	orf, hypothetical protein	2.2	3.5
b3903	*rhaA*	L-rhamnose isomerase	3.6	2.5
b3989	*htrC*	heat shock protein htrC	2.5	2.0
b4072	*nrfC*	formate-dependent nitrite reductase; Fe-S centers	2.2	2.0
b4075	*nrfF*	part of formate-dependent nitrite reductase complex	2.3	2.8
b4116	*adiY*	putative ARAC-type regulatory protein	2.6	3.3
b4239	*treC*	trehalase 6-P hydrolase	2.3	2.2
b4247	*yjgG*	orf, hypothetical protein	3.1	3.5

[a] Abbreviations: ORF, open reading frame

To report the number of genes differentially expressed, we took the commonly used 2-fold induction ratio as a cutoff limit (126). There were 119 and 27 genes induced and repressed, respectively, at least 2-fold by *lsrR*, and there were 108 and 32 genes induced and repressed, respectively, by *lsrK*. Among these, 78 genes were both regulated by *lsrR* and *lsrK* (Fig 4-6). Surprisingly, only the *lsr* transporter operon genes (including *lsrABCDFG*, *tam*) and *appY* were divergently regulated according to the repressor/derepressor model in Fig.4-1, while all the others were regulated by *lsrR, lsrK* according to an alternative model (Table 4-1). That is, for the divergently co-regulated genes, LsrR works as a repressor while phospho-AI-2 works as an anti-repressor. For the apparent co-regulated genes, we suspect that a totally different regulatory mechanism exists, i.e. that in which LsrR is a repressor (and at times activator) and its repression is enhanced by AI-2 in a complex. That the number of genes affected by each mutation represents the majority of the entire set of genes affected by both mutations, and that the relative induction ratios are consistent with a hypothetical activator complex, supports this hypothesis. An *lsrR* mutation leads to deficient LsrR expression while an *lsrK* mutation results in a lack of phospho-AI-2, which is not only an inducer for LsrR expression but also an integral component for LsrR-phospho-AI-2 complex formation. Therefore, LsrR and LsrR-phospho-AI-2 are two putative candidates for this regulator complex. We suggest further, that non-phosphorylated AI-2, participates as an activator of LsrR activity and that this mode of activity is the dominant feature of LsrR-mediated quorum sensing. Finally, we prefer this signaling modality for AI-2 mediated quorum sensing for two reasons: first, quorum-sensing signals have been shown to be global regulators hence cells

must have a purpose for importing and processing AI-2; second, *lsrR* and *lsrK* belong to the same operon and AI-2 mediated regulon (277). Thus, it is not surprising that *E. coli* utilizes the product of this operon to globally control cellular phenotype. Our transcriptome results agree with this model since most of the *lsrRK*-regulated genes are related to the cell's secretion systems (e.g. *flu*, *yheE*), transcriptional regulators (e.g., *mhpR*, *tdcA*, *envR*), small RNAs or "ribo"-regulators (e.g., dsrA), and regulatory proteins for stress responses and nutrient depletion (e.g., *adiY*, *glnK*, *cspF*) (Table 4-1). Most target genes that are induced in Δ*lsrR* and Δ*lsrK*, AI-2 probably works as a repressor, otherwise may serve as activator.

Interestingly, *flu*, which encodes a phase variable protein antigen 43 (Ag43), was dramatically depressed, 10.8 and 6.3-fold in Δ*lsrR*, Δ*lsrK* mutants, respectively. Ag43 belongs to an autotransporter protein family, which contains all information required for traversing the bacterial membrane and routing itself to the bacterial cell surface. Ag43 mediates cell-to-cell aggregation thus dramatically enhances biofilm formation (49, 144, 215). Recently, glycosylated Ag43 with an adhesive phenotype toward human cell lines was discovered (234). As Ag43 plays an important role in the intial recognition and attachment to host tissue surfaces, it also plays a role in the pathogenesis of disease-causing *E. coli*: (116). We carried out an autoaggregation assay to elucidate the potential role of *lsrRK* on aggregation. Consistent with Ag43's autoaggregation function, more wild type cells settled to the bottom of the tubes than did both mutant strains (Fig. 4-7 A), even though complete resolution of the assay took two days (Fig 4-7 B). We suspect fimbriae blockage of autoaggregation may have contributed to this delay (111). Complete deficiency in autoaggregation of both

lsrR and *lsrK* mutants is consistent with our microarray results and regulatory model involving LsrR and LsrK.

(A)

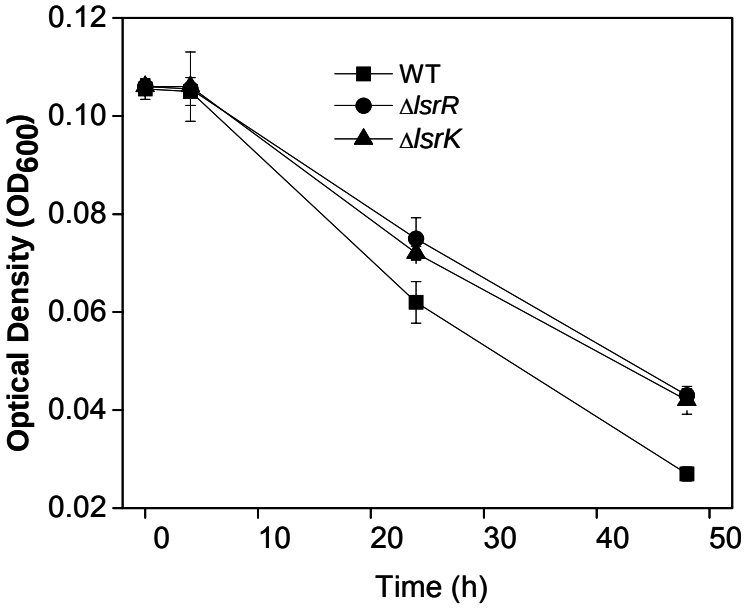

(B)

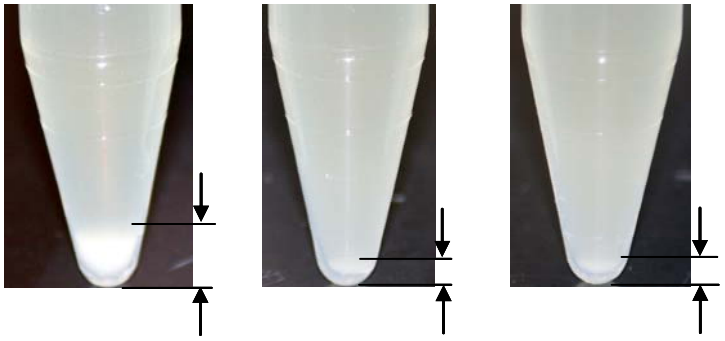

Figure4-7 Autoaggregation assay of W3110, and *lsrR*, *lsrK* mutants
(A) Cell density changes as cells settle down (B) Pictures of the autoaggregated cells at the bottom of the tubes, from left to right: W3110, W3110 Δ*lsrR*, Δ*lsrK*

Another interesting finding is that *yheE* (also called *gspC)*, a gene encoding a putative secretion protein, was induced 2.4- and 2.1-fold in *lsrR* and *lsrK* mutants respectively (Table 4-1). In *E. coli*, *gspC* is a member of an operon of genes (*gspC-O*) which is not normally expressed, but is homologous to those encoding type II secretion in *Klebsiella oxytoca* and *Aeromonase hydrophila* (82, 83). Type II secretion machinery allows most Gram-negative bacteria to deliver virulence factors into their surroundings. GspC has been shown, to interact with the cytoplasmic membrane through the formation of heterooligomers with GspE, GspL and GspM (204, 208, 222). Another component of *gspC-O* family, *yheF* (*gspD*) was induced more than 2-fold in the *lsrR* mutant (details below). Other components of this complex were not revealed here, perhaps due to their typically low levels of expression (82).

There are 68 genes regulated by *lsrR* only and among these, 25 are hypothetical proteins with unknown function (Table 4-2). We report a preponderance of genes associated with attachment, defense, and pathogenicity affected by *lsrR*. For example, a curli production assembly/transport component, *csgE,* from the 2nd curli operon was negatively regulated in the *lsrR* mutant. Curli is associated with biofilm formation, host cell adhesion and invasion, and immune system activation, where CsgA is the major fiber subunit and CsgE, CsgF and CsgG are non-structural proteins involved in curli biogenesis (12, 216). *htrE*, a homolog to *papD* involved in type II pili assembly (209) was

Table 4-2 Genes regulated by *lsrR* only

B. no	gene	Gene product	Fold change Δ*lsrR*/WT
b0139	*htrE*	probable outer membrane porin protein involved in fimbrial assembly	-3.2
b1039	*csgE*	curli production assembly/transport component, 2nd curli operon	-3.0
b0586	*entF*	ATP-dependent serine activating enzyme (may be part of enterobactin synthase as component F)	-2.3
b1849	*purT*	phosphoribosylglycinamide formyltransferase 2	-2.3
b1393	*ydbS*	putative enzyme	-2.2
b4131	*cadA*	lysine decarboxylase 1	-2.2
b0270	*yagG*	putative permease	-2.1
b0484	*ybaR*	putative ATPase	-2.0
b0596	*entA*	2,3-dihydro-2,3-dihydroxybenzoate dehydrogenase, enterochelin biosynthesis	-2.0
b1963		orf, hypothetical protein	-2.0
b2230	*yfaA*	orf, hypothetical protein	-2.0
b2725	*hycA*	transcriptional repression of hyc and hyp operons	-2.0
b0615	*citF*	citrate lyase alpha chain	-2.0
b0999	*yccD*	orf, hypothetical protein	-2.0
b1293	*sapB*	homolog of Salmonella peptide transport permease protein	-2.0
b1776		putative oxidoreductase	-2.0
b1141		orf, hypothetical protein	2.0
b0709	*ybgH*	putative transport protein	2.0
b1456	*rhsE*	rhsE protein in rhs element	2.0
b1550		orf, hypothetical protein	2.0
b1588		putative oxidoreductase, major subunit	2.0
b2497	*uraA*	uracil transport	2.0
b2775	*yqcE*	putative transport protein	2.0
b3060	*ygiP*	putative transcriptional regulator LYSR-type	2.0
b3214	*gltF*	regulator of gltBDF operon, induction of Ntr enzymes	2.0
b3215	*yhcA*	putative chaperone	2.0
b2648		orf, hypothetical protein	2.1
b1229	*tpr*	a protaminelike protein	2.1
b0236	*prfH*	probable peptide chain release factor	2.1
b0363	*yaiP*	polysaccharide metabolism	2.1
b0984	*ymcA*	orf, hypothetical protein	2.1
b1122	*ymfA*	orf, hypothetical protein	2.1
b1155		orf, hypothetical protein	2.1
b3159	*yhbV*	orf, hypothetical protein	2.1
b4063	*soxR*	redox-sensing activator of soxS	2.1
b4246	*pyrL*	pyrBI operon leader peptide	2.1
b4300	*sgcR*	putative DEOR-type transcriptional regulator	2.1
b0942		putative fimbrial-like protein	2.2
b1146		orf, hypothetical protein	2.2
b1720		orf, hypothetical protein	2.2
b2120	*yehM*	orf, hypothetical protein	2.2
b2123	*yehR*	orf, hypothetical protein	2.2
b2646	*ypjF*	orf, hypothetical protein	2.2
b3325	*yheF*	putative general protein secretion protein	2.2

Table 4-2 continued

b3944	*yijF*	orf, hypothetical protein	2.2
b4212	*ytfH*	orf, hypothetical protein	2.2
b1265	*trpL*	trp operon leader peptide	2.3
b1675		orf, hypothetical protein	2.3
b2387		putative PTS system enzyme IIB component	2.3
b2657		putative enzyme	2.3
b0806	*ybiM*	orf, hypothetical protein	2.4
b1028		orf, hypothetical protein	2.4
b3437	*gntK*	gluconokinase 2, thermoresistant	2.4
b4204	*yjfZ*	orf, hypothetical protein	2.4
b1121		homolog of virulence factor	2.5
b2105	*yohL*	orf, hypothetical protein	2.5
b2852	*ygeH*	putative invasion protein	2.5
b3517	*gadA*	glutamate decarboxylase isozyme	2.5
b3564	*xylB*	xylulokinase	2.6
b0717	*ybgP*	putative chaperone	2.8
b1350	*recE*	exonuclease VIII, ds DNA exonuclease, 5 --> 3 specific	2.9
b4071	*nrfB*	formate-dependent nitrite reductase; a penta-haeme cytochrome c	2.9
b2348	*argW*	Arginine tRNA5	3.4
b0246	*yafW*	orf, hypothetical protein	3.4
b2059	*wcaA*	putative regulator	3.5
b3504	*yhiS*	orf, hypothetical protein	3.9
b3875	*yshA*	orf, hypothetical protein	4.3
b3119	*tdcR*	threonine dehydratase operon activator protein	5.1

negatively regulated. Another putative fimbrial-like protein, from b0942, was upregulated 2-fold in the *lsrR* mutant. A transmembrane domain, from *sapB* of the SapABCD system (homologs of the *Salmonella typhimurium* SapABCD proteins) (195), which are required for virulence and resistance to antimicrobial peptides, melittin and protamine, was repressed in the *lsrR* mutant. Meanwhile, an increase in the transcription of a protamine like protein *tpr* was observed. *YheF* (also called GspD), which belongs to a large family of homologous proteins called secretins and is involved in virulence and filamentous phage extrusion (92). YheF proteins are not normally expressed and are silenced by the nucleoid-structuring protein H-NS (82). The upregulation of *yheF* from *lsrR* deletion is likely a capability of bacterial self-protection.

There are 71 genes regulated by *lsrK* only and among these 38 are hypothetical proteins with unclear function (Table 4-3). Again, a number of genes associated with attachment, defense, and pathogenicity was found regulated by *lsrK*. *ppdD*, which encodes a putative major type IV pilin, was repressed 2-fold in *lsrK* mutant. PpdD was able to form type IV pili when expressed in *Pseudomonas aeruginosa* as determined by immunogold labeling (224). PpdD also formed pili when the pullulanase secretion from *Klebsiella oxytoca* and *ppdD* was expressed in *E. coli* (225). Genes for two putative fimbrial proteins, *yadK* and *yadN,* were repressed 2.4- and 2-fold respectively in the *lsrK* mutant. *mcrA*, a type IV site-specific deoxyribonuclease defending cells against

Table 4-3 Genes regulated by *lsrK* only

B. no	gene	Gene product	Fold change
b0396	*araJ*	involved in either transport or processing of arabinose polymers	-2.7
b0136	*yadK*	putative fimbrial protein	-2.4
b1980		orf, hypothetical protein	-2.4
b2651		orf, hypothetical protein	-2.1
b1318	*ycjV*	putative ATP-binding component of a transport system	-2.1
b2634	*yfjR*	orf, hypothetical protein	-2.1
b2932	*yggP*	orf, hypothetical protein	-2.1
b0044	*fixX*	putative ferredoxin	-2.0
b0108	*ppdD*	prelipin peptidase dependent protein	-2.0
b0141	*yadN*	putative fimbrial-like protein	-2.0
b0263		putative transport system permease protein	-2.0
b1256	*yciD*	putative outer membrane protein	-2.0
b1896	*otsA*	trehalose-6-phosphate synthase	-2.0
b2384		orf, hypothetical protein	-2.0
b1357	*ydaS*	orf, hypothetical protein	2.0
b1576	*ydfD*	orf, hypothetical protein	2.0
b0528	*ybcJ*	orf, hypothetical protein	2.0
b0901	*ycaK*	orf, hypothetical protein	2.0
b1012		orf, hypothetical protein	2.0
b1029	*ycdU*	orf, hypothetical protein	2.0
b1358	*ydaT*	orf, hypothetical protein	2.0
b1956		orf, hypothetical protein	2.0
b2253		putative enzyme	2.0
b2371	*yfdE*	putative enzyme	2.0
b2399	*yfeD*	orf, hypothetical protein	2.0
b2902	*ygfF*	putative oxidoreductase	2.0
b2921	*ygfI*	putative transcriptional regulator LYSR-type	2.0
b2972		putative peptidase	2.0
b3117	*tdcB*	threonine dehydratase, catabolic	2.0
b3489	*yhiK*	orf, hypothetical protein	2.0
b3556	*cspA*	cold shock protein 7.4, transcriptional activator of hns	2.0
b4338	*yjiP*	orf, hypothetical protein	2.0
b0532	*sfmD*	putative outer membrane protein, export function	2.1
b1409		putative phosphatidate cytidiltransferase	2.1
b1455		orf, hypothetical protein	2.1
b2374		putative enzyme	2.1
b3078	*ygjI*	putative oxidoreductase	2.1
b3906	*rhaR*	positive regulator for rhaRS operon	2.1
b3937	*yiiX*	orf, hypothetical protein	2.1
b4038	*yjbI*	orf, hypothetical protein	2.1
b1147	*ymfL*	orf, hypothetical protein	2.2
b2969	*yghE*	putative general secretion pathway for protein export (GSP)	2.2
b3547	*yhjX*	putative resistance protein	2.2
b3808		orf, hypothetical protein	2.2
b4076	*nrfG*	part of formate-dependent nitrite reductase complex	2.2
b0702	*ybfB*	orf, hypothetical protein	2.3
b0691	*ybfH*	orf, hypothetical protein	2.3

Table 4-3 continued			
b2886	*ygfS*	putative oxidoreductase, Fe-S subunit	2.3
b3659	*yicK*	two-module transport protein	2.3
b2853		orf, hypothetical protein	2.4
b0157	*yadS*	orf, hypothetical protein	2.4
b1159	*mcrA*	restriction of DNA at 5-methylcytosine residues; at locus of e14 element	2.4
b1557	*cspB*	cold shock protein; may affect transcription	2.4
b2357	*yfdN*	orf, hypothetical protein	2.4
b2846	*yqeH*	orf, hypothetical protein	2.4
b2849	*yqeK*	orf, hypothetical protein	2.4
b1353	*sieB*	phage superinfection exclusion protein	2.5
b1375	*ynaE*	orf, hypothetical protein	2.5
b2626	*yfjJ*	orf, hypothetical protein	2.5
b4066	*yjcF*	orf, hypothetical protein	2.5
b0364	*yaiS*	orf, hypothetical protein	2.6
b1722		orf, hypothetical protein	2.6
b3063	*ygjE*	orf, hypothetical protein	2.6
b3552	*yiaD*	putative outer membrane protein	2.6
b4205	*ytfA*	orf, hypothetical protein	2.8
b4385	*yjjJ*	orf, hypothetical protein	2.8
b0544	*ybcK*	orf, hypothetical protein	2.9
b1476	*fdnI*	formate dehydrogenase-N, nitrate-inducible, cytochrome B556(Fdn) gamma subunit	2.9
b1877	*yecT*	orf, hypothetical protein	2.9
b0558	*ybcV*	putative an envelop protein	3.0
b3946	*talC*	putative transaldolase	3.0

foreign DNA such as bacteriophage (7), was upregulated 2.4-fold. *SieB*, similar to a λ gene responsible for preventing phage superinfection (77), was also upregulated 2.5-fold. These findings suggest that AI-2 signaling molecules interact with their uptake kinase to protect the bacteria against foreign DNA infections.

lsrR and _lsrK_ regulate biofilm architecture and formation through the colanic acid synthesis gene, _wza_, and the autotransporter gene, _flu_

It has been reported that flagella, fimbriae, type I pili, curli fibers, the antigen 43, exopolysaccharides (EPS) and other outer membrane adhesions are critical for biofilm development in *E. coli* (49, 50, 206, 215). However, the flagellar-related and the motility-associated genes, such as motility master regulon, *flh*DC, and type I adhesin, showed no evident changes in the mutants, *lsrR* and *lsrK*, as compared to the parental strain (observed fold change was less than 2). Also the two-component, quorum-sensing controlled motility regulatory system, QseBC (248) did not change under the tested conditions in this work. Previous research has already demonstrated that cell-to-cell communication signal is critical for forming complex biofilm structures. For example in *Pseudomonas aeruginosa* and *V. cholerae*, quorum sensing controls maturated biofilm formation through the regulation of exopolysacchride (EPS) production synthesis (52, 105).

Colanic acid synthesis has been demonstrated necessary for forming (EPS) and capsular polysaccharides (CPS) during the biofilm development (50, 193, 206). *Wza*, associated with colanic acid synthesis, is involved in EPS and CPS surface expression and assembling (19, 67, 68, 188, 214, 281). Wza in the outer membrane are believed to provide a channel for polymer exportions in group 1 CPS assembly in

E. coli. Wza recently was demonstrated indispensable for the functioning of the colanic acid synthase Wzc (281). Previous elaborate literatures already thoroughly demonstrated that *wza* is indispensable for biofilm formation, and that the change of *wza* expression will affect biofilm architecture in *E. coli* (50, 193, 206).

Table 4-4 Biofilm related gene mediated by *lsrR, lsrK*

B no.	Gene	Gene product	Fold Change	
			Δ*lsrR*/WT	Δ*lsrK*/WT
b2000	*flu*	outer membrane fluffing protein, similar to adhesin	-10.8	-6.3
b2062	*wza*	putative polysaccharide export protein	3.7	3.5
b0139	*htrE*	probable outer membrane porin protein involved in fimbrial assembly	-3.2	--
b1039	*csgE*	curli production assembly/transport component, 2nd curli operon	-3.0	--
b0942		putative fimbrial-like protein	2.2	--
b2059	*wcaA*	putative regulator	3.5	--
b0141	*yadN*	putative fimbrial-like protein	--	-2.0
b0136	*yadK*	putative fimbrial protein	--	-2.4

Remarkably, this gene was induced 3.7- and 3.5-fold in *lsrR*, *lsrK* mutants. Another biofilm related gene, an autotransporter gene, *flu*, was repressed 10.8- and 6.8- fold in both mutants respectively (Table 4-1). A putative regulator for colanic acid synthesis, *wcaA* was induced 3.5 fold in *lsrR* mutants. The biofilm related curli

gene, *csgE,* and a putative fimbrial assembly gene, *htrE,* were down regulated due to *lsrR* deletion. In *lsrK* mutants, two putative fimbrial related genes, *yadK* and *yadN,* were downregulated more than 2-fold. All biofilm related genes affected ≥2-fold from our microarray analysis are assembled in Table 4-4.

While our crystal violet biofilm assays found no significant differences in biofilm quantity between the two mutants and the wild type at 24 hrs and slight differences after 30 hrs (Fig.4-3), our SEM analysis revealed significant differences in cell-based fimbriae and matrices of both mutants compared to the wild type (Fig. 4-4). In order to further elucidate the overall variations in biofilm formation between the wild type and mutants, we utilized confocal scanning microscopy to scrutinize the biofilm formation (methods see Materials and Methods). In confocal images (Fig 4-8), more biofilm was formed at the substrate surface in both mutant strains as compared to the wild type. Also, Imaris imaging demonstrated that the biofilm thickness of the mutants was much less than that of the wild type. Hence, the mean thickness and biomass of the wild type was higher while the substratum coverage was lower than that of the mutants (because more of the mutant biofilm was at the bottom, see Fig. 4-8 and corresponding data listed in Table 4-5). We note results of the *lsrR* mutant had a larger standard deviation than that of the *lsrK* mutant; the biofilm height was observed to fluctuate in the flow chamber. In summary, the wild type formed more biofilm than the mutant, however, at the bottom layer adjacent to the substrate, the mutants formed more biofilm; they tended (276) to collapse and pack tightly onto surface of the substrate.

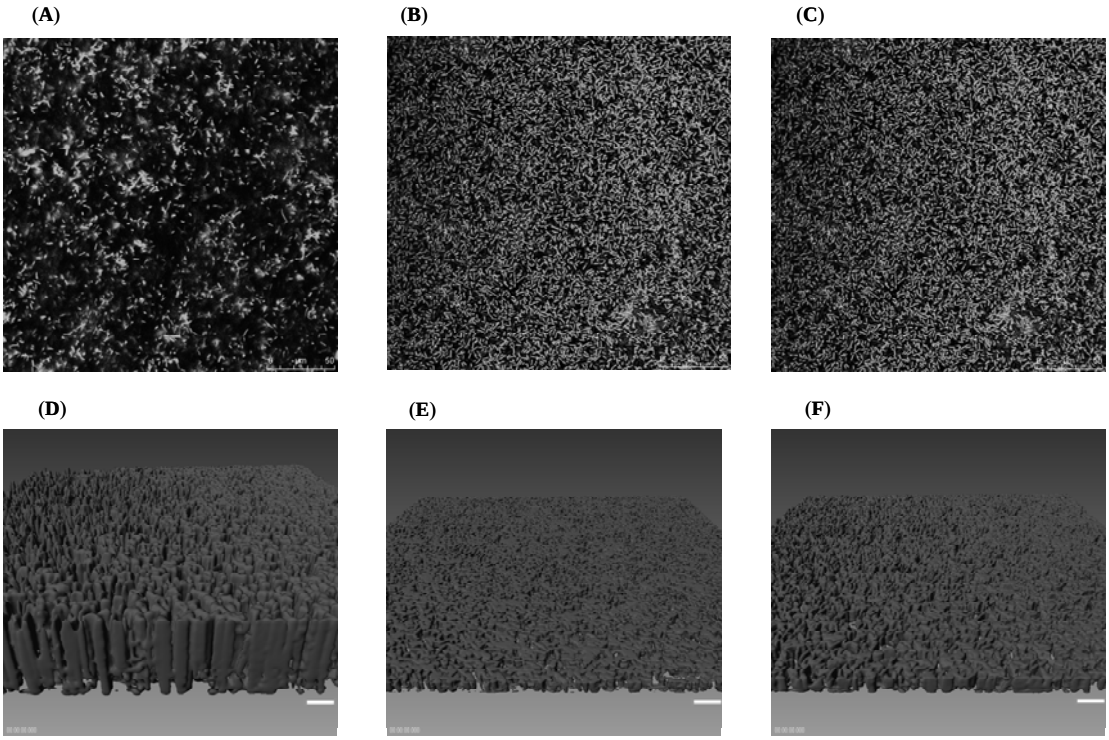

Figure 4-8 Biofilm flow cell images from Scanning Confocal Laser Microscopy

(A) & (D) wild type W3110; (B) & (E) W3110 Δ*lsrR*; (C) & (F) W3110 Δ*lsrK*

Table 4-5 Confocal analysis results of biofilm flow cell assay

	Biomass (μm^2/ μm^3)	Substratum Coverage (%)	Mean thickness (μm)	Roughness coefficient
W3110 type/pCM18	32.02± 3.2	20.4± 6.4	25.45 ±2.8	0.196± 0.08
ΔlsrK:kan^r/pCM18	3.64± 1.05	50.8 ± 4.7	2.95± 1.24	0.235± 0.05
ΔlsrR:kan^r/pCM18	13.43 ±14.43	44.6± 21.4	10.86± 11.85	0.229± 0.11

Colanic acid is critical for the formation of complex, three-dimensional biofilm structures in *E. coli* even though it is dispensable during the initial adhesion and biofilm development (50, 193, 206). The absence of colanic acid synthesis results in limited biofilm thickness and close cell-to-cell association within the microcolonies. From our array results, *wza* was upregulated in both mutants. Wza is necessary for the function of a tyrosine kinase, Wzc (214), which negatively regulates colanic acid biosynthesis through its autophosphorylation (246, 274). Tyrosine phosphorylation is associated with the production of exopolysaccharide in several bacterial pathogens (274). We note that in many species, including *Salmonella*, the production of exopolysaccharides and *luxS* expression have been linked with biofilm formation (55). Therefore, we suggest it is possible that the induced expression of *wza* in the *lsrR*, *lsrK* deletion strains resulted in more tyrosine kinase, *wzc*, which in turn negatively regulated colanic acid biosynthesis and lead to deficiency in the formation of the complex three-dimensional biofilm structure.

At the same time, the dramatically reduced *flu* gene, together with other reduced biofilm-related genes, probably resulted in less biofilm formation in both mutants overall in the flow cells. Genes controlling initial attachment (motility and flagellar associated genes) show no evident changes due to *lsrR*, *lsrK* deletion. We suspect the crystal violet assay is influenced by the removal of cells loosely attached to the surface through repetitive rinses, and instead reflects the number of firmly attached cells (mainly from initial adhesion). Similarly the SEM study probably eliminated the floating cells on the surface during the rigorous washes and kept the

basic adhesive matrix at the bottom resulting in mutant biofilm structures that were distinct from wild type structures (Fig 4-4).

In summary, the AI-2 uptake regulators, LsrR and LsrK, mediate biofilm formation and structure by the coordination of different biofilm-related genes, concluding the autotransporter gene, *flu*, and the colanic acid synthesis regulator, *wza*.

Small RNAs (sRNAs) are mediated by lsrR and lsrK

We searched the intergenic regions of the microarrays for known and putative sRNAs (Table 4-6). Interestingly, global sRNA regulator, DsrA, was induced 3.6- and 4.4-fold in Δ*lsrR*, Δ*lsrK,* respectively. DsrA is a riboregulator for RpoS and H-NS production, wherein DsrA enhances the translation of *rpoS* RNA by stabilizing *rpoS* mRNA but inhibits the H-NS translation by sharply increasing *hns* mRNA turn over (157, 164). DsrA RNA affects the biosynthesis of capsular polysaccharides via the increased production of the activator RcsA, due to the inhibition of H-NS mediated transcriptional silencing (238). DsrA also plays a regulatory role in acid resistance and has been identified to induce other genes through microarray analysis (158). The regulatory effects of DsrA are mediated by specific RNA-to-RNA pairing interactions while the stability and activity require the recruitment of an Hfq protein (28, 181, 239, 243). Since RpoS and H-NS play an important role in globally regulating many genes in response to a changing environment and function in the adaptation to many different kinds of stresses, it is not surprising that quorum sensing networks utilize its uptake regulators together with DsrA, in a hierarchical modality, for mediating prompt responses to environmental stimuli and extracellular stresses. Induction of components (*yheE*, *yheF*) in the type II secretion complex, GspC-O, is a good

example of DsrA regulation: type II secretion was silenced by H-NS in the wild type *E. coli* K-12 (82), while DsrA antagonizes the H-NS-mediated silencing of numerous promoters (238). Therefore, the QS-mediated induction of DsrA, resulting from the *lsrR* and *lsrK* deletions, lead to amplified expression of *yheE*, *yheF* (seemingly in *lsrR* mutant only). Even though the *lsr* operon transporters are subjected to *rpoS* regulation, the effect of DsrA's positive induction on *lsr* is unclear. This is because there are many interacting players; *rpoS* also negatively regulates small RNA, RydB, which can, in turn, influence *rpoS*. Also, *lsr* is directly mediated by other regulators such as LsrR, LsrK and cAMP/CRP (276).

Small RNA cell division inhibitor, DicF, was induced ≥2-fold in both *lsrR* and *lsrK* mutants. This is along with the more than 2-fold increase in expression of the cell division gene *dicB* since both genes belong to the same cell division operon (TABLE 1) (25). *DicF* inhibits cell division in *E. coli* by decreasing the abundance and activity of FtsZ, therefore, DicF affects the septum formation and separation of the replicated chromosomes into the daughter nucleoids (267, 268). However, this inhibition effect can be suppressed by an *rpoB* mutation, and the inhibition effect is partially counteracted by an *rpoS* mutation (31). We note however, that we did not see elongated cells in *lsrR* and *lsrK* mutants in our SEM studies. This probably because cell division is a complex process controlled by many modes of regulation (1, 36, 103, 273).

Table 4-6 Small RNAs affected by *lsrR*, *lsrK*

Name	Start	End	Flanking gene	Fold Change		condition
				Δ*lsrR*/WT	Δ*lsrK*/WT	
dsrA	2023233	2023532	*dsrB*/*yedP*	3.6	4.4	confirmed
DicF	1647459	1647632	*rzpQ*/*dicB*	2.0	2.5	confirmed
RydB/tpe7	1762411	1762957	*sufA(ydiC)*/*ydiH*	4.9	--	confirmed
IS102	2069234	2069404	*yeeP*/*flu*	-2.3	-1.5	confirmed
tpke70	2494586	2496690	*ddg*/*yfdZ*	2.0	--	confirmed
MicC (ISO63)	1434918	1435283	*ompN*/*ydbK*	3.2	--	confirmed
ayjiW	4577468	4577637	opposite *yjiW*	2.5	2.1	confirmed
SokX	2885243	2885600		--	3.5	confirmed
Unknown	2468480	2468778	*yfdI*/*tfaS*	2.3	3.2	predicted

Another small RNA, immediately upstream of the *flu* gene, was repressed in both mutants. This might account for the dramatic decrease of *flu*, 10.8- and 6.3- fold respectively, in *lsrR* and *lsrK* mutants (Table4-1) although a monocistronic RNA has not been identified. Two other small RNAs were found co-regulated by *lsrR* and *lsrK*: ayjiW and one flanking the genes, *yfdI/tfaS*. The function of these ribo-regulators remains unclear and awaits further research.

For the *lsrR* mutant, there were three additional small RNAs induced more than 2-fold: RydB, MicC and tpke70. High-copy expression of RydB decreased *rpoS* expression during the stationary phase in LB (278). It is possible that the AI-2 uptake repressor associates with RydB to fine-tune the genetic network through the regulation of the global regulator, RpoS. Expression of MicC was induced when growing at low temperatures or in minimal media (37).

MicC works as an antisense, negatively regulating the translation of an outer membrane protein, *OmpC* (38). We did not see evident changes in *ompC* expression nor changes in the expression of its regulator *ompF*, which is because *ompC* regulated posttranscriptionally by MicC. Therefore, mRNA might not be affected and there still could be changes in protein level. Tpke70 is an antisense with an unclarified function. In *lsrK* mutants, SokX, of unknown function, was induced 3.5-fold.

Discussion

In contrast to our previous microarray study of W3110 and *luxS* mutants, where fewer than 50 genes were significantly affected (277), our current study found 146 genes significantly affected by an *lsrR* deletion and 140 affected by an *lsrK* mutation. Among these, 78 genes were both regulated by *lsrR* and *lsrK* and 69 were identically regulated in both mutants. Our analysis of *lsrR*, *lsrK* deletion revealed many quorum sensing regulated genes (Table 4-1, 4-2 & 4-3). Deletion of *lsrR* resulted in the induction of the *lsr* operon (including *lsrACDBFG* and *tam* gene), while deletion of *lsrK* resulted in the depression of those genes, which is exactly consistent with the reported regulatory structure of this regulon (276, 293). At least one difference between these two mutants and the *luxS* mutant can be attributed to the roles of these proteins in signal generation versus signal perception. This is confounded by our discovery that the genes affected by *luxS*, differ depending on the growth phase and presence or absence of glucose (277). Further, we have recently predicted and demonstrated the existence of non-*luxS* synthesis for AI-2 (161), as has been noted by others (113, 264). The present study, however, enables a linkage between *lsrR* and *lsrK* to AI-2 as a signal molecule.

A key to this understanding was revealed previously but not reported for its importance (276, 277): The *lsr*-lacZ and *lsrR*-lacZ reporters in *lsrR* and *lsr* operon mutants were upregulated manifold. Specifically, the *lsr* transcription rate in an *lsr* operon mutant was upregulated to an almost equivalent extent as in an *lsrR* mutant strain, even though cells import AI-2 at a much slower rate than *lsrR* mutants (due to lack of Lsr transporter). The same transcriptional reporter plasmid was nearly completely inactive in the *lsrK* mutant (consistent with the derepression afforded by phospho-AI-2). These results suggest that AI-2, taken in by an alternative transporter (alluded to in Wang *et al*, 2005) or otherwise unsecreted AI-2, may still be phosphorylated by LsrK. Interestingly, the extracellular AI-2 level in LsrK mutants never drops; AI-2 is not taken up by the cells. These findings suggest that (1) the Lsr transporter does not function without LsrK and that (2) LsrK can work with another transporter. These findings, coupled with the observation that *lsrR* and *lsrK* mutants regulate the same genes in nearly the same manner (with the exception of its uptake transporter), suggest that AI-2, in addition to phospho-AI-2 is an LsrR regulator.

That is, the apparent co-regulation by *lsrR* and *lsrK* genes could be differentiated from *luxS* regulated genes in that *luxS* is an enzyme that acts on a main metabolic pathway and *lsrR*, *lsrK* only mediates cellular determinants when combined with the quorum signal, AI-2. We propose that the signaling role of AI-2 is therefore mediated by at least LsrR and LsrK in a transcriptional regulatory complex. AI-2 is perhaps a global regulator of *E. coli* (292) only when it is coupled to another regulator (e.g., LuxP in *V. harveyi*, LsrR in *E. coli*). Hence the genetic and phenotypic responses from deletion of central metabolic enzyme, *luxS,* are different than that of

lsrR, lsrK mutants (277). Many of the *lsrR* and *lsrK* affected genes are related to biofilm formation, stress responses and protection against foreign DNA, directly in line with quorum sensing as a global signaling mechanism for mediating behavior.

Our finding that a significant number of small RNA regulators was also induced or repressed (Table 4-6) by *lsrR* and *lsrK*, provides the first evidence that small RNAs interact with quorum sensing regulators in *E. coli* K-12. Previous reports have conclusively demonstrated that 4 small RNAs are intimately involved in the quorum sensing networks of *V. harveyi* and *V. cholerae* and act through RNA chaperone, Hfq (159). Coupled destruction of small RNA and cognate target mRNA imposes an ultrasensitive response to environmental stimuli for fine-tuning quorum-sensing circuitry (28, 159). It is possible that *E. coli* quorum sensing utilizes these small RNAs for auto-initiating the AI-2 uptake process as cells approach the stationary phase, thus promptly responding to environmental stimuli. Among the ribo-regulators, *dsrA*, coregulated by *lsrR* and *lsrK*, was significantly induced in both mutants. DsrA encodes a small, untranslated RNA, which post-transcriptionally mediates RpoS and H-NS synthesis in *E. coli* via specific RNA-to-RNA interactions with the help of an Hfq binding protein (239, 243). This finding is the first to suggest convergence of an *E. coli* QS signaling system onto the Hfq/LuxO transduction process of *V. harveyi* and suggests yet one more modality for which bacterial autoinducer signal transduction occurs.

Another striking result of this investigation was that *lsrR* and *lsrK* regulate biofilm architecture and formation by coordinately regulating interactions of bio-film related genes, including the colanic acid synthesis regulator, *wza*, and the *flu* gene.

The influence of these genes on biofilm structure has already been elucidated – its QS dependence is shown here for the first time. Induced colanic acid regulator, *wza*, downregulates colanic synthesis by interacting with the tysosine kinase ,*wzc*, (246, 274) which, in turn, leads to a deficiency in the formation of three-dimensional structures (seen in Figs 4-4 & 4-8). All other biofilm related genes are repressed (except for *b0942)* in *lsrR* mutants. Among these, Ag43, encoded by *flu* gene, can increase biofilm-formation. Thus, overall biofilm formation probably halted in both mutants due to the repressed *flu* gene together with other repressed bio-film related genes (Table 4-5). This is consistent with our confocal microscopy results. However, in our crystal violet assay, before 24 hours, we could not see any differences in biofilm formation between two mutants and the wild type strain. After 30 hours, we started see more biofilm in mutants than in wild type. These different results with different time points suggest that biofilm formation emerges with time, which is reasonable since biofilm development does involve the dynamic processes of attachment and detachment of planktonic cells onto substrates and into growth medium (193).

In a previous study, *in vitro* AI-2 stimulates biofilm formation through the cooperation of a motility regulator, MqsR that mediates QseBC and motility. The addition of *in vitro* AI-2 significantly induced lots of motility related genes thus enhanced biofilm formation, which is correlated with an increased *lsr*-lacZ transcription (98). Herzberg *et al*. also demonstrated that the deletion of an AI-2 exporter YdgG led to higher *lsr*-lacZ level thus increased biofilm formation, and that the recovery of *ydgG* expression increased extracellular AI-2 therefore depressed

biofilm formation (119). In these two systems, the uptake regulators LsrR, LsrK are still active and principally deactivated by AI-2 addition through phospho-AI-2. While in ours, AI-2 uptake regulators are mutated, which are deficient in repressor LsrR. As stated above, this repressor probably mediates cellular processes with the help of AI-2/phospho-AI-2 molecules. It is perhaps interesting that in some cases the phospho-AI-2 is important and in others, AI-2 is important. These suggest that two different biofilm regulatory modes associate with quorum signal AI-2 in *E. coli,* and that AI-2 can associate with different regulators to regulate biofilm formation under different conditions. De Keersmaecker *et al*. recently also demonstrated that expression of the addition of synthetic DPD(i.e., *in vitro* AI-2) can rescue AI-2 uptake transporter *lsr* operon but not biofilm formation in a *luxS* mutant of *S. typhimurim* (55). This example from a homologous *E. coli* organism demonstrated that biofilm formation processes are not necessarily associated with *lsr* transcriptional mediated AI-2 signaling pathway.

Quorum sensing signals cooperating with their repressors or receptors to regulate gene expression are commonly existed. For examples, AI-1 signal binds with its repressor LuxR type protein to regulate bioluminescence (90). AI-2 ligand cooperates with its receptor protein LuxP to trigger the transition *V. harveyi* into quorum sensing mode (187). An AI-2/phospho-AI-2 ligand-induced quorum sensing regulations in *E. coli* is proposed based on our previous researches and current investigations (Fig. 4-9): when extracellular AI-2 signaling accumulates in supernatants, imported AI-2 molecule binds with LsrR to relieve its repression (activation) on gene (such as *dsrA*, *flu*, *wza*) expression. When cells sense the nutrient

depletion, imported AI-2 signal will be phosphorylated. The phosphorylated of AI-2 signal probably results in the conformational changes of repressor LsrR, which then triggers the disassociation of AI-2 molecule and association of phospho-AI-2 with LsrR. The binding of phospho-AI-2 with LsrR probably serves as a flip-off switch to turn off genetic regulations associated with LsrR-AI-2, and to turn on the genetic expression subject to LsrR and phospho-AI-2, that is, initiate the positive feedback regulation of *lsr* operon transporter to recycle AI-2 molecule for metabolisms. This regulatory mode associates with complex hierarchy and dynamic responses. But how these two different regulatory modes switch and regulate different cellular processes still remains enigma. Hopefully, the *de novo* unity of current knowledge with mathematical simulations, which successfully uncovered a hidden alternative AI-2 synthesis pathway (161), will lead us to the right solution.

All in all, from our transcriptome analysis, we demonstrate that there are three different groups of genes regulated by the AI-2 uptake repressor, LsrR, and the AI-2 kinase, LsrK: (1) genes divergently regulated by LsrR and LsrK (e.g., *lsr* operon) wherein LsrR serves as a repressor and LsrK provides inducer, phospho-AI-2; (2) genes co-regulated by both LsrR and LsrK, among which biofilm formation genes are examples in that both LsrR and LsrK seemingly work together to modulate gene expression. This two different type of regulations associated with lsrR, lsrK first tiem demonstrated clearly that AI-2 signal in *E. coli* system is a singalling molecule. (3) genes regulated either by LsrR or LsrK, which suggests that LsrR and LsrK have their own specific functions other than working together as stated above. For the first time,

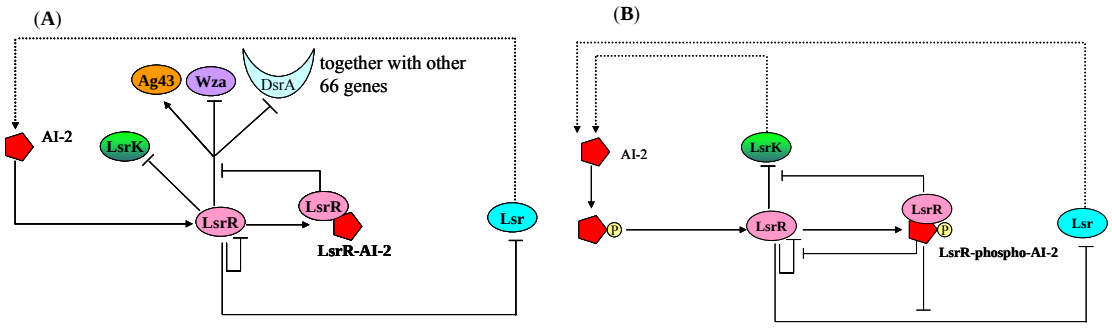

Figure 4-9 Proposed regulatory mechanisms associated with *lsrR, lsrK*
(A) LsrR represses (in some case activate, like *flu* gene (AG43)) gene expression, such as *wza*, *dsrA*. AI-2 molecule or some AI-2 anomers can bind with this repressor to derepress its repression on gene expression, thus globally control cell societal behaviors and dynamic response. Crescent shape represents small RNA. (B) When extracellular AI-2 concentration reaches some threshold, *lsr* imported AI-2 back inside the cells as cells sense nutrients depletion. The imported AI-2 signal will be phosphorylated to phospho-AI-2. This molecule probably will change the conformation of LsrR repressor thus to deassociate AI-2 molecule with this repressor and terminate their related gene expression. At the same time, phosphor-AI-2 binds/associates with this repressor to relieve its repression on *lsr* transporter operon, which will also trigger the positive feedback regulation of *lsr* operon thus further processing phospho-AI-2 for recycling this molecule into cell metabolism.

several small RNAs were shown to interact with the quorum sensing regulators *lsrR* and *lsrK*. It is possible that bacteria utilize these self-limiting small RNA regulators to fine tune *lsrR* and *lsrK* which in turn imposes various mediations on cellular phenotype and gene expression. This study sheds light on this connectivity while the specific crosstalk between these regulators (small RNAs and *lsrR, lsrK*) still awaits further investigation.

Acknowledgements

I would like to thank Mr. Alvaro Godínez for assistance in the DNA microarray experiments, Tim Maugel for scanning electron microscopy (SEM) experiments. This work was supported by the National Science Foundation (Grants BES-0124401, BES-0222687) and the Center for Biosystems Research, UMBI.

Chapter 5: Conclusions and Future Directions

It has been demonstrated that addition of PTS sugar can increase the AI-2 level significantly. There is no direct evidence that explains this dramatic increase even though some researchers have suggested it is due to the catabolic repression of AI-2 uptake regulators. First, this study utilized the combined efforts of mathematical simulations and experimental tools to explore the metabolic pathways and regulatory mechanisms associated with this phenomenon in *E. coli*. Our results demonstrated that this phenomenon is not due to AI-2 synthase *luxS*, *pfs* transcript levels nor their corresponding protein amounts. Also, increased metabolic flux due to the addition of glucose can not substantially account for this increase. Our predictions indicate that this increase is due to the existence of alternative pathways for AI-2 synthesis. This was validated by observing AI-2 activity from cellular extracts of *luxS/pfs* mutants supplemented with adenosine. We believe the coupling of experimental measurements together with mathematical modeling analysis is needed to uncover hidden mechanisms and dynamics associated with partially elucidated metabolic pathways. This is a key component in making systems biology a successful endeavor in the industrial sector.

In addition, the mechanisms associated with AI-2 uptake regulators were studied in detail using recombinant lacZ reporter and genomic profiling. In particular, *lsrR*-lacZ, *lsrK*-lacZ reporters were constructed to elucidate the transcriptional profile associated with AI-2 uptake repressor LsrR and its kinase LsrK. *lsrR*, *lsrK* transcription was found subject to catabolite repression and LsrR repression. Activation of *lsrR* expression also depends on induction of the *luxS* and *lsrK* genes

while activation of *lsrK* promoter does not depend on these factors. The existence of monocistronic transcript, spanning the whole coding region between *lsrR* and *lsrK*, demonstrated that *lsrR* and *lsrK* belong to the same operon. *LsrK* gene is mainly subject to the *lsrR* promoter regulation, and additionally to *lsrK* promoter mediation.

Genomic profiling of *lsrR*, *lsrK* mutations revealed many genes subject to the regulations of the AI-2 uptake regulators. This is an interesting and important result. The existence of coregulated genes by both *lsrR* and *lsrK* demonstrated that there exists another type of regulation controlled by these regulators. This is probably because *lsrR* and *lsrK* belong to the same operon and *lsrR*'s regulation is epistatic. That is, LsrR probably binds with imported AI-2 or unsecreted intracellular AI-2 or its anomers to coregulate gene expression. While the phosphorylation of signaling molecule results in association of phospho-AI-2 with LsrR, which in turn, terminates the LsrR-AI-2 mediated cellular processes and triggers the *lsr* operon mediated expression. At the same time, there are also different groups of genes regulated by *lsrR* and *lsrK* respectively. This is probably because both regulators have their own specific roles and functions. In quorum sensing AI-2 uptake, LsrR works as a repressor while LsrK acts as a kinase. Hence, different gene groups are regulated by different regulators. Another striking finding from genomic profiling is that AI-2 uptake regulators, were for the first time demonstrated to be involved with many small RNAs. There are five small RNA coregulated by *lsrR* and *lsrK*, while another two small RNAs regulated by *lsrR* and *lsrK* respectively. Recently, numerous reports have identified that small RNA works as a secondary messenger for mediating cellular processes and/or metabolism in a variety of bacterial species, such as *V.*

cholerae, *Pseudomonas fluorescens* (139, 159). It is not surprising that *E. coli* quorum sensing systems utilize the ribo-regulators to globally mediate responses to environmental stimuli. Remarkably, *lsrR* and *lsrK* mutations resulted in deficiency in forming complex three-dimensional biofilm structures, as compared to their wild type parent. This is a solid example of *lsrR* and *lsrK* coregulating phenotype. These discoveries have led to the new regulatory pathways associated with the *E. coli* quorum sensing uptake network, and broaden our knowledge about the current quorum sensing circuitry in *E. coli*. New directions in research are sure to result.

For example, in order to discover more molecular interactions and the cellular regulations associated with AI-2 uptake, we need identify the binding site of LsrR. That is, we need to refine the gel motility assay for the binding between LsrR with its DNA operator *lsr* and *lsrR* promoters. We found that *lsr*-lacZ transcription was repressed due to the *lsrR* expression (Fig 3-5) in *vivo*. Current results from the gel shift binding assay did not show apparent shift, which is probably because we did not include the activator CRP's binding site in the DNA sequence during the assay or some other molecules that were necessary for the binding. Refined binding assays will be performed as stated in Chapter 3. A successful binding assay will provide evidence for LsrR as a repressor on the *lsr* transporter during the auto-initiated AI-2 uptake process. Further investigations of the protein structure and function of LsrR, based on homologous analysis and crystal studies, will also provide valuable information for elaborating the regulations of quorum sensing in *E. coli*.

Since LsrK was already demonstrated as a kinase in *S. typhimurium* and a similar function was proposed in *E. coli* (260, 276, 293), where the phosphorylation

process was suggested to be an indispensable part of the quorum sensing network. Phosphorylation processes were demonstrated as an active signal transduction step for linking quorum sensing systems in *V. harveyi* and *V. cholerae* (32, 85). In eukaryotic systems phosphorylation processes are related to abundant signal transduction networks, such as MAPK kinase, p53 factor etc (231). It is also commonly known that cellular regulations are often associated with biological molecule's phosphorylation and dephosphorylation. Therefore, further investigations of this quorum sensing kinase, LsrK, will provide valuable information on the state of phosphorylated signal transduction in *E. coli*. Investigations of proteins LsrF and LsrG will shed light on how this signaling molecule reconnected to cell metabolism.

Further elucidation of the interactions between small RNAs with LsrR, LsrK, the *lsr* operon will also help to uncover the hidden mechanisms for this auto-induced regulatory network. A promosing way will be the investigation of Hfq protein level in *lsrR*, *lsrK* mutants and their isogenic parent strains. Bassler's group studied phenotypic changes, including bioluminescence and toxin-coregulated pilus, from the *hfq* mutation, and analyzed Hfq associated *hapR* mRNA stability by Northern blots (159). We probably can also utilizse Northern blots to test whether *hfq* level has changed in both *lsrR*, *lsrK* mutants. We can test the interactions between LsrR, LsrK and Hfq by co-immunoprecipitation and directly detect the bound RNAs on genomic microarrays to identify members of this small RNA family. This approach was extremely sensitive in previous work: even Hfq-binding small RNAs expressed at low levels were readily detected (300). Alternatively, a comparative transcriptome analysis of wild type gene with *hfq* mutant or *lsrR hfq* double mutant (244) will be

useful for further explaining the signal transduction network associated with quorum sensing. Analysis the membrane receptor protein and sensory protein from the genomic profiling will also provide more information for AI-2 signal export process, and help to discover what other genetic regulatory network are crosstalking with quorum sensing circuitry.

As a result of this dissertation, we found out that quorum sensing uptake regulators *lsrR*, *lsrK* together with the *lsr* operon formed different interlocking positive-negative feedback loops in response to different input signals (Fig 4-9). However, how these feedback loops help the cells self-perptuate different states, and drive phenotype changes still remain mysterious. Our results also suggest that these uptake circuits interact with other unidentified pathways for mediating societal activity and systematical behaviors, such as small RNAs and biofilm formation. Mathematical models can help formulate the mechanistic hypotheses, derive the physiological implications, and uncover the associated dynamic switch responses originated from meshed feeback regulation (79, 271). Hence, we can test different types of interactions between uptake repressor LsrR, kinase LsrK, the *lsr* operon and signaling molecule AI-2/phospho-AI-2 by mathematically simulating the regulatory networks in Fig 4-9. Flow cytometry for the density distribution will be helpful for dynamic measuring the responses in this regulatory network. Hopefully, this in turn will help to to unmask the hidden mechanisms and dynamics associated with these pathways, help to explain more quorum-sensing associated behaviors, and provide better ways for reengineering this auto-initiated processes. Hence, this combined

approach will provide a more comprehensive picture of *E. coli* quorum sensing system and provide new insights for further research.

Bibliography

1. **Aarsman, M. E., A. Piette, C. Fraipont, T. M. Vinkenvleugel, M. Nguyen-Disteche, and T. den Blaauwen.** 2005. Maturation of the Escherichia coli divisome occurs in two steps. Mol Microbiol **55:**1631-45.
2. **Adar, Y. Y., M. Simaan, and S. Ulitzur.** 1992. Formation of the LuxR protein in the Vibrio fischeri lux system is controlled by HtpR through the GroESL proteins. J Bacteriol **174:**7138-43.
3. **Adar, Y. Y., and S. Ulitzur.** 1993. GroESL proteins facilitate binding of externally added inducer by LuxR protein-containing E. coli cells. J Biolumin Chemilumin **8:**261-6.
4. **Aguzzi, A., and C. Weissmann.** 1996. Spongiform encephalopathies: a suspicious signature. Nature **383:**666-7.
5. **Ahmer, B. M.** 2004. Cell-to-cell signalling in Escherichia coli and Salmonella enterica. Mol Microbiol **52:**933-45.
6. **Almaas, E., Kovacs B, Vicsek T, Oltvai ZN, and A. Barabasi.** 2004. Global organization of metabolic fluxes in the bacterium *Escherichia coli*. Nature **427:**839-843.
7. **Anton, B. P., and E. A. Raleigh.** 2004. Transposon-mediated linker insertion scanning mutagenesis of the Escherichia coli McrA endonuclease. J Bacteriol **186:**5699-707.
8. **Arkin, A., J. Ross, and H. H. McAdams.** 1998. Stochastic kinetic analysis of developmental pathway bifurcation in phage lambda-infected *Escherichia coli* cells. Genetics **149:**1633-48.
9. **Asanuma, N., T. Yoshii, and T. Hino.** 2004. Molecular characterization and transcription of the luxS gene that encodes LuxS autoinducer 2 synthase in Streptococcus bovis. Curr Microbiol **49:**366-71.
10. **Balestrino, D., J. A. Haagensen, C. Rich, and C. Forestier.** 2005. Characterization of type 2 quorum sensing in *Klebsiella pneumoniae* and relationship with biofilm formation. J Bacteriol **187:**2870-80.
11. **Baltimore, D.** 1970. RNA-dependent DNA polymerase in virions of RNA tumour viruses. Nature **226:**1209-11.
12. **Barnhart, M. M., and M. R. Chapman.** 2006. Curli Biogenesis and Function. Annu Rev Microbiol.
13. **Barrett, C. L., T. Y. Kim, H. U. Kim, B. O. Palsson, and S. Y. Lee.** 2006. Systems biology as a foundation for genome-scale synthetic biology. Curr Opin Biotechnol **17:**488-92.
14. **Bassler, B. L., E. P. Greenberg, and A. M. Stevens.** 1997. Cross-species induction of luminescence in the quorum-sensing bacterium Vibrio harveyi. J Bacteriol **179:**4043-5.
15. **Bassler, B. L., M. Wright, R. E. Showalter, and M. R. Silverman.** 1993. Intercellular signalling in *Vibrio harveyi*: sequence and function of genes regulating expression of luminescence. Mol Microbiol **9:**773-86.
16. **Bassler, B. L., M. Wright, and M. R. Silverman.** 1994. Multiple signalling systems controlling expression of luminescence in *Vibrio harveyi*: sequence

and function of genes encoding a second sensory pathway. Mol Microbiol **13:**273-86.
17. **Becskei, A., and L. Serrano.** 2000. Engineering stability in gene networks by autoregulation. Nature **405:**590-3.
18. **Beeston, A. L., and M. G. Surette.** 2002. pfs-dependent regulation of autoinducer 2 production in Salmonella enterica serovar Typhimurium. J Bacteriol **184:**3450-6.
19. **Beis, K., R. F. Collins, R. C. Ford, A. B. Kamis, C. Whitfield, and J. H. Naismith.** 2004. Three-dimensional structure of Wza, the protein required for translocation of group 1 capsular polysaccharide across the outer membrane of Escherichia coli. J Biol Chem **279:**28227-32.
20. **Berg, O. G.** 1978. A model for the statistical fluctuations of protein numbers in a microbial population. J Theor Biol **71:**587-603.
21. **Berg, O. G., J. Paulsson, and M. Ehrenberg.** 2000. Fluctuations and quality of control in biological cells: zero-order ultrasensitivity reinvestigated. Biophys J **79:**1228-36.
22. **Bettenbrock, K., S. Fischer, A. Kremling, K. Jahreis, T. Sauter, and E. D. Gilles.** 2006. A quantitative approach to catabolite repression in Escherichia coli. J Biol Chem **281:**2578-84.
23. **Blake, W. J., K. A. M, C. R. Cantor, and J. J. Collins.** 2003. Noise in eukaryotic gene expression. Nature **422:**633-7.
24. **Bohannon, D. E., N. Connell, J. Keener, A. Tormo, M. Espinosa-Urgel, M. M. Zambrano, and R. Kolter.** 1991. Stationary-phase-inducible "gearbox" promoters: differential effects of *katF* mutations and role of sigma 70. J Bacteriol **173:**4482-92.
25. **Bouche, F., and J. P. Bouche.** 1989. Genetic evidence that DicF, a second division inhibitor encoded by the Escherichia coli dicB operon, is probably RNA. Mol Microbiol **3:**991-4.
26. **Bowman, W. H., C. W. Tabor, and H. Tabor.** 1973. Spermidine biosynthesis. Purification and properties of propylamine transferase from Escherichia coli. J Biol Chem **248:**2480-6.
27. **Bremer, H., and P. Dennis.** 1996. Modulation of chemical composition and other parameters of the cell by growth rate, p. 1553-1569. *In* F. Neidhardt (ed.), *Escherichia coli* and *Salmonella*: cellular and molecular biology, 2nd ed, vol. 2. ASM Press, Washington, DC.
28. **Brescia, C. C., P. J. Mikulecky, A. L. Feig, and D. D. Sledjeski.** 2003. Identification of the Hfq-binding site on DsrA RNA: Hfq binds without altering DsrA secondary structure. Rna **9:**33-43.
29. **Burr, T., A. M. Barnard, M. J. Corbett, C. L. Pemberton, N. J. Simpson, and G. P. Salmond.** 2006. Identification of the central quorum sensing regulator of virulence in the enteric phytopathogen, Erwinia carotovora: the VirR repressor. Mol Microbiol **59:**113-25.
30. **Cadieux, N., C. Bradbeer, E. Reeger-Schneider, W. Koster, A. K. Mohanty, and M. C. Wiener, and R.J. Kadner.** 2002. Identification of the periplasmic cobalamin-binding protein BtuF of *Escherichia coli*. J. Bacteriol. **184:**706-717.

31. **Cam, K., A. Cuzange, and J. P. Bouche.** 1995. Sigma S-dependent overexpression of ftsZ in an Escherichia coli K-12 rpoB mutant that is resistant to the division inhibitors DicB and DicF RNA. Mol Gen Genet **248:**190-4.
32. **Camara, M., A. Hardman, P. Williams, and D. Milton.** 2002. Quorum sensing in Vibrio cholerae. Nat Genet **32:**217-8.
33. **Camas, F. M., J. Blazquez, and J. F. Poyatos.** 2006. Autogenous and nonautogenous control of response in a genetic network. Proc Natl Acad Sci U S A.
34. **Camilli, A., and B. L. Bassler.** 2006. Bacterial small-molecule signaling pathways. Science **311:**1113-6.
35. **Cao, J. G., and E. A. Meighen.** 1989. Purification and structural identification of an autoinducer for the luminescence system of Vibrio harveyi. J Biol Chem **264:**21670-6.
36. **Chen, J. C., and J. Beckwith.** 2001. FtsQ, FtsL and FtsI require FtsK, but not FtsN, for co-localization with FtsZ during Escherichia coli cell division. Mol Microbiol **42:**395-413.
37. **Chen, S., E. A. Lesnik, T. A. Hall, R. Sampath, R. H. Griffey, D. J. Ecker, and L. B. Blyn.** 2002. A bioinformatics based approach to discover small RNA genes in the Escherichia coli genome. Biosystems **65:**157-177.
38. **Chen, S., A. Zhang, L. B. Blyn, and G. Storz.** 2004. MicC, a second small-RNA regulator of Omp protein expression in Escherichia coli. J Bacteriol **186:**6689-97.
39. **Chen, X., S. Schauder, N. Potier, A. Van Dorsselaer, I. Pelczer, B. L. Bassler, and F. M. Hughson.** 2002. Structural identification of a bacterial quorum-sensing signal containing boron. Nature **415:**545-549.
40. **Chen, Y. W., P. Zhao, R. Borup, and E. P. Hoffman.** 2000. Expression profiling in the muscular dystrophies: identification of novel aspects of molecular pathophysiology. J Cell Biol **151:**1321-36.
41. **Choi, S. H., and E. P. Greenberg.** 1991. The C-terminal region of the *Vibrio fischeri* LuxR protein contains an inducer-independent *lux* gene activating domain. Proc Natl Acad Sci U S A **88:**11115-9.
42. **Choo, Q. L., G. Kuo, A. J. Weiner, L. R. Overby, D. W. Bradley, and M. Houghton.** 1989. Isolation of a cDNA clone derived from a blood-borne non-A, non-B viral hepatitis genome. Science **244:**359-62.
43. **Coburn, P. S., C. M. Pillar, B. D. Jett, W. Haas, and M. S. Gilmore.** 2004. Enterococcus faecalis senses target cells and in response expresses cytolysin. Science **306:**2270-2.
44. **Cohen, S.** 1998. A guide to the polyamines. Oxford University Press, New York.
45. **Connell, N., Z. Han, F. Moreno, and R. Kolter.** 1987. An *E. coli* promoter induced by the cessation of growth. Mol Microbiol **1:**195-201.
46. **Cook, D. L., A. N. Gerber, and S. J. Tapscott.** 1998. Modeling stochastic gene expression: implications for haploinsufficiency. Proc Natl Acad Sci U S A **95:**15641-6.
47. **Crick, F.** 1970. Central dogma of molecular biology. Nature **227:**561-3.

48. **Crick, F. H.** 1958. On protein synthesis. Symp Soc Exp Biol **12:**138-63.
49. **Danese, P. N., L. A. Pratt, S. L. Dove, and R. Kolter.** 2000. The outer membrane protein, antigen 43, mediates cell-to-cell interactions within Escherichia coli biofilms. Mol Microbiol **37:**424-32.
50. **Danese, P. N., L. A. Pratt, and R. Kolter.** 2000. Exopolysaccharide production is required for development of Escherichia coli K-12 biofilm architecture. J Bacteriol **182:**3593-6.
51. **Davidson, E. H., J. P. Rast, P. Oliveri, A. Ransick, C. Calestani, C. H. Yuh, T. Minokawa, G. Amore, V. Hinman, C. Arenas-Mena, O. Otim, C. T. Brown, C. B. Livi, P. Y. Lee, R. Revilla, A. G. Rust, Z. Pan, M. J. Schilstra, P. J. Clarke, M. I. Arnone, L. Rowen, R. A. Cameron, D. R. McClay, L. Hood, and H. Bolouri.** 2002. A genomic regulatory network for development. Science **295:**1669-78.
52. **Davies, D. G., M. R. Parsek, J. P. Pearson, B. H. Iglewski, J. W. Costerton, and E. P. Greenberg.** 1998. The involvement of cell-to-cell signals in the development of a bacterial biofilm. Science **280:**295-8.
53. **de Jong, H.** 2002. Modeling and simulation of genetic regulatory systems: a literature review. J Comput Biol **9:**67-103.
54. **De Keersmaecker, S. C., K. Sonck, and J. Vanderleyden.** 2006. Let LuxS speak up in AI-2 signaling. Trends Microbiol **14:**114-119.
55. **De Keersmaecker, S. C., C. Varszegi, N. van Boxel, L. W. Habel, K. Metzger, R. Daniels, K. Marchal, D. De Vos, and J. Vanderleyden.** 2005. Chemical synthesis of (S)-4,5-dihydroxy-2,3-pentanedione, a bacterial signal molecule precursor, and validation of its activity in Salmonella typhimurium. J Biol Chem **280:**19563-8.
56. **de Kievit, T. R., and B. H. Iglewski.** 2000. Bacterial quorum sensing in pathogenic relationships. Infect Immun **68:**4839-49.
57. **de la Fuente, A., and P. Mendes.** 2003. Integrative modelling of gene expression and cell metabolism. Appl Bioinformatics **2:**79-90.
58. **DeLisa, M. P., J. J. Valdes, and W. E. Bentley.** 2001. Mapping stress-induced changes in autoinducer AI-2 production in chemostat-cultivated *Escherichia coli* K-12. J Bacteriol **183:**2918-2928.
59. **DeLisa, M. P., J. J. Valdes, and W. E. Bentley.** 2001. Quorum signaling via AI-2 communicates the "Metabolic Burden" associated with heterologous protein production in *Escherichia coli*. Biotechnol Bioeng **75:**439-450.
60. **DeLisa, M. P., J. J. Valdes, and W. E. Bentley.** 2001. Quorum signaling via AI-2 communicates the "Metabolic Burden" associated with heterologous protein production in *Escherichia coli*. Biotechnol Bioeng **75:**439-50.
61. **Della Ragione, F., M. Porcelli, M. Cartenì-Farina, and V. a. P. Zappia, A E.** 1985. Escherichia coli S-adenosylhomocysteine/5'-methylthioadenosine nucleosidase. Purification, substrate specificity and mechanism of action. Biochem J **232:**335-341.
62. **Derzelle, S., E. Duchaud, F. Kunst, A. Danchin, and P. Bertin.** 2002. Identification, characterization, and regulation of a cluster of genes involved in carbapenem biosynthesis in Photorhabdus luminescens. Appl Environ Microbiol **68:**3780-9.

63. **Devine, J. H., G. S. Shadel, and T. O. Baldwin.** 1989. Identification of the operator of the *lux* regulon from the *Vibrio fischeri* strain ATCC7744. Proc Natl Acad Sci U S A **86:**5688-92.
64. **Dong, Y. H., L. H. Wang, J. L. Xu, H. B. Zhang, X. F. Zhang, and L. H. Zhang.** 2001. Quenching quorum-sensing-dependent bacterial infection by an N-acyl homoserine lactonase. Nature **411:**813-7.
65. **Dong, Y. H., J. L. Xu, X. Z. Li, and L. H. Zhang.** 2000. AiiA, an enzyme that inactivates the acylhomoserine lactone quorum-sensing signal and attenuates the virulence of Erwinia carotovora. Proc Natl Acad Sci U S A **97:**3526-31.
66. **Draper, D.** 1996. Tranlational initiation, p. 902-921. *In* F. C. Neidhardt (ed.), Escherichia coli and Salmonella, vol. I. ASM press, Washington, DC.
67. **Drummelsmith, J., and C. Whitfield.** 1999. Gene products required for surface expression of the capsular form of the group 1 K antigen in Escherichia coli (O9a:K30). Mol Microbiol **31:**1321-32.
68. **Drummelsmith, J., and C. Whitfield.** 2000. Translocation of group 1 capsular polysaccharide to the surface of Escherichia coli requires a multimeric complex in the outer membrane. Embo J **19:**57-66.
69. **Dudda-Subramanya, R., G. Lucchese, D. Kanduc, and A. A. Sinha.** 2003. Clinical applications of DNA microarray analysis. J Exp Ther Oncol **3:**297-304.
70. **Duerre, J.** 1962. A Hydrolytic Nucleosidase acting on S-Adenosylhomocysteine and on 5'-Methlthioadenosine. The journal of biological chemistry **237:**3737-3741.
71. **Dufour, P., S. Jarraud, F. Vandenesch, T. Greenland, R. P. Novick, M. Bes, J. Etienne, and G. Lina.** 2002. High genetic variability of the agr locus in Staphylococcus species. J Bacteriol **184:**1180-6.
72. **Ebeling, W., L. Schimansky-Geier, and Y. M. Romanovsky.** 2002. Stochastic Dynamics of Reacting Biomolecules. World Scientific Publishing Co., Singpapore.
73. **Eberhard, A., T. Longin, C. A. Widrig, and S. J. Stranick.** 1991. Synthesis of the lux gene autoinducer in Vibrio fischeri is positively autoregulated. Arch Microbiol **155:**294-297.
74. **Eberl, L.** 1999. N-acyl homoserinelactone-mediated gene regulation in gram-negative bacteria. Syst Appl Microbiol **22:**493-506.
75. **Elowitz, M. B., A. J. Levine, E. D. Siggia, and P. S. Swain.** 2002. Stochastic gene expression in a single cell. Science **297:**1183-6.
76. **Erdi, P., and J. Toth.** 1989. Mathematical models of chemical reactions:theory and applications of deterministic and stochastic models. Princeton Univ press, Princeton.
77. **Faubladier, M., and J. P. Bouche.** 1994. Division inhibition gene dicF of Escherichia coli reveals a widespread group of prophage sequences in bacterial genomes. J Bacteriol **176:**1150-6.
78. **Federle, M. J., and B. L. Bassler.** 2003. Interspecies communication in bacteria. J Clin Invest **112:**1291-9.

79. **Ferrell, J. E., Jr.** 2002. Self-perpetuating states in signal transduction: positive feedback, double-negative feedback and bistability. Curr Opin Cell Biol **14:**140-8.
80. **Finnegan, E. J., and M. A. Matzke.** 2003. The small RNA world. J Cell Sci **116:**4689-93.
81. **Fire, A., S. Xu, M. K. Montgomery, S. A. Kostas, S. E. Driver, and C. C. Mello.** 1998. Potent and specific genetic interference by double-stranded RNA in Caenorhabditis elegans. Nature **391:**806-11.
82. **Francetic, O., D. Belin, C. Badaut, and A. P. Pugsley.** 2000. Expression of the endogenous type II secretion pathway in Escherichia coli leads to chitinase secretion. Embo J **19:**6697-703.
83. **Francetic, O., and A. P. Pugsley.** 1996. The cryptic general secretory pathway (gsp) operon of Escherichia coli K-12 encodes functional proteins. J Bacteriol **178:**3544-9.
84. **Franks, P. W., J. L. Mesa, A. H. Harding, and N. J. Wareham.** 2006. Gene-lifestyle interaction on risk of type 2 diabetes. Nutr Metab Cardiovasc Dis.
85. **Freeman, J. A., B. N. Lilley, and B. L. Bassler.** 2000. A genetic analysis of the functions of LuxN: a two-component hybrid sensor kinase that regulates quorum sensing in Vibrio harveyi. Mol Microbiol **35:**139-49.
86. **Fuqua, C., and Greenberg, E. P.** 1998. Self perception in bacteria: quorum sensing with acylated homoserine lactones. Curr Opin Microbiol **1:**183-189.
87. **Fuqua, C., M. R. Parsek, and E. P. Greenberg.** 2001. Regulation of gene expression by cell-to-cell communication: acyl-homoserine lactone quorum sensing. Annu Rev Genet **35:**439-68.
88. **Fuqua, C., and S. C. Winans.** 1996. Conserved cis-acting promoter elements are required for density-dependent transcription of *Agrobacterium tumefaciens* conjugal transfer genes. J Bacteriol **178:**435-40.
89. **Fuqua, C., S. C. Winans, and E. P. Greenberg.** 1996. Census and consensus in bacterial ecosystems: the LuxR-LuxI family of quorum-sensing transcriptional regulators. Annu Rev Microbiol **50:**727-51.
90. **Fuqua, W. C., S. C. Winans, and E. P. Greenberg.** 1994. Quorum sensing in bacteria: the LuxR-LuxI family of cell density-responsive transcriptional regulators. J Bacteriol **176:**269-75.
91. **Gardner, T. S., C. R. Cantor, and J. J. Collins.** 2000. Construction of a genetic toggle switch in Escherichia coli. Nature **403:**339-42.
92. **Genin, S., and C. A. Boucher.** 1994. A superfamily of proteins involved in different secretion pathways in gram-negative bacteria: modular structure and specificity of the N-terminal domain. Mol Gen Genet **243:**112-8.
93. **Gibson, M. A., and E. Mjolsness.** 2001. Modeling of the activity of signle genes, p. 1-48. *In* J. M. B. a. H. Bolouri (ed.), Computational modeling of genetic and biochemical networks. MIT Press, Cambrige.
94. **Gillespie, D. T.** 1977. Exact stochastic simulation of coupled chemical reactions. J. Phys. Chem. **81:**2340-2361.
95. **Gillespie, D. T.** 1977. Exact stochastic simulation of coupled chemical reactions. J. Phys. Chem. **81:**2340~2361.

96. **Gillespie, D. T.** 1976. A general method for numerically simulating the stochastic time evolution of coupled chemical reactions. J. Comput . Phys. **22:**403-434.
97. **Glass, L., and S. A. Kauffman.** 1973. The logical analysis of continuous, non-linear biochemical control networks. J Theor Biol **39:**103-29.
98. **Gonzalez Barrios, A. F., R. Zuo, Y. Hashimoto, L. Yang, W. E. Bentley, and T. K. Wood.** 2006. Autoinducer 2 controls biofilm formation in Escherichia coli through a novel motility quorum-sensing regulator (MqsR, B3022). J Bacteriol **188:**305-16.
99. **Goss, P. J., and J. Peccoud.** 1998. Quantitative modeling of stochastic systems in molecular biology by using stochastic Petri nets. Proc Natl Acad Sci U S A **95:**6750-5.
100. **Grebe, T. W., and J. B. Stock.** 1999. The histidine protein kinase superfamily. Adv Microb Physiol **41:**139-227.
101. **Guptasarma, P.** 1995. Does replication-induced transcription regulate synthesis of the myriad low copy number proteins of Escherichia coli? Bioessays **17:**987-97.
102. **Haken, H.** 1982. Nonequilibrium phase transitions and self-organization in biological systems. *In* A. Zotin (ed.), Thermodynamics and Kinetics of Biological Processes. Walter de Gruyter, Berlin, Germany.
103. **Hale, C. A., and P. A. de Boer.** 2002. ZipA is required for recruitment of FtsK, FtsQ, FtsL, and FtsN to the septal ring in Escherichia coli. J Bacteriol **184:**2552-6.
104. **Hamada, K., H. Ago, M. Sugahara, Y. Nodake, S. Kuramitsu, and M. Miyano.** 2003. Oxyanion hole-stabilized stereospecific isomerization in ribose-5-phosphate isomerase (Rpi). J Biol Chem **278:**49183-90.
105. **Hammer, B. K., and B. L. Bassler.** 2003. Quorum sensing controls biofilm formation in Vibrio cholerae. Mol Microbiol **50:**101-4.
106. **Hammond, S. M., E. Bernstein, D. Beach, and G. J. Hannon.** 2000. An RNA-directed nuclease mediates post-transcriptional gene silencing in Drosophila cells. Nature **404:**293-6.
107. **Hannon, G. J.** 2002. RNA interference. Nature **418:**244-51.
108. **Hanzelka, B. L., M. R. Parsek, D. L. Val, P. V. Dunlap, J. E. Cronan, Jr., and E. P. Greenberg.** 1999. Acylhomoserine lactone synthase activity of the *Vibrio fischeri* AinS protein. J Bacteriol **181:**5766-70.
109. **Hardie, K. R., C. Cooksley, A. D. Green, and K. Winzer.** 2003. Autoinducer 2 activity in Escherichia coli culture supernatants can be actively reduced despite maintenance of an active synthase, LuxS. Microbiology **149:**715-28.
110. **Hardy, S., and P. N. Robillard.** 2004. Modeling and simulation of molecular biology systems using petri nets: modeling goals of various approaches. J Bioinform Comput Biol **2:**595-613.
111. **Hasman, H., T. Chakraborty, and P. Klemm.** 1999. Antigen-43-mediated autoaggregation of Escherichia coli is blocked by fimbriation. J Bacteriol **181:**4834-41.

112. **Hasty, J., D. McMillen, and J. J. Collins.** 2002. Engineered gene circuits. Nature **420:**224-30.
113. **Hauck, T., Y. Hubner, F. Bruhlmann, and W. Schwab.** 2003. Alternative pathway for the formation of 4,5-dihydroxy-2,3-pentanedione, the proposed precursor of 4-hydroxy-5-methyl-3(2H)-furanone as well as autoinducer-2, and its detection as natural constituent of tomato fruit. Biochim Biophys Acta **1623:**109-19.
114. **Havarstein, L. S., G. Coomaraswamy, and D. A. Morrison.** 1995. An unmodified heptadecapeptide pheromone induces competence for genetic transformation in Streptococcus pneumoniae. Proc Natl Acad Sci U S A **92:**11140-4.
115. **Havarstein, L. S., R. Hakenbeck, and P. Gaustad.** 1997. Natural competence in the genus Streptococcus: evidence that streptococci can change pherotype by interspecies recombinational exchanges. J Bacteriol **179:**6589-94.
116. **Henderson, I. R., F. Navarro-Garcia, M. Desvaux, R. C. Fernandez, and D. Ala'Aldeen.** 2004. Type V protein secretion pathway: the autotransporter story. Microbiol Mol Biol Rev **68:**692-744.
117. **Henke, J. M., and B. L. Bassler.** 2004. Quorum sensing regulates type III secretion in Vibrio harveyi and Vibrio parahaemolyticus. J Bacteriol **186:**3794-805.
118. **Henke, J. M., and B. L. Bassler.** 2004. Three parallel quorum-sensing systems regulate gene expression in Vibrio harveyi. J Bacteriol **186:**6902-14.
119. **Herzberg, M., I. K. Kaye, W. Peti, and T. K. Wood.** 2006. YdgG (TqsA) controls biofilm formation in Escherichia coli K-12 through autoinducer 2 transport. J Bacteriol **188:**587-98.
120. **Hilgers, M. T., and M. L. Ludwig.** 2001. Crystal structure of the quorum-sensing protein LuxS reveals a catalytic metal site. Proc Natl Acad Sci U S A **98:**11169-74.
121. **Hofmann, T.** 1998. Characterization of the chemical structure of novel colored Maillard reaction products from furan-2-carboxaldehyde and amino acids. J Agric Food Chem **46:**932-940.
122. **Holms, H.** 1996. Flux analysis and control of the central metabolic pathways in *E. coli*. FEMS Microbiology Reviews **19:**85-116.
123. **Hornberg, J. J., F. J. Bruggeman, H. V. Westerhoff, and J. Lankelma.** 2006. Cancer: a Systems Biology disease. Biosystems **83:**81-90.
124. **Houdt, R., A. Aertsen, P. Moons, K. Vanoirbeek, and C. W. Michiels.** 2006. N-acyl-l-homoserine lactone signal interception by Escherichia coli. FEMS Microbiol Lett **256:**83-9.
125. **Huang, C. Y., and J. E. Ferrell, Jr.** 1996. Ultrasensitivity in the mitogen-activated protein kinase cascade. Proc Natl Acad Sci U S A **93:**10078-83.
126. **Ichikawa, J. K., A. Norris, M. G. Bangera, G. K. Geiss, A. B. van 't Wout, R. E. Bumgarner, and S. Lory.** 2000. Interaction of pseudomonas aeruginosa with epithelial cells: identification of differentially regulated genes by expression microarray analysis of human cDNAs. Proc Natl Acad Sci U S A **97:**9659-64.

127. **Ingraham, J., O. Maaloe, and F. Neidhardt.** 1983. Growth of the Bacterial Cell. Sinaeur Associates Inc., Sunderland, MA.
128. **Isbell, H. S., and W. Pigman.** 1969. Mutarotation of sugars in solutions: II. Catalytic processes, isotope effects, reaction mechanisms, and biochemical aspects. Advances in Carbohydrate Chemistry and Biochemistry **24:**13-65.
129. **Jarraud, S., G. J. Lyon, A. M. Figueiredo, L. Gerard, F. Vandenesch, J. Etienne, T. W. Muir, and R. P. Novick.** 2000. Exfoliatin-producing strains define a fourth agr specificity group in Staphylococcus aureus. J Bacteriol **182:**6517-22.
130. **Jobling, M. G., and R. K. Holmes.** 1997. Characterization of hapR, a positive regulator of the Vibrio cholerae HA/protease gene hap, and its identification as a functional homologue of the Vibrio harveyi luxR gene. Mol Microbiol **26:**1023-34.
131. **Joel, K.** 1987. Statistical Thermodynamics of Nonequlibrium Processes. Springer-Verlag, Berlin.
132. **Joung, J. K., E. H. Chung, G. King, C. Yu, A. S. Hirsh, and A. Hochschild.** 1995. Genetic strategy for analyzing specificity of dimer formation: *Escherichia coli* cyclic AMP receptor protein mutant altered in its dimerization specificity. Genes Dev **9:**2986-96.
133. **Kahn, D., and G. Ditta.** 1991. Modular structure of FixJ: homology of the transcriptional activator domain with the -35 binding domain of sigma factors. Mol Microbiol **5:**987-97.
134. **Kansal, A. R.** 2004. Modeling approaches to type 2 diabetes. Diabetes Technol Ther **6:**39-47.
135. **Kaplan, H. B., and E. P. Greenberg.** 1987. Overproduction and purification of the luxR gene product: Transcriptional activator of the Vibrio fischeri luminescence system. Proc Natl Acad Sci U S A **84:**6639-6643.
136. **Kashiwagi, K., R. Pistocchi, S. Shibuya, S. Sugiyama, K. Morikawa, and K. Igarashi.** 1996. Spermidine-preferential uptake system in Escherichia coli. Identification of amino acids involved in polyamine binding in PotD protein. J Biol Chem **271:**12205-8.
137. **Kauffman, S. A.** 1969. Metabolic stability and epigenesis in randomly constructed genetic nets. J Theor Biol **22:**437-67.
138. **Kaufmann, G. F., R. Sartorio, S. H. Lee, J. M. Mee, L. J. Altobell, 3rd, D. P. Kujawa, E. Jeffries, B. Clapham, M. M. Meijler, and K. D. Janda.** 2006. Antibody interference with N-acyl homoserine lactone-mediated bacterial quorum sensing. J Am Chem Soc **128:**2802-3.
139. **Kay, E., C. Dubuis, and D. Haas.** 2005. Three small RNAs jointly ensure secondary metabolism and biocontrol in Pseudomonas fluorescens CHA0. Proc Natl Acad Sci U S A **102:**17136-41.
140. **Keller, L., and M. G. Surette.** 2006. Communication in bacteria: an ecological and evolutionary perspective. Nat Rev Microbiol.
141. **Kepler, T. B., and T. C. Elston.** 2001. Stochasticity in transcriptional regulation: origins, consequences, and mathematical representations. Biophys J **81:**3116-36.

142. **Kimata, K., H. Takahashi, T. Inada, P. Postma, and H. Aiba.** 1997. cAMP receptor protein-cAMP plays a crucial role in glucose-lactose diauxie by activating the major glucose transporter gene in *Escherichia coli*. Proc Natl Acad Sci U S A **94:**12914-9.
143. **Kitano, H.** 2002. Systems biology: a brief overview. Science **295:**1662-4.
144. **Kjaergaard, K., M. A. Schembri, C. Ramos, S. Molin, and P. Klemm.** 2000. Antigen 43 facilitates formation of multispecies biofilms. Environ Microbiol **2:**695-702.
145. **Kleerebezem, M., L. E. Quadri, O. P. Kuipers, and W. M. de Vos.** 1997. Quorum sensing by peptide pheromones and two-component signal-transduction systems in Gram-positive bacteria. Mol Microbiol **24:**895-904.
146. **Kolibachuk, D., and E. P. Greenberg.** 1993. The Vibrio fischeri luminescence gene activator LuxR is a membrane-associated protein. J Bacteriol **175:**7307-12.
147. **Koop, A. H., M. E. Hartley, and S. Bourgeois.** 1987. A low-copy-number vector utilizing beta-galactosidase for the analysis of gene control elements. Gene **52:**245-56.
148. **Kovacikova, G., and K. Skorupski.** 2002. Regulation of virulence gene expression in Vibrio cholerae by quorum sensing: HapR functions at the aphA promoter. Mol Microbiol **46:**1135-47.
149. **Kremling, A., S. Fischer, T. Sauter, K. Bettenbrock, and E. D. Gilles.** 2004. Time hierarchies in the Escherichia coli carbohydrate uptake and metabolism. Biosystems **73:**57-71.
150. **Kremling, A., R. Heermann, F. Centler, K. Jung, and E. D. Gilles.** 2004. Analysis of two-component signal transduction by mathematical modeling using the KdpD/KdpE system of Escherichia coli. Biosystems **78:**23-37.
151. **Kuipers, O. P., M. M. Beerthuyzen, P. G. de Ruyter, E. J. Luesink, and W. M. de Vos.** 1995. Autoregulation of nisin biosynthesis in Lactococcus lactis by signal transduction. J Biol Chem **270:**27299-304.
152. **Kuo, G., Q. L. Choo, H. J. Alter, G. L. Gitnick, A. G. Redeker, R. H. Purcell, T. Miyamura, J. L. Dienstag, M. J. Alter, C. E. Stevens, and et al.** 1989. An assay for circulating antibodies to a major etiologic virus of human non-A, non-B hepatitis. Science **244:**362-4.
153. **Kuroda, M., T. Ohta, I. Uchiyama, T. Baba, H. Yuzawa, I. Kobayashi, L. Cui, A. Oguchi, K. Aoki, Y. Nagai, J. Lian, T. Ito, M. Kanamori, H. Matsumaru, A. Maruyama, H. Murakami, A. Hosoyama, Y. Mizutani-Ui, N. K. Takahashi, T. Sawano, R. Inoue, C. Kaito, K. Sekimizu, H. Hirakawa, S. Kuhara, S. Goto, J. Yabuzaki, M. Kanehisa, A. Yamashita, K. Oshima, K. Furuya, C. Yoshino, T. Shiba, M. Hattori, N. Ogasawara, H. Hayashi, and K. Hiramatsu.** 2001. Whole genome sequencing of meticillin-resistant Staphylococcus aureus. Lancet **357:**1225-40.
154. **Kurtz, T. G.** 1972. The relationship between stochastic and deterministic models for chemical reactions. J. Chem. Phys **57:**2976-2978.
155. **Kushner, S.** 1996. mRNA decay, p. 849-860. *In* F. C. Neidhardt (ed.), Escherichia coli and Salmonella, 2 ed, vol. I. SAM press, Washington, DC.

156. **Laurent, M., and N. Kellershohn.** 1999. Multistability: a major means of differentiation and evolution in biological systems. Trends Biochem Sci **24:**418-22.
157. **Lease, R. A., and M. Belfort.** 2000. A trans-acting RNA as a control switch in Escherichia coli: DsrA modulates function by forming alternative structures. Proc Natl Acad Sci U S A **97:**9919-24.
158. **Lease, R. A., D. Smith, K. McDonough, and M. Belfort.** 2004. The small noncoding DsrA RNA is an acid resistance regulator in Escherichia coli. J Bacteriol **186:**6179-85.
159. **Lenz, D. H., K. C. Mok, B. N. Lilley, R. V. Kulkarni, N. S. Wingreen, and B. L. Bassler.** 2004. The small RNA chaperone Hfq and multiple small RNAs control quorum sensing in Vibrio harveyi and Vibrio cholerae. Cell **118:**69-82.
160. **Lewis, H. A., E. B. Furlong, B. Laubert, G. A. Eroshkina, Y. Batiyenko, J. M. Adams, M. G. Bergseid, C. D. Marsh, T. S. Peat, W. E. Sanderson, J. M. Sauder, and S. G. Buchanan.** 2001. A structural genomics approach to the study of quorum sensing: crystal structures of three LuxS orthologs. Structure **9:**527-37.
161. **Li, J., L. Wang, Y. Hashimoto, C. Y. Tsao, J. J. Valdes, T. K. Wood, E. Zafiriou, and W. E. Bentley.** in press. A Stochastic Model of *E. coli* AI-2 Quorum Signal Circuit Reveals Alternative Synthesis Pathways. Molecular System Biology.
162. **Li, J., L. Wang, E. Zafiriou, and W. E. Bentley.** 2004. Presented at the AICHE Annual meeting, Houston, TX.
163. **Li, Z., and C. Chan.** 2004. Inferring pathways and networks with a Bayesian framework. Faseb J **18:**746-8.
164. **Majdalani, N., C. Cunning, D. Sledjeski, T. Elliott, and S. Gottesman.** 1998. DsrA RNA regulates translation of RpoS message by an anti-antisense mechanism, independent of its action as an antisilencer of transcription. Proc Natl Acad Sci U S A **95:**12462-7.
165. **Marson , M. A. B., G. Conte, G., Donatelli, S., Franceschinis, G. ,.** 1995. Modeling with Generalized Stochastic Petri nets. John Wiley & Sons.
166. **Matsuno, H., A. Doi, M. Nagasaki, and S. Miyano.** 2000. Hybrid Petri nets representation of gene regulatory network, vol. 5. Singapore, World Scientific Publishing .
167. **McAdams, H. H., and A. Arkin.** 1999. It's a noisy business! Genetic regulation at the nanomolar scale. Trends Genet **15:**65-9.
168. **McAdams, H. H., and A. Arkin.** 1998. Simulation of prokaryotic genetic circuits. Annu Rev Biophys Biomol Struct **27:**199-224.
169. **McAdams, H. H., and A. Arkin.** 1997. Stochastic mechanism in gene expression. . Proceedings of National Academic Science U. S. A. **94:** 814-819.
170. **McQuarrie, D. A.** 1967. Stochastic Approach to Chemical Kinetics. Journal of Applied Probability **4:**413-478.
171. **Meijler, M. M., L. G. Hom, G. F. Kaufmann, K. M. McKenzie, C. Sun, J. A. Moss, M. Matsushita, and K. D. Janda.** 2004. Synthesis and biological

validation of a ubiquitous quorum-sensing molecule. Angew Chem Int Ed Engl **43:**2106-8.
172. **Mendes, P., D. Camacho, and A. de la Fuente.** 2005. Modelling and simulation for metabolomics data analysis. Biochem Soc Trans **33:**1427-9.
173. **Mettetal, J. T., D. Muzzey, J. M. Pedraza, E. M. Ozbudak, and A. van Oudenaarden.** 2006. Predicting stochastic gene expression dynamics in single cells. Proc Natl Acad Sci U S A **103:**7304-9.
174. **Miller, C. H., and J. A. Duerre.** 1968. S-ribosylhomocysteine cleavage enzyme from Escherichia coli. J Biol Chem **243:**92-7.
175. **Miller, J. H.** 1972. Experiments in molecular genetics. Cold Spring Harbor Laboratory, [Cold Spring Harbor, N.Y.].
176. **Miller, M. B., and B. L. Bassler.** 2001. Quorum sensing in bacteria. Annu Rev Microbiol **55:**165-199.
177. **Miller, M. B., K. Skorupski, D. H. Lenz, R. K. Taylor, and B. L. Bassler.** 2002. Parallel quorum sensing systems converge to regulate virulence in Vibrio cholerae. Cell **110:**303-14.
178. **Miller, S. T., K. B. Xavier, S. R. Campagna, M. E. Taga, M. F. Semmelhack, B. L. Bassler, and F. M. Hughson.** 2004. *Salmonella typhimurium* Recognizes a Chemically Distinct Form of the Bacterial Quorum-Sensing Signal AI-2. Mol Cell **15:**677-687.
179. **Minogue, T. D., M. Wehland-von Trebra, F. Bernhard, and S. B. von Bodman.** 2002. The autoregulatory role of EsaR, a quorum-sensing regulator in *Pantoea stewartii* ssp. *stewartii*: evidence for a repressor function. Mol Microbiol **44:**1625-35.
180. **Miyamoto, C. M., P. V. Dunlap, E. G. Ruby, and E. A. Meighen.** 2003. LuxO controls luxR expression in Vibrio harveyi: evidence for a common regulatory mechanism in Vibrio. Mol Microbiol **48:**537-48.
181. **Moll, I., T. Afonyushkin, O. Vytvytska, V. R. Kaberdin, and U. Blasi.** 2003. Coincident Hfq binding and RNase E cleavage sites on mRNA and small regulatory RNAs. Rna **9:**1308-14.
182. **More, M. I., L. D. Finger, J. L. Stryker, C. Fuqua, A. Eberhard, and S. C. Winans.** 1996. Enzymatic synthesis of a quorum-sensing autoinducer through use of defined substrates. Science **272:**1655-8.
183. **Nakayama, J., Y. Cao, T. Horii, S. Sakuda, A. D. Akkermans, W. M. de Vos, and H. Nagasawa.** 2001. Gelatinase biosynthesis-activating pheromone: a peptide lactone that mediates a quorum sensing in Enterococcus faecalis. Mol Microbiol **41:**145-54.
184. **Nealson, K. H., T. Platt, and J. W. Hastings.** 1970. Cellular control of the synthesis and activity of the bacterial luminescence system. J Bacteriol **104:**313-322.
185. **Neddermann, P., C. Gargioli, E. Muraglia, S. Sambucini, F. Bonelli, R. De Francesco, and R. Cortese.** 2003. A novel, inducible, eukaryotic gene expression system based on the quorum-sensing transcription factor TraR. EMBO Rep **4:**159-65.

186. **Neidhardt, F., J. Ingraham, and M. Schaechter.** 1990. p. 8-9, Physiology of the Bacterial Cell: a Molecular Approach. Sinauer Associates Inc, Sunderland, Mass.
187. **Neiditch, M. B., M. J. Federle, A. J. Pompeani, R. C. Kelly, D. L. Swem, P. D. Jeffrey, B. L. Bassler, and F. M. Hughson.** 2006. Ligand-induced asymmetry in histidine sensor kinase complex regulates quorum sensing. Cell **126:**1095-108.
188. **Nesper, J., C. M. Hill, A. Paiment, G. Harauz, K. Beis, J. H. Naismith, and C. Whitfield.** 2003. Translocation of group 1 capsular polysaccharide in Escherichia coli serotype K30. Structural and functional analysis of the outer membrane lipoprotein Wza. J Biol Chem **278:**49763-72.
189. **Newman, E. B., L. I. Budman, E. C. Chan, R. C. Greene, R. T. Lin, C. L. Woldringh, and R. D'Ari.** 1998. Lack of S-adenosylmethionine results in a cell division defect in Escherichia coli. J Bacteriol **180:**3614-9.
190. **Novozhilov, A. S., F. S. Berezovskaya, E. V. Koonin, and G. P. Karev.** 2006. Mathematical modeling of tumor therapy with oncolytic viruses: regimes with complete tumor elimination within the framework of deterministic models. Biol Direct **1:**6.
191. **Oh, M. K., and J. C. Liao.** 2000. Gene expression profiling by DNA microarrays and metabolic fluxes in *Escherichia coli*. Biotechnol Prog **16:**278-86.
192. **Ohtani, K., H. Hayashi, and T. Shimizu.** 2002. The *luxS* gene is involved in cell-cell signalling for toxin production in *Clostridium perfringens*. Mol Microbiol **44:**171-9.
193. **O'Toole, G., H. B. Kaplan, and R. Kolter.** 2000. Biofilm formation as microbial development. Annu Rev Microbiol **54:**49-79.
194. **Parkinson, J.** 1995. Genetic approaches for signalling pathways and proteins, p. 9-23. *In* J. Hoch and T. Silhavy (ed.), Two-Component Signal Transduction. American Society for Microbiology Press, Washington, DC.
195. **Parra-Lopez, C., M. T. Baer, and E. A. Groisman.** 1993. Molecular genetic analysis of a locus required for resistance to antimicrobial peptides in Salmonella typhimurium. Embo J **12:**4053-62.
196. **Parsek, M. R., and E. P. Greenberg.** 2000. Acyl-homoserine lactone quorum sensing in gram-negative bacteria: a signaling mechanism involved in associations with higher organisms. Proc Natl Acad Sci U S A **97:**8789-93.
197. **Parsek, M. R., and E. P. Greenberg.** 2005. Sociomicrobiology: the connections between quorum sensing and biofilms. Trends Microbiol **13:**27-33.
198. **Parsek, M. R., D. L. Val, B. L. Hanzelka, J. E. Cronan, Jr., and E. P. Greenberg.** 1999. Acyl homoserine-lactone quorum-sensing signal generation. Proc Natl Acad Sci U S A **96:**4360-5.
199. **Pedersen, S., P. Bloch, S. Reeh, and F. Neidhardt.** 1978. Patterns of Protein Synthesis in E. coli: a Catalog of the Amount of 140 Individual Proteins at Different Growth Rates. Cell **14:**179-190.
200. **Pennisi, E.** 2003. Systems biology. Tracing life's circuitry. Science **302:**1646-9.

201. **Peterson , J. L.** 1981. Petri net theory and the modeling of systems. Prentice Hall, Englewood Cliffs, N. J.
202. **Pigman, W., and H. S. Isbell.** 1968. Mutarotation of sugars in solution: I. History, Basic Kinetics, and Composition of sugar solutions. Advances in Carbohydrate Chemistry **23:**11-57.
203. **Posnick, L. M., and L. D. Samson.** 1999. Influence of S-adenosylmethionine pool size on spontaneous mutation, dam methylation, and cell growth of *Escherichia coli*. J Bacteriol **181:**6756-62.
204. **Possot, O. M., G. Vignon, N. Bomchil, F. Ebel, and A. P. Pugsley.** 2000. Multiple interactions between pullulanase secreton components involved in stabilization and cytoplasmic membrane association of PulE. J Bacteriol **182:**2142-52.
205. **Pratt, L. A., and R. Kolter.** 1998. Genetic analysis of *Escherichia coli* biofilm formation: roles of flagella, motility, chemotaxis and type I pili. Mol Microbiol **30:**285-93.
206. **Prigent-Combaret, C., G. Prensier, T. T. Le Thi, O. Vidal, P. Lejeune, and C. Dorel.** 2000. Developmental pathway for biofilm formation in curli-producing Escherichia coli strains: role of flagella, curli and colanic acid. Environ Microbiol **2:**450-64.
207. **Prouty, A. M., W. H. Schwesinger, and J. S. Gunn.** 2002. Biofilm formation and interaction with the surfaces of gallstones by *Salmonella* spp. Infect Immun **70:**2640-9.
208. **Py, B., L. Loiseau, and F. Barras.** 2001. An inner membrane platform in the type II secretion machinery of Gram-negative bacteria. EMBO Rep **2:**244-8.
209. **Raina, S., D. Missiakas, L. Baird, S. Kumar, and C. Georgopoulos.** 1993. Identification and transcriptional analysis of the Escherichia coli htrE operon which is homologous to pap and related pilin operons. J Bacteriol **175:**5009-21.
210. **Rajan, R., J. Zhu, X. Hu, D. Pei, and C. E. Bell.** 2005. Crystal structure of S-ribosylhomocysteinase (LuxS) in complex with a catalytic 2-ketone intermediate. Biochemistry **44:**3745-53.
211. **Raychaudhuri, S., V. Jain, and M. Dongre.** 2006. Identification of a constitutively active variant of LuxO that affects production of HA/protease and biofilm development in a non-O1, non-O139 Vibrio cholerae O110. Gene **369:**126-33.
212. **Records Jr., M. T., W. S. Reznikoff, M. L. Craig, K. L. McQuade, and P. J. Schlax.** 1996. *Escherichia coli* RNA polymerase(Esigma70), Promoters, and the kinetics of the steps of Transcription initiation, p. 792-820. *In* F. C. Neidhardt (ed.), Escherichia coli and Salmonella, 2 ed, vol. I. ASM press, Washington, DC.
213. **Reddy, V. N., M. L. Mavrovouniotis, and M. N. Liebman.** 1993. Petri net representations in metabolic pathways. *In* D. S. a. J. S. L. Hunter (ed.), Proc of the First. Intl. Conf. on Intell. Sys. for Mol. Biol. AAAI/MIT Press, Menlo Park, CA.
214. **Reid, A. N., and C. Whitfield.** 2005. functional analysis of conserved gene products involved in assembly of Escherichia coli capsules and

exopolysaccharides: evidence for molecular recognition between Wza and Wzc for colanic acid biosynthesis. J Bacteriol **187:**5470-81.

215. **Reisner, A., J. A. Haagensen, M. A. Schembri, E. L. Zechner, and S. Molin.** 2003. Development and maturation of Escherichia coli K-12 biofilms. Mol Microbiol **48:**933-46.
216. **Robinson, L. S., E. M. Ashman, S. J. Hultgren, and M. R. Chapman.** 2006. Secretion of curli fibre subunits is mediated by the outer membrane-localized CsgG protein. Mol Microbiol **59:**870-81.
217. **Roe, A. J., C. O'Byrne, D. McLaggan, and I. R. Booth.** 2002. Inhibition of Escherichia coli growth by acetic acid: a problem with methionine biosynthesis and homocysteine toxicity. Microbiology **148:**2215-22.
218. **Rosenfeld, N., M. B. Elowitz, and U. Alon.** 2002. Negative autoregulation speeds the response times of transcription networks. J Mol Biol **323:**785-93.
219. **Ruby, E. G.** 1996. Lessons from a cooperative, bacterial-animal association: the *Vibrio fischeri-Euprymna scolopes* light organ symbiosis. Annu Rev Microbiol **50:**591-624.
220. **Rust, L., E. C. Pesci, and B. H. Iglewski.** 1996. Analysis of the *Pseudomonas aeruginosa* elastase (*lasB*) regulatory region. J Bacteriol **178:**1134-40.
221. **Sambrook, J., E. F. Fritsch, and T. Maniatis.** 1989. Molecular cloning: a laboratory manual, 2nd ed. Cold Spring Harbor laboratory Press, Cold Spring Harbor, N. Y.
222. **Sandkvist, M., J. M. Keith, M. Bagdasarian, and S. P. Howard.** 2000. Two regions of EpsL involved in species-specific protein-protein interactions with EpsE and EpsM of the general secretion pathway in Vibrio cholerae. J Bacteriol **182:**742-8.
223. **Sauter, T., and E. D. Gilles.** 2004. Modeling and experimental validation of the signal transduction via the Escherichia coli sucrose phospho transferase system. J Biotechnol **110:**181-99.
224. **Sauvonnet, N., P. Gounon, and A. P. Pugsley.** 2000. PpdD type IV pilin of Escherichia coli K-12 can Be assembled into pili in Pseudomonas aeruginosa. J Bacteriol **182:**848-54.
225. **Sauvonnet, N., G. Vignon, A. P. Pugsley, and P. Gounon.** 2000. Pilus formation and protein secretion by the same machinery in Escherichia coli. Embo J **19:**2221-8.
226. **Schaefer, A. L., D. L. Val, B. L. Hanzelka, J. E. Cronan, Jr., and E. P. Greenberg.** 1996. Generation of cell-to-cell signals in quorum sensing: acyl homoserine lactone synthase activity of a purified Vibrio fischeri LuxI protein. Proc Natl Acad Sci U S A **93:**9505-9.
227. **Schauder, S., K. Shokat, M. G. Surette, and B. L. Bassler.** 2001. The LuxS family of bacterial autoinducers: biosynthesis of a novel quorum-sensing signal molecule. Mol Microbiol **41:**463-476.
228. **Schlitt, T., and A. Brazma.** 2006. Modelling in molecular biology: describing transcription regulatory networks at different scales. Philos Trans R Soc Lond B Biol Sci **361:**483-94.

229. **Schramke, V., D. M. Sheedy, A. M. Denli, C. Bonila, K. Ekwall, G. J. Hannon, and R. C. Allshire.** 2005. RNA-interference-directed chromatin modification coupled to RNA polymerase II transcription. Nature **435:**1275-9.
230. **Schroeder, H. R., C. J. Barnes, R. C. Bohinski, and M. F. Mallette.** 1973. Biological production of 5-methylthioribose. Can. J. Microbiol. **19:**1347-1354.
231. **Seger, R., and E. G. Krebs.** 1995. The MAPK signaling cascade. Faseb J **9:**726-35.
232. **Semmelhack, M. F., S. R. Campagna, M. J. Federle, and B. L. Bassler.** 2005. An expeditious synthesis of DPD and boron binding studies. Org Lett **7:**569-72.
233. **Semmelhack, M. F., S. R. Campagna, C. Hwa, M. J. Federle, and B. L. Bassler.** 2004. Boron binding with the quorum sensing signal AI-2 and analogues. Org Lett **6:**2635-7.
234. **Sherlock, O., U. Dobrindt, J. B. Jensen, R. Munk Vejborg, and P. Klemm.** 2006. Glycosylation of the self-recognizing Escherichia coli Ag43 autotransporter protein. J Bacteriol **188:**1798-807.
235. **Simms, S. A., A. M. Stock, and J. B. Stock.** 1987. Purification and characterization of the S-adenosylmethionine:glutamyl methyltransferase that modifies membrane chemoreceptor proteins in bacteria. J Biol Chem **262:**8537-43.
236. **Simpson, M. L., C. D. Cox, and G. S. Sayler.** 2004. Frequency domain chemical Langevin analysis of stochasticity in gene transcriptional regulation. J Theor Biol **229:**383-94.
237. **Sitnikov, D. M., J. B. Schineller, and T. O. Baldwin.** 1996. Control of cell division in Escherichia coli: regulation of transcription of ftsQA involves both rpoS and SdiA-mediated autoinduction. Proc Natl Acad Sci U S A **93:**336-41.
238. **Sledjeski, D., and S. Gottesman.** 1995. A small RNA acts as an antisilencer of the H-NS-silenced rcsA gene of Escherichia coli. Proc Natl Acad Sci U S A **92:**2003-7.
239. **Sledjeski, D. D., C. Whitman, and A. Zhang.** 2001. Hfq is necessary for regulation by the untranslated RNA DsrA. J Bacteriol **183:**1997-2005.
240. **Slock, J., D. VanRiet, D. Kolibachuk, and E. P. Greenberg.** 1990. Critical regions of the Vibrio fischeri luxR protein defined by mutational analysis. J Bacteriol **172:**3974-9.
241. **Slonim, D. K.** 2002. From patterns to pathways: gene expression data analysis comes of age. Nat Genet **32 Suppl:**502-8.
242. **Smolen, P., D. A. Baxter, and J. H. Byrne.** 2000. Mathematical modeling of gene networks. Neuron **26:**567-80.
243. **Sonnleitner, E., J. Napetschnig, T. Afonyushkin, K. Ecker, B. Vecerek, I. Moll, V. R. Kaberdin, and U. Blasi.** 2004. Functional effects of variants of the RNA chaperone Hfq. Biochem Biophys Res Commun **323:**1017-23.
244. **Sonnleitner, E., M. Schuster, T. Sorger-Domenigg, E. P. Greenberg, and U. Blasi.** 2006. Hfq-dependent alterations of the transcriptome profile and effects on quorum sensing in Pseudomonas aeruginosa. Mol Microbiol **59:**1542-58.

245. **Sorensen, K. I., and B. Hove-Jensen.** 1996. Ribose catabolism of Escherichia coli: characterization of the rpiB gene encoding ribose phosphate isomerase B and of the rpiR gene, which is involved in regulation of rpiB expression. J Bacteriol **178:**1003-11.
246. **Soutourina, J., S. Blanquet, and P. Plateau.** 2001. Role of D-cysteine desulfhydrase in the adaptation of Escherichia coli to D-cysteine. J Biol Chem **276:**40864-72.
247. **Sperandio, V., A. G. Torres, B. Jarvis, J. P. Nataro, and J. B. Kaper.** 2003. Bacteria-host communication: the language of hormones. Proc Natl Acad Sci U S A **100:**8951-6.
248. **Sperandio, V., A. G. Torres, and J. B. Kaper.** 2002. Quorum sensing *Escherichia coli* regulators B and C (QseBC): a novel two-component regulatory system involved in the regulation of flagella and motility by quorum sensing in *E. coli*. Mol Microbiol **43:**809-821.
249. **Srivastava, R., M. S. Peterson, and W. E. Bentley** 2001. Stochastic kinetic analysis of the *Escherichia coli* stress circuit using sigma (32)-targeted antisense. Biotechnol Bioeng **75:**120-129.
250. **Srivastava, R., L. You, J. Summers, and J. Yin.** 2002. Stochastic vs. deterministic modeling of intracellular viral kinetics. J Theor Biol **218:**309-21.
251. **Stevens, A. M., K. M. Dolan, and E. P. Greenberg.** 1994. Synergistic binding of the *Vibrio fischeri* LuxR transcriptional activator domain and RNA polymerase to the *lux* promoter region. Proc Natl Acad Sci U S A **91:**12619-23.
252. **Stevens, A. M., N. Fujita, A. Ishihama, and E. P. Greenberg.** 1999. Involvement of the RNA polymerase alpha-subunit C-terminal domain in LuxR-dependent activation of the *Vibrio fischeri* luminescence genes. J Bacteriol **181:**4704-7.
253. **Stevens, A. M., and E. P. Greenberg.** 1997. Quorum sensing in *Vibrio fischeri*: essential elements for activation of the luminescence genes. J Bacteriol **179:**557-62.
254. **Strohman, R. C.** 1997. The coming Kuhnian revolution in biology. Nat Biotechnol **15:**194-200.
255. **Sturme, M. H., M. Kleerebezem, J. Nakayama, A. D. Akkermans, E. E. Vaugha, and W. M. de Vos.** 2002. Cell to cell communication by autoinducing peptides in gram-positive bacteria. Antonie Van Leeuwenhoek **81:**233-43.
256. **Sun, J., R. Daniel, I. Wagner-Dobler, and A. P. Zeng.** 2004. Is autoinducer-2 a universal signal for interspecies communication: a comparative genomic and phylogenetic analysis of the synthesis and signal transduction pathways. BMC Evol Biol **4:**36.
257. **Surette, M. G., and B. L. Bassler.** 1998. Quorum sensing in *Escherichia coli* and *Salmonella typhimurium*. Proc Natl Acad Sci U S A **95:**7046-50.
258. **Surette, M. G., and B. L. Bassler.** 1998. Quorum sensing in *Escherichia coli* and *Salmonella typhimurium*. Proc Natl Acad Sci U S A **95:**7046-7050.

259. **Surette, M. G., M. B. Miller, and B. L. Bassler.** 1999. Quorum sensing in *Escherichia coli*, *Salmonella typhimurium*, and *Vibrio harveyi*: a new family of genes responsible for autoinducer production. Proc Natl Acad Sci U S A **96:**1639-44.
260. **Taga, M. E., S. T. Miller, and B. L. Bassler.** 2003. Lsr-mediated transport and processing of AI-2 in *Salmonella typhimurium*. Mol Microbiol **50:**1411-1427.
261. **Taga, M. E., J. L. Semmelhack, and B. L. Bassler.** 2001. The LuxS-dependent autoinducer AI-2 controls the expression of an ABC transporter that functions in AI-2 uptake in Salmonella typhimurium. Mol Microbiol **42:**777-93.
262. **Taira, K.** 2006. Induction of DNA methylation and gene silencing by short interfering RNAs in human cells. Nature **441:**1176.
263. **Tao, Y.** 2004. Intrinsic and external noise in an auto-regulatory genetic network. J Theor Biol **229:**147-56.
264. **Tavender, T., Baldwin, TJ, Hardie, KR and Winzer, K.** 2004. Presented at the ASM 2004 general meeting.
265. **Taylor, J. C., F. Takusagawa, and G. D. Markham.** 2002. The active site loop of S-adenosylmethionine synthetase modulates catalytic efficiency. Biochemistry **41:**9358-69.
266. **Temin, H. M., and S. Mizutani.** 1970. RNA-dependent DNA polymerase in virions of Rous sarcoma virus. Nature **226:**1211-3.
267. **Tetart, F., R. Albigot, A. Conter, E. Mulder, and J. P. Bouche.** 1992. Involvement of FtsZ in coupling of nucleoid separation with septation. Mol Microbiol **6:**621-7.
268. **Tetart, F., and J. P. Bouche.** 1992. Regulation of the expression of the cell-cycle gene ftsZ by DicF antisense RNA. Division does not require a fixed number of FtsZ molecules. Mol Microbiol **6:**615-20.
269. **Tian, T., and K. Burrage.** 2004. Bistability and switching in the lysis/lysogeny genetic regulatory network of bacteriophage lambda. J Theor Biol **227:**229-37.
270. **Tortosa, P., L. Logsdon, B. Kraigher, Y. Itoh, I. Mandic-Mulec, and D. Dubnau.** 2001. Specificity and genetic polymorphism of the Bacillus competence quorum-sensing system. J Bacteriol **183:**451-60.
271. **Tyson, J. J., K. C. Chen, and B. Novak.** 2003. Sniffers, buzzers, toggles and blinkers: dynamics of regulatory and signaling pathways in the cell. Curr Opin Cell Biol **15:**221-31.
272. **Vendeville, A., K. Winzer, K. Heurlier, C. M. Tang, and K. R. Hardie.** 2005. Making 'sense' of metabolism: autoinducer-2, LuxS and pathogenic bacteria. Nat Rev Microbiol **3:**383-96.
273. **Vicente, M., and A. I. Rico.** 2006. The order of the ring: assembly of Escherichia coli cell division components. Mol Microbiol **61:**5-8.
274. **Vincent, C., B. Duclos, C. Grangeasse, E. Vaganay, M. Riberty, A. J. Cozzone, and P. Doublet.** 2000. Relationship between exopolysaccharide production and protein-tyrosine phosphorylation in gram-negative bacteria. J Mol Biol **304:**311-21.

275. **Walters, M., and V. Sperandio.** 2006. Quorum sensing in Escherichia coli and Salmonella. Int J Med Microbiol.
276. **Wang, L., Y. Hashimato, C. Y. Tsao, J. J. Valdes, and W. E. Bentley.** 2005. Cyclic AMP (cAMP) and cAMP receptor protein influence both synthesis and uptake of extracellular autoinducer 2 in *Escherichia coli*. J Bacteriol **187:**2066-2076.
277. **Wang, L., J. Li, J. C. March, J. J. Valdes, and W. E. Bentley.** 2005. luxS-dependent gene regulation in Escherichia coli K-12 revealed by genomic expression profiling. J Bacteriol **187:**8350-60.
278. **Wassarman, K. M., F. Repoila, C. Rosenow, G. Storz, and S. Gottesman.** 2001. Identification of novel small RNAs using comparative genomics and microarrays. Genes Dev **15:**1637-51.
279. **Westerhoff, H. V., and B. O. Palsson.** 2004. The evolution of molecular biology into systems biology. Nat Biotechnol **22:**1249-52.
280. **Whitehead, N. A., A. M. Barnard, H. Slater, N. J. Simpson, and G. P. Salmond.** 2001. Quorum-sensing in Gram-negative bacteria. FEMS Microbiol Rev **25:**365-404.
281. **Whitfield, C., and A. Paiment.** 2003. Biosynthesis and assembly of Group 1 capsular polysaccharides in Escherichia coli and related extracellular polysaccharides in other bacteria. Carbohydr Res **338:**2491-502.
282. **Wickner, R. B.** 1994. [URE3] as an altered URE2 protein: evidence for a prion analog in Saccharomyces cerevisiae. Science **264:**566-9.
283. **Wickner, R. B., C. W. Tabor, and H. Tabor.** 1970. Purification of adenosylmethionine decarboxylase from Escherichia coli W: evidence for covalently bound pyruvate. J Biol Chem **245:**2132-9.
284. **Williams, S. C., E. K. Patterson, N. L. Carty, J. A. Griswold, A. N. Hamood, and K. P. Rumbaugh.** 2004. *Pseudomonas aeruginosa* autoinducer enters and functions in mammalian cells. J Bacteriol **186:**2281-7.
285. **Winzer, K., K. R. Hardie, N. Burgess, N. Doherty, D. Kirke, M. T. Holden, R. Linforth, K. A. Cornell, A. J. Taylor, P. J. Hill, and P. Williams.** 2002. LuxS: its role in central metabolism and the in vitro synthesis of 4-hydroxy-5-methyl-3(2H)-furanone. Microbiology **148:**909-22.
286. **Winzer, K., K. R. Hardie, N. Burgess, N. Doherty, D. Kirke, M. T. Holden, R. Linforth, K. A. Cornell, A. J. Taylor, P. J. Hill, and P. Williams.** 2002. LuxS: its role in central metabolism and the in vitro synthesis of 4-hydroxy-5-methyl-3(2H)-furanone. Microbiology **148:**909-922.
287. **Winzer, K., K. R. Hardie, and P. Williams.** 2003. LuxS and autoinducer-2: their contribution to quorum sensing and metabolism in bacteria. Adv Appl Microbiol **53:**291-396.
288. **Withers, H., S. Swift, and P. Williams.** 2001. Quorum sensing as an integral component of gene regulatory networks in Gram-negative bacteria. Curr Opin Microbiol **4:**186-93.
289. **Wong, P., S. Gladney, and J. D. Keasling.** 1997. Mathematical model of the lac operon: inducer exclusion, catabolite repression, and diauxic growth on glucose and lactose. Biotechnol Prog **13:**132-43.

290. **Wong, W. W., and J. C. Liao.** 2006. The design of intracellular oscillators that interact with metabolism. Cell Mol Life Sci **63:**1215-20.
291. **Xavier, K. B., and B. L. Bassler.** 2005. Interference with AI-2-mediated bacterial cell-cell communication. Nature **437:**750-3.
292. **Xavier, K. B., and B. L. Bassler.** 2003. LuxS quorum sensing: more than just a numbers game. Curr Opin Microbiol **6:**191-7.
293. **Xavier, K. B., and B. L. Bassler.** 2005. Regulation of uptake and processing of the quorum-sensing autoinducer AI-2 in Escherichia coli. J Bacteriol **187:**238-48.
294. **Xie, Q. W., C. W. Tabor, and H. Tabor.** 1989. Spermidine biosynthesis in Escherichia coli: promoter and termination regions of the speED operon. J Bacteriol **171:**4457-65.
295. **Yebra, M. J., A. Veyrat, M. A. Santos, and G. Perez-Martinez.** 2000. Genetics of L-sorbose transport and metabolism in Lactobacillus casei. J Bacteriol **182:**155-63.
296. **Yi, X., and R. M. Weis.** 2002. The receptor docking segment and S-adenosyl-L-homocysteine bind independently to the methyltransferase of bacterial chemotaxis. Biochim Biophys Acta **1596:**28-35.
297. **Yoshida, A., T. Ansai, T. Takehara, and H. K. Kuramitsu.** 2005. LuxS-Based Signaling Affects *Streptococcus* mutants Biofilm Formation. Appl Environ Microbiol **71:**2372-80.
298. **You, L., R. S. Cox, 3rd, R. Weiss, and F. H. Arnold.** 2004. Programmed population control by cell-cell communication and regulated killing. Nature **428:**868-71.
299. **Zeng, X., and H. H. Saxild.** 1999. Identification and characterization of a DeoR-specific operator sequence essential for induction of dra-nupC-pdp operon expression in Bacillus subtilis. J Bacteriol **181:**1719-27.
300. **Zhang, A., K. M. Wassarman, C. Rosenow, B. C. Tjaden, G. Storz, and S. Gottesman.** 2003. Global analysis of small RNA and mRNA targets of Hfq. Mol Microbiol **50:**1111-24.
301. **Zhu, J., E. Dizin, X. Hu, A. Wavreille, and J. a. P. Park, D.** 2003. S-Ribosylhomocysteinase (LuxS) is a mononuclear iron protein. Biochemistry **42:**4717-4726.
302. **Zhu, J., E. Dizin, X. Hu, A. S. Wavreille, J. Park, and D. Pei.** 2003. S-Ribosylhomocysteinase (LuxS) is a mononuclear iron protein. Biochemistry **42:**4717-26.
303. **Zhu, J., M. B. Miller, R. E. Vance, M. Dziejman, B. L. Bassler, and J. J. Mekalanos.** 2002. Quorum-sensing regulators control virulence gene expression in Vibrio cholerae. Proc Natl Acad Sci U S A **99:**3129-34.